EPA/540/R-95/526
September 1995

EMERGING TECHNOLOGY REPORT: DEVELOPMENT OF A PHOTOTHERMAL DETOXIFICATION UNIT

by

John L. Graham
Barry Dellinger
Joseph Swartzbaugh

Environmental Science and Engineering Group
University of Dayton Research Institute
Dayton, Ohio 45469-0132

Cooperative Agreement No. CR8 19594-01-0

Project Officer

Chien T. Chen
National Risk Management Research Laboratory
Water Supply and Water Resources Division
(formerly Superfund Technology Demonstration Division)
Edison, NJ 08837

This study was conducted
in cooperation with
U. S. Environmental Protection Agency

NATIONAL RISK MANAGEMENT RESEARCH LABORATORY
OFFICE OF RESEARCH AND DEVELOPMENT
U. S. ENVIRONMENTAL PROTECTION AGENCY
CINCINNATI, OH 45268

TECHNICAL REPORT DATA

(Please read Instructions on the reverse before completing)

1. REPORT NO.	2.	3. RECIPIENT'S ACCESSION NO.

4. TITLE AND SUBTITLE
Emerging Technology Report: Development of a Photothermal Detoxification Unit

5. REPORT DATE
August 1995

6. PERFORMING ORGANIZATION CODE

7. AUTHOR(S)
John L. Graham, Barry Dellinger, John Swartzbaugh

8. PERFORMING ORGANIZATION REPORT NO.

9. PERFORMING ORGANIZATION NAME AND ADDRESS
Environmental Science and Engineering Group
University of Dayton Research Institute
300 College Park
Dayton, OH 45469-0132

10. PROGRAM ELEMENT NO.

11. CONTRACT/GRANT NO.
CR819594-01-0

12. SPONSORING AGENCY NAME AND ADDRESS
National Risk Management Research Laboratory
Office of Research and Development
U.S. Environmental Protection Agency
Cincinnati, OH 45268

13. TYPE OF REPORT AND PERIOD COVERED
Final Report 10/92 - 12/94

14. SPONSORING AGENCY CODE
EPA/600/14

15. SUPPLEMENTARY NOTES
Chien T. Chen, Telephone No. (908) 906-6985 Technology, 15 (2), 1995

16. ABSTRACT

There has long been interest in utilizing photochemical methods for destroying hazardous organic materials. Unfortunately, the direct application of classic, low temperature photochemical processes to hazardous waste detoxification are often too slow to be practical for wide spread use. Furthermore, low-temperature photochemical processes often fail to completely convert targeted wastes to mineral products of complete conversion which are either harmless to the environment or easily scrubbed from the system effluent. Researchers at the University of Dayton Research Institute (UDRI) have developed a unique photothermal process that overcomes many of the problems previously encountered with direct photochemical detoxification techniques. Specifically, it has been found that there are numerous advantages to conducting photochemical detoxification at relatively high temperatures. Under the conditions of simultaneous exposure to heat and ultraviolet (UV) radiation the rate of destructive photothermal reactions can be greatly increased and that these reactions result in the complete mineralization of the waste feed. Furthermore, it has been demonstrated that at the elevated temperatures used in this process the efficiency of UV radiation absorption also increases resulting in an overall improvement in process efficiency. These features (i.e., fast, efficient, and complete destruction of organic wastes) makes this process a promising technique for destroying hazardous organic wastes in the gas-phase. The authors present the theoretical foundation for the photothermal detoxification process along with a summary of the results from a bench-scale flow reactor system. The basic design, capital cost, and operating cost for a full-scale flow reactor system using currently available industrial illumination equipment is also presented.

17. KEY WORDS AND DOCUMENT ANALYSIS

a. DESCRIPTORS	b. IDENTIFIERS/OPEN ENDED TERMS	c. COSATI Field/Group
Trichloroethylene, Tetrachloroethylene, Benzene, Toluene, Ethylbenzene, Xylene, Photothermal Reaction		

18. DISTRIBUTION STATEMENT	19. SECURITY CLASS *(This Report)*	21. NO. OF PAGES
Release to the public	unclassified	
	20. SECURITY CLASS *(This page)*	22. PRICE
	unclassified	

EPA Form 2220-1 (9-73)

DISCLAIMER

The information in this document has been funded wholly or in part by the United States Environmental Protection Agency through Cooperative Agreement No.: CR819594-01-0 to the University of Dayton Research Institute. It has been subjected to the Agency's peer and administrative review, and it has been approved for publication as an EPA document. Mention of trade names or commercial products does not constitute endorsement or recommendation for use.

FOREWORD

The U.S. Environmental Protection Agency is charged by Congress with protecting the Nation's land, air, and water resources. Under a mandate of national environmental laws, the Agency strives to formulate and implement actions leading to a compatible balance between human activities and the ability of natural systems to support and nurture life. To meet this mandate, EPA's research program is providing data and technical support for solving environmental problems today and building a science knowledge base necessary to manage our ecological resources wisely, understand how pollutants affect our health, and prevent or reduce environmental risks in the future.

The National Risk Management Research Laboratory is the Agency's center for investigation of technological and management approaches for reducing risks from threats to human health and the environment. The focus of the Laboratory's research program is on methods for the prevention and control of pollution to air, land, water and subsurface resources; protection of water quality in public water systems ; remediation of contaminated sites and ground water; and prevention and control of indoor air pollution. The goal of this research effort is to catalyze development and implementation of innovative, cost-effective environmental technologies; develop scientific and engineering information needed by EPA to support regulatory and policy decisions; and provide technical support and information transfer to ensure effective implementation of environmental regulations and strategies.

This publication has been produced as part of the Laboratory's strategic long-term research plan. It is published and made available by EPA's Office of Research and Development to assist the user community and to link researchers with their clients.

E. Timothy Oppelt, Director
National Risk Management Research Laboratory

ABSTRACT

There has long been interest in utilizing photochemical methods for destroying hazardous organic materials. Unfortunately, the direct application of classic, low temperature photochemical processes to hazardous waste detoxification are often too slow to be practical for wide spread use. Furthermore, low-temperature photochemical processes often fail to completely convert the targeted wastes to mineral products of complete conversion which are either harmless to the environment or easily scrubbed from the system effluent. Researchers at the University of Dayton Research Institute (UDRI) have deveioped a unique photothermal process that overcomes many of the problems previously encountered with direct photochemical detoxification techniques. Specifically, it has been found that there are numerous advantages to conducting photochemical detoxification at relatively high temperatures. Under the conditions of simultaneous exposure to heat and ultraviolet (UV) radiation the rate of destructive photothermal reactions can be greatly increased and that these reactions result in the complete mineralization of the waste feed, Furthermore, it has been demonstrated that at the elevated temperatures used in this process the efficiency of UV radiation absorption also increases resulting in an overall improvement in process efficiency. These features (i.e., fast, efficient, and complete destruction of organic wastes) makes this process a promising technique for destroying hazardous organic wastes in the gas-phase. The authors present the theoretical foundation for the photothermal detoxification process along with a summary of the results from a bench-scale flow reactor system. The basic design, capital cost, and operating cost for a full-scale flow reactor system using currently available industrial illumination equipment is also presented.

This report was submitted in fulfillment of Cooperative Agreement CR819594-01-0 by the University of Dayton Research Institute, Environmental Science and Engineering Croup, under the (partial) sponsorship of the U. S. Environmental Protection Agency. This report covers a period from1 October 1992 to 30 December 1994, and work was completed as of 30 December

CONTENTS

CONTENTS (continued)

FIGURES

FIGURES (continued)

FIGURES (continued)

FIGURES (continued)

FIGURES (continued)

FIGURES (continued)

FIGURES (continued)

FIGURES (continued)

FIGURES (continued)

TABLES

TABLES (continued)

TABLES (continued)

TABLES (continued)

ABBREVIATIONS AND SYMBOLS

Symbol	Definition
°C	Degrees Centigrade
°K	Degrees Kelvin
A	Arrhenius coefficient
AMU	Atomic Mass Units
BTEX	Benzene. Toluene. Ethyl Benzene, Xylene mixture
Bz	Benzene
C	Concentration
cal	Calories
cfm	Cubic Feet per Minute
Clfrm	Chloroform
cm	Centimeter
Ctet	Carbon Tetrachloride
d	Distance
DCBz	o-Dichlorobenzene
E_a	Activation Energy
$\varepsilon_{\lambda i}$	Extinction coefficient at wavelength λ_i
ESE	Environmental Science and Engineering
EthBz	Ethyl Benzene
exp(n)	Exponentiation of n (e^n)
F	Flow rate
FID	Flame Ionization Detector
f_r	Fraction Remaining
ϕ_r	Quantum Yield
g	Grams
GC	Gas Chromatograph
HTAS	High Temperature Absorption Spectrophotometer
I	Intensity
$I_{0\lambda i}$	Initial Intensity at wavelength λ_i
I_{avg}	Average Intensity
in	Inch
k_{ab}	Photon absorption rate constant
k_{gnd}	Ground state reaction rate constant
kW	Kilowatts
L	Liter
l	Length
λ_i	Wavelength of i
ln	Natural logarithm
LS-PDU	Laboratory Scale-Photothermal Detoxification Unit
m	Meter
MCBz	Monochlorobenzene
min	Minute

ABBREVIATIONS AND SYMBOLS (continued)

Symbol	Definition
ml	Milliliter
µl	Microliter
mm	Millimeter
mol	Mole
MS	Mass Spectrometer
N	Number of tanks
NIST	National Institute of Standards and Technology
nm	Nanometer
OMA	Optical Multichannel Analyzer
P	Power
P_e	Power at a volume element
PCB	Polychlorinated Biphenyl
PCDD	Polychlorinated Dibenzo-p-dioxin
PCDF	Polychlorinated Dibenzo-p-furan
PCE	Teuachloroethylene
PDU	Photothermal Detoxification Unit
PIC	Product of Incomplete Conversion
Pn	Unidentified organic product n
PNA	Polynuclear Aromatic
ppm	Part Per Million
psig	Pounds per Square Inch Gauge
R	Universal Gas Constant
R	Radius
RSD	Relative Standard Deviation
Σ	Summation
scfm	Standard Cubic Feet per Minute (dry @ 20°C)
sec	Second
S_n	Singlet state n
SVE	Soil Vapor Extraction
T	Temperature
T_{PDU}	Temperature of the PDU
Tref	Reference Temperature
t	Time
t_r	Mean residence time
t_{99}	Time required for 99% conversion
TCDD	1,2,3,4-Tetrachlorodibenzo-p-dioxin
TCE	Trichloroethylene
T_n	Triplet state n
Tol	Toluene
UDRI	University of Dayton Research Institute
UV	Ultraviolet
V	Volume
W	Watts
Xyl	m-Xylene

ACKNOWLEDGMENT

We would like to gratefully acknowledge the United States Environmental Protection Agency for funding this project under Cooperative Agreement No: CR819594-01-0. We would also like to express our appreciation to Norma M. Lewis, Chief, Emerging Technology Section, for her support and encouragement. We would also like to acknowledge the Project Officer for this program, Dr. Chien T. Chen, for his assistance throughout this project. And finally, we would like to thank the reviewers who did an excellent job helping us prepare this final report

SECTION 1

INTRODUCTION

The University of Dayton Research Institute's (UDRI) Environmental Science and Engineering Group (ESE) has developed a new process based on a photochemical technology that is well suited for treating the dilute gas-phase waste streams that are associated with several types of Superfund site cleanup operations (e.g., soil vapor extraction, thermal desorption, etc.) and may also find other applications such as a retrofit on conventional hazardous waste incinerators to assist in the destruction process or even as a primary destruction technology in special cases such as mixed wastes. Specifically, previous work on the use of concentrated solar energy to destroy hazardous organic wastes has demonstrated that a photothermal process (a high-temperature photochemical process) can destroy toxic organic materials far more efficiently and cleanly than conventional methods such as thermal oxidation.[1,2] Given the limited quantity of short-wavelength ultraviolet (UV) radiation in sunlight as compared to artificial sources,[3,4] it was felt that the results of the solar research only hinted at the potential for a photothermal treatment process. Therefore, the solar-based photothermal technology was generalized to include the use of nearly any source of thermal and W energy to make the concept of a Photothermal Detoxification Unit (PDU) available for Superfund site remediation. In this specific application, the PDU will serve as an off-gas cleanup device used in conjunction with various conventional soil and debris decontamination systems.

1.1 SYSTEM DESCRIPTION

The PDU is conceptually a relatively simple device that can be included as a new unit operation on existing treatment technologies requiring little or no change in the overall design of these systems. Specifically, the PDU could conceivably be designed to be retrofitted to existing gas handling systems with the subsequent elimination of activated carbon filters or other treatment devices such as condensers and separators. This eliminates the capital and operating

costs of this equipme nt and the transport and disposal of the collected wastes. Indeed, it is possible that the inclusion of a PDU in the design of a treatment system may result in significant savings by eliminating storage transportation, and treatment costs.

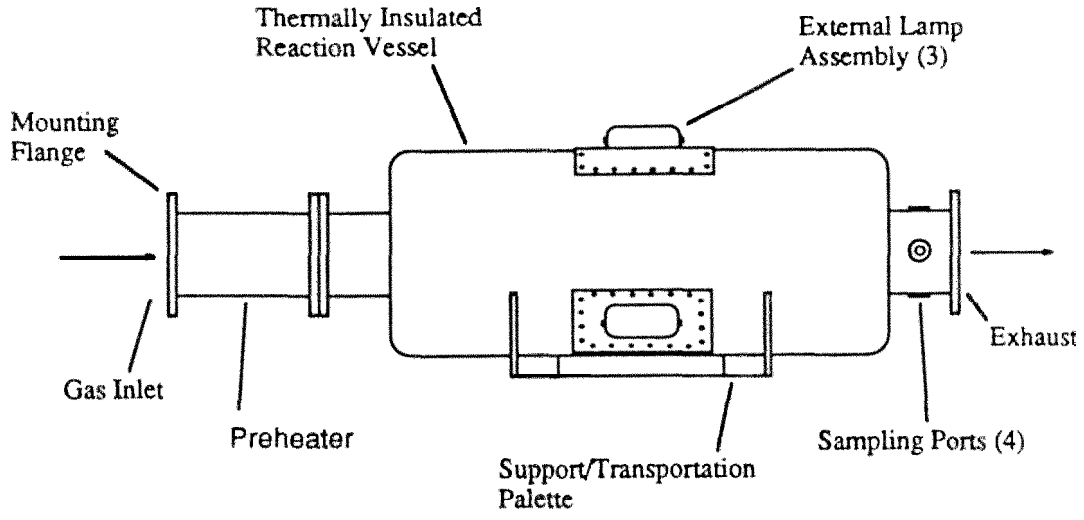

Figure 1.1. Conceptual schematic of a prototype Photothermal Detoxification Unit (PDU) showing the basic elements of the system including the reactor vessel and illumination system.

The basic concept of the PDU is fairly simple; a flowing gas stream is heated to a relatively high temperatur (>200°C) and exposed to intense UV radiation for a duration long enough to destroy the hazardous organic components. While the exact configuration of the PDU may take many forms depending on the specific application of a given unit, a general schematic of a conceptual prototype unit is shown in Figure 1.1. In this Figure, the PDU is shown as a thermally insulated, cylindrical vessel with high intensity UV lamps mounted around the perimeter so that the interior of the reactor can be evenly illuminated. Regardless of the final form of the PDU, all designs share the same central concept; exposing a flowing gas-phase stream to a relatively high temperature and intense UV radiation long enough to achieve an acceptably complete mineralization (i.e., decomposition to mineral products of complete conversion such as water, carbon dioxide, hydrogen chloride, etc.) of the hazardous organic components. It is the problem of determining the necessary conditions of time, temperature, and

radiant intensity as well as the optimization of these parameters that present a unique design challenge.

1.2 THEORY OF PHOTOTHERMAL DETOXIFICATION

Various photophysical and photochemical processes that may take place in a photochemical reactor operating at a relatively high temperature can be described by the energy versus reaction coordinate diagram presented in Figure 1.2. This figure illustrates the potential energy surfaces for the thermochemical and photochemical reaction pathways available in this

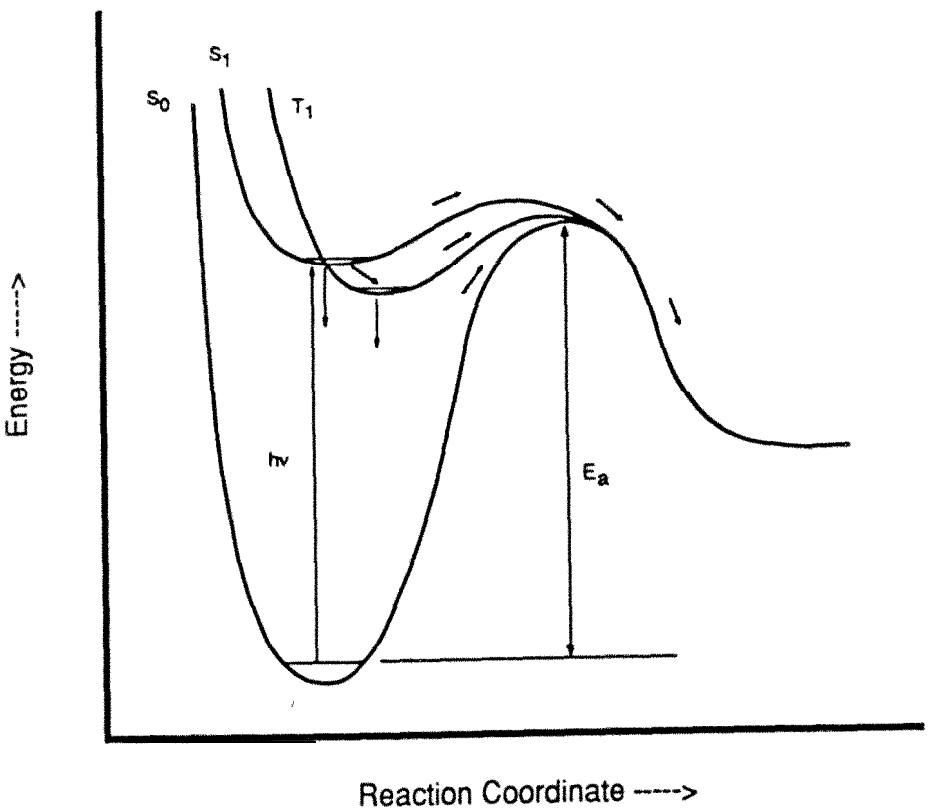

Figure 1.2. General energy versus reaction coordinated diagram illustrating the relative energy requirements for thermal (curve S_0) and photothermal (curves S_1 and T_1) decomposition processes.

In Figure 1.2 the hazardous organic molecules present in a process stream are considered to be initially near the lowest vibrational energy state of the ground electronic state (i.e., near the

bottom of curve S_0 in Figure 1.2). The combustion literature demonstrates that molecules on the ground state surface require approximately 30-100 kcal/mol of thermal energy to initiate oxidation reactions.[5] It is this relatively high activation energy barrier that makes it necessary for purely thermal processors (i.e., incinerators) to operate at such high temperatures, often in excess of 1,000°C. In the conventional thermal treatment of hazardous wastes there is little that can be done to improve the efficiency of the fundamental thermal process. Specifically, exposure time, temperature, and excess air are the only process variables that can be readily changed in an effort to achieve more efficient destruction.

When the option of introducing intense UV radiation to the system is considered, we find that we are no longer restricted to ground state, thermal chemistry. If organic molecules are exposed to UV radiation of an appropriate wavelength, they can be promoted to electronically excited states as shown by the curve S_1. Molecules absorbing a photon of UV radiation store that energy by promoting an electron to a higher energy state. This new electronic configuration tends to weaken the molecular bonds, thereby reducing the energy required to induce chemical reactions. Hence smaller activation energy barriers to destructive reactions are the result (cf. Figure 1.2).

The excited state most readily accessible from the ground state is the lowest energy singlet state, labeled S_1 in Figure 1.2, in which the spin of the promoted electron is preserved. When using sunlight as the radiation source, which has a UV cutoff of about 300 nm, only S_1 is accessible in most hazardous waste molecules. Literature values suggest the activation energy from this state is typically on the order of 2-10 kcal/mol,[6] so molecules in S_1 should react far more rapidly than those in the parent ground state at a given temperature. Furthermore, if UV radiation sources are used which generate shorter wavelength UV photons, higher energy singlet states (S_2, S_3, etc.) may be reached. In these higher energy states, activation energy decreases still further, and the states may even be dissociative, requiring no additional thermal energy for reactions to proceed.

One consequence of the preservation of electron spin in excited singlet states is that the deactivation of the state through rapid processes, such as re-emission of the energy as

fluorescence, is readily allowed. Therefore, the lifetime of these states can be quite short, often on the order of nanoseconds. By necessity, then, only very fast reactions can occur from these states before they return to the ground state. However, the spin of the excited electron may change and the molecule converts to what is referred to as triplet state, shown as T_1 in Figure 1.2. Like their associated singlet states, the activation energies from triplet states is quite small, often less than 5 kcal/mol. However, unlike molecules in excited singlet states, molecules in excited triplet states relax through much slower processes, such as phosphorescence so there is far greater opportunity for reactions to occur from excited triplet states than excited singlet states, interestingly, one of the dominant promoters of conversion of a singlet to a triplet state is the presence of heteroatoms such as chlorine, bromine, sulfur, nitrogen, and oxygen.[6] Therefore, molecules that tend to be of environmental concern (chlorinated solvents, pesticides, PCBs, PCDDs, PCDFs, etc.) also have the tendency to reside in excited triplet states upon irradiation and should be particularly susceptible to photothermal destruction.

In addition to the radiative relaxation processes described above (fluorescence and phosphorescence) molecules in either excited singlet or triplet states can relax back to the ground state through radiationless paths These pathways may take several forms and depend upon the particular molecule involved. Consequently, the relative rate and efficiency of these processes cannot be generalized. However, the possibility that a molecule will absorb UV radiation and still remain refractory must be considered. The existence of these rapid radiationless processes further exacerbates the need far high-temperature to accelerate the photochemical reactions to the point that they successfully compete with deactivation.

1.3 EXPERIMENTAL DESIGN

The photothermal detoxification process described above and illustrated in Figure I.2 may also be described mathematically as; [I]

$$f_r = \exp[-(k_{gnd} + \phi_r k_{ab})t_r] \qquad (1.1)$$

where f_r is the fraction of reactant(s) remaining, k_{gnd} is the rate constant of ground state (purely thermal) oxidation (sec^{-1}), ϕ_r is the photochemical quantum yield (mol/Einstein), k_{ab} is the UV photon absorption rate constant (sec^{-1}), and t_r is the mean residence time in the reactor

(sec). Equation 1.1 represents the global plug flow reactor performance model for the photothermal detoxification process In order to use Equation 1.1 to predict the performance of a prototype PDU, and hence aid in the design of the prototype unit, we must have knowledge of typical values of k_{gnd}, ϕ_r, and k_{ab}. Therefore, the experimental portion of this project will concentrate on obtaining these values for selected example compounds.

It has been shown that the rate of thermal oxidation of many organic compounds can be adequately described by simple pseudo-first-order kinetic models.[5] Specifically,

$$f_r = \exp(- k_{gnd} t_r) \tag{1.2}$$

so,

$$k_{gnd} = \ln(1/f_r)/t_r \tag{1.3}$$

Therefore, k_{gnd} may be found by measuring the fraction remaining following a purely thermal exposure of known duration Furthermore, the temperature dependence of k_{gnd} usually follows the Arrhenius, thermal activation expression;

$$k_{gnd} = A\exp(-E_a/RT) \tag{1.4}$$

or,

$$\ln(k_{gnd}) = \ln(A) - E_a/RT \tag{1.5}$$

where A is the frequency factor (sec^{-1}), E_a is the molar activation energy (cal mol^{-1}), R is the universal gas constant (1.987 cal mol^{-1} $°K^{-1}$), and T is temperature (°K). Therefore, by measuring the reaction rate (Equation 1.3) at a minimum of two temperatures, E_a and A can be calculated from Equation 1.5. Once these values are known, k_{gnd} may be calculated at any temperature using Equation 1.4.

In a fashion similar to the measurement of the rate of purely thermal (i.e., ground state) oxidation, has been shown that the photochemical quantum yield may be found from; [1]

$$\phi_r = \ln[f_r(0)/f_r(I_0)]/k_{ab}t_r \tag{1.6}$$

where $f_r(0)$ is the fraction remaining following a purely thermal exposure, fr(Io) is the fraction remaining following an identical exposure but with the reactor being illuminated with radiant intensity I_0 (W cm^{-2}). The rate coefficient of UV photon absorption, k_{ab}, may be calculated as;

$$k_{ab} = 1.92X\,10^{-5}\Sigma\varepsilon_{\lambda i}\lambda_i I_{0\lambda i} \qquad (1.7)$$

where $\varepsilon_{\lambda i}$ is the molar extinction coefficient (L $mol^{-1}cm^{-1}$) of the waste at wavelength λ_i (nm), and $I_{0\lambda i}$ is the radiant intensity (W cm^{-2}) between λ_{i-1} and λ_i. The summation is carried over the wavelength region of overlap between the absorption spectrum of the waste and the emission spectrum of the illumination source.

Reviewing Equations 1.1 through 1.7 shows that the important experimental values are temperature, time, radiant intensity, spectral distribution, molar extinction, and fraction remaining. It should also be noted that these models were developed for use in oxidizing systems (though not necessarily limited to oxidation) so initial concentrations must be such that excess air is available for complete oxidation. Therefore, the overall experimental plan is to measure the molar extinction spectra (the molar extinction as a function of wavelength) of individual selected organic compounds and measure the fraction remaining following carefully controlled laboratory experiments, and then use this data to obtain the fundamental parameters of E_a, A, k_{ab}, and ϕ_r. Once this information is available for several example compounds, the Performance of a pilot scale PDU may be estimated thereby providing guidance on the system specifications.

1.4 LABORATORY SYSTEMS

To conduct the experiments required to investigate high temperature photothermal destruction of hazardous organic wastes, two dedicated instrumentation systems have been constructed. Shown in Figures 1.3 and 1.4, respectively, these are the High-Temperature Absorption Spectrophotometer (HTAS), and the Laboratory Scale-Photothermal Detoxification Unit (LS-PDU). With these systems the most important aspects of photothermal destruction can be studied under controlled, laboratory conditions. Specifically, the HTAS is used to directly measure how strongly molecules absorb light by taking high-temperature, gas-phase absorption spectra, and the LS-PDU is used for thermal and photothermal studies using various radiation

sources such as simulated solar radiation, xenon, xenon/mercury, and mercury arc lamps, and lasers.

1.4.1 **The High-Temperature Absorption Spectrophotometer**

The HTAS, shown in Figure 1.3, is a custom built, single-beam spectrophotometer capable of operating at temperatures as high as 1,000°C. Since the organic molecules for which the HTAS was designed to study tend to decompose with prolonged exposures at elevated temperatures, the system is fitted with a flow cell rather than a static cell found in most commercial spectrophotometers. Furthermore, an inert carrier gas (i.e., nitrogen) is used for sample transport to eliminate the possibility of sample oxidation. By flowing a carrier gas laden with the sample of interest through the cell, the length of exposure to elevated temperatures can be kept short (typically 1 second) to limit destruction of the sample at very high temperatures.

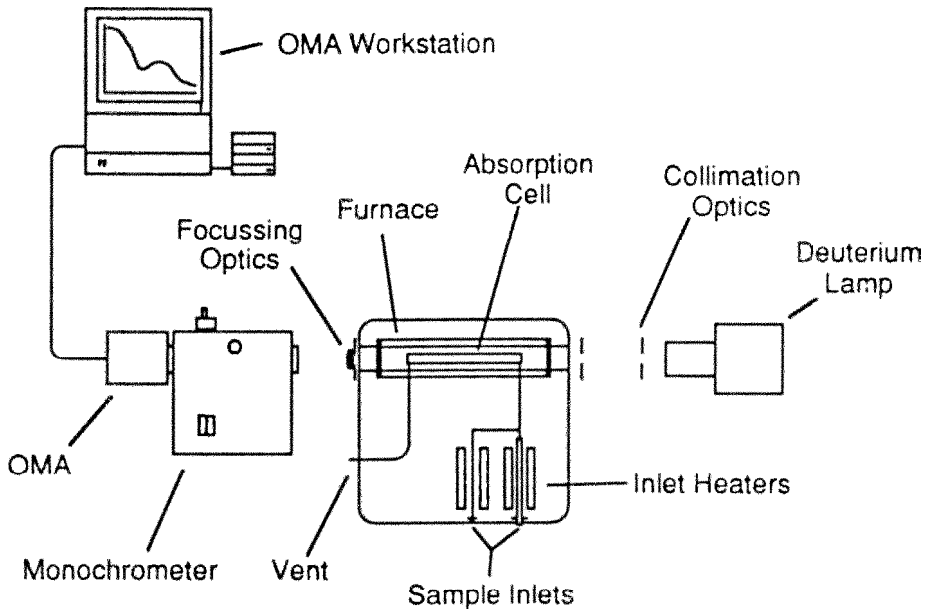

Figure 1.3. General schematic of the High Temperature Absorption Spectrophotometer (HTAS) showing the principal elements of this system.

Referring to Figure 1.3, the absorption cell assembly consists of a thermally insulated enclosure which houses a pair of sample inlet chambers and the absorption cell itself. The two

heated inlets include a low volume inlet specifically designed for gasses and liquids, and a high volume inlet which may be fitted with a variety of probe inserts for admitting gases, liquids, solids, and even mixed phase samples. During normal operation carrier gas is admitted to the system through both chambers to prevent back-diffusion into the unused channel. The flow from the two inlets join together into a single transfer line which is fused to the sidewall of the absorption cell, The cell is in the form of a cylinder, 1.2 cm in diameter by 20 cm long, and is mounted along the centerline of a conduit which passes completely through the housing. Heat is provided by half-cylinder ceramic heaters which are closed at either end with flat quartz windows which prevent convection currents from passing through the heated zone. The exhaust from the cell exits the housing through a heated transfer line, then passes through a particulate filter, an activated carbon filter, and finally to a fume hood. For the sake of chemical inertness, structural integrity, and UV transparency, the entire flow system, from the inlets to the exhaust, is fabricated from fused quartz. The cell is illuminated with collimated radiation from a deuterium lamp and the light leaving the cell is dispersed with a 0.25 m monochrometer and detected with a 512 channel optical multi-channel analyzer (OMA).

Operation of the HTAS is described in detail in Section 2. Briefly, molar extinction spectra were obtained by comparing reference (system blank) and sample spectra taking into account the cell length and the calculated molar concentration of sample in the cell.

1.4.2 The Laboratory Scale-Photothermal Detoxification Unit

The LS-PDU, shown in Figure 1.4, is a dedicated flow reactor system capable of obtaining thermal and photothermal decomposition data on a great variety of compounds. Structurally, the LS-PDU shares many features with the HTAS. For example, the LS-PDU includes dual sample inlets connected to a cylindrical vessel through a single sample transfer line. However, whereas the HTAS was designed to prevent reactions from taking place in the system, the LS-PDU was designed to conduct reactions under carefully defined conditions and analyze the products of those reactions. For this purpose the vessel connected to the inlet line is a small cylindrical reactor measuring 1.2 cm in diameter by 8.4 cm long. The exhaust from the reactor flows through a heated transfer line to a trapping system which collects all of the condensable materials from the flowing gas, This trap is a single tube-in-shell design similar

a laboratory condenser. The shell side is cooled with nitrogen gas which has in turn been cooled by a liquid nitrogen bath. This allows the trap to operate at temperatures as low as -180°C, though -160°C is routinely used. During the condensate collection phase of operation the exhaust from the trap is vented to a fume hood. In preparation to analyze the collected condensate, this vent is closed which directs the flow of gas to an inline analytical system consisting of a programmed temperature, capillary column gas chromatograph (GC) fitted with dual columns and an inlet splitter. One of the columns is connected to a scanning quadrapole mass spectrometer (MS), the other to a hydrogen flame ionization detector (FID). The LS-PDU may be used with nearly any UV radiation source and it is currently configured with a pulsed dye laser, solar simulator, and a high pressure xenon arc lamp.

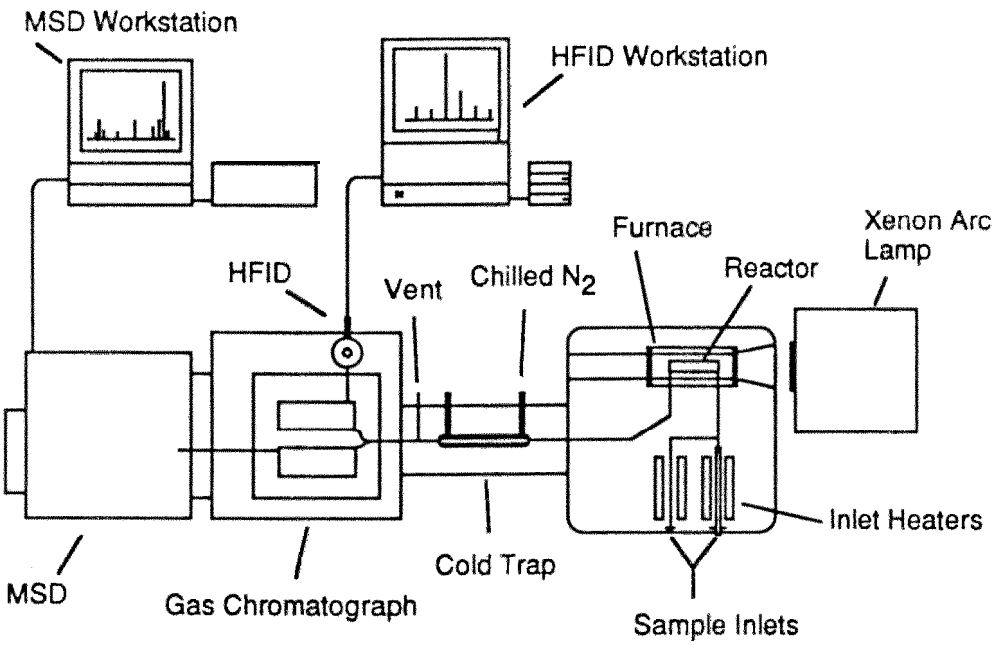

Figure 1.4. General schematic of the Laboratory Scale-Photothermal Detoxification Unit (LS-PDU) showing the principal elements of this system.

The operation of the LS-PDU is described in detail in Section 2. Briefly, the fraction remaining (the fraction of organic feed surviving the exposure in the reactor) is calculated by comparing integrated chromatographic peak areas measured under destructive conditions with values obtained from non-destructive tests (e.g., 300*C purely thermal). Quantitative organic

product yields were calculated by comparing the integrated peaks with those from known amounts of analytical standards. Qualitative organic product yields were calculated by comparison with the initial peak area of the parent species from non-destructive tests.

SECTION 2

EXPERIMENTAL PROCEDURES AND QUALITY ASSURANCE/QUALITY CONTROL

Before a detailed design could be considered for the prototype PDU it was necessary to obtain fundamental spectroscopic, thermochemical, and photochemical data on the types of compounds which would be considered candidate for photothermal detoxification. This data collection was one subject of this research project, and Section 6 presents the design for a prototype PDU.

As described below, the spectroscopic information was collected using the HTAS, while the LS-PDU was used to obtain the thermochemical and photochemical data. In addition to the general operating procedures, the quality assurance and quality control procedures are described.

2.1 HIGH TEMPERATURE ABSORPTION SPECTROPHOTOMETER

Referring to the general schematic of the HTAS as shown in Figure 1.3, operation of this system began with checking the gas supply pressure and making sure the supply valves were fully open. Next, the deuterium lamp (Oriel Model 6316), data system (Apple IIe), and computer interface (Tracor Northern Model 6100/6200) were switched on to allow them to stabilize while the absorption cell system was set up for a specific analysis. Once the deuterium lamp was started, the beam exiting the absorption cell assembly was inspected to ensure it was properly centered on the entrance slit of the monochrometer (Jarrel-Ash Model 82-410).

With the subsystems on and stabilizing, the temperature of the inlet chamber, absorption cell, and exhaust line were set as needed. These were typically already set at 100°C from previous operations in what is referred to as an idle mode. The temperature sensors (type K thermocouples) and readouts (dedicated thermocouple readers) were calibrated using a National Institute of Standards and Technology (NIST) traceable thermocouple calibrator (Omega Model CL23A). The temperature of the absorption cell was considered critical, so a calibration table

was assembled for the cell's temperature controller. The measurement of the cell temperature was repeated 5 times to ensure the precision (2% relative standard deviation) and accuracy (+/- 5°K absolute difference) was met. The inlet chamber and exhaust line temperatures were considered noncritical so the indicated temperature was used. The initial temperature was set to 100, 200, or 300°C depending on the boiling point of the sample,

Once the system temperatures were set, the flow rate of gas through the absorption cell was measured with a soap film flow meter (Alltech Model 4047). The operation and typical accuracy and precision of this device has been described in the literature.[7] The indicated volume of this device was calibrated by water displacement using volumetric flasks (0.05% accuracy) and found to be within the accuracy of the measurement, therefore the indicated volume was taken as the actual volume, The timer used to make the flow measurement (Fisher Model 14-649-7) was checked against time signals from WWV, the NIST broadcast time standard. The measurement of five replicates of 60 seconds each showed the timer to be accurate to within 0.005 sec. and precise to within 0.084% relative standard deviation (RSD), The flow through the test cell was measured 5 times to insure it was within the acceptance criteria of +/- 0.2 ml/sec and 5% RSD, A nominal flow rate of 12 ml/s at 20°C was set (with the actual value being measured and recorded) to give a nominal mean residence time in the cell of 1 second at 300°C.

Along with the system flow rates, the ambient pressure was recorded using a vacuum-over-mercury barometer (Sargernt-Welch Model S4565). The pressure in the absorption cell was taken as ambient.

With the flow of the carrier gas through the system set, the monochrometer wavelength selector was set to the desired value. The wavelength indicator was calibrated using a mercury vapor lamp and was found to be within the required acceptance criteria of 5% relative standard deviation and +/- 1 nm absolute difference.

With clean carrier gas (i.e., dry nitrogen) flowing through the cell a reference spectrum was taken and stared on the data system's floppy disk. The test sample was then admitted to the system at a controlled rate using a syringe pump (Sage Instruments Model 341B). The samples used in this project were kept in a special storage area and restricted to use for this project. A

manifest accompanied each sample to record when samples were drawn from the stock, how much, and by whom. The purity of each sample as specified by the manufacturer is summarized in Table 2.1. The flow rate of sample into the system was determined by measuring the time required for the syringe plunger to admit a predetermined volume. This measurement was repeated 5 times to insure the acceptance criteria of 5% RSD and +/-1 ppm absolute difference in concentration was met. With sample flowing through the cell, a second spectrum is taken and stored on disk.

Table 2.1
Summary Of Sample Purity As Specified By The Suppliers

Name	Purity	Supplier
Benzene	99.9+%	Sigma-Aldrich
Carbon Tetrachloride	99.9+%	Sigma-Aldrich
Chloroform	99.9%	Sigma-Aldrich
o-Dichlorobenzene	99%	Sigma-Aldrich
Ethyl Benzene	99+%	Sigma-Aldrich
n-Hexane	99+%	Sigma-Aldrich
Monochlorobenzene	99.99%	Sigma-Aldrich
1,2,3,4-Tetrachlorodibenzo-p-dioxin	98+%	Ultra Scientific
Tetrachloroethylene	99.9+%	Sigma-Aldrich
Toluene	99.8%	Sigma-Aldrich
Trichloroethylene	99+%	Sigma-Aldrich
2,2,4-Trimethylpentane	99%	Sigma-Aldrich
m-Xylene	99+%	Sigma-Aldrich

From the reference spectrum, the sample spectrum, and the calculated concentration of sample in the cell, the molar extinction spectrum is determined by;

$$\varepsilon_\lambda = \log_{10}(I_{0\lambda}/I_\lambda)/(lC) \qquad (2.1)$$

where ε_λ is the molar extinction coefficient (L/mol-cm) at wavelength λ (nm), $I_{0\lambda}$ is the reference intensity at λ (detector counts), I_λ is the measured intensity with sample flowing

through the cell with a molar concentration of C (mol/L), and with a cell. path length of l(cm). The molar concentration of sample in the cell is calculated from the measured flow rates of sample and carrier gas (L/s), the measured molar flow rate of sample (mol/s), and the measured cell temperature (to correct for the temperature difference between the point of measurement and the ceil). The temperature of the flow meter was taken as ambient, a condition confirmed by direct measurement" The overall procedure was checked using a NIST UV absorption standard and procedure (Standard Reference Material 935a, potassium dichromate) and was found to be within the acceptance criteria of 5% relative standard deviation and +/-0.05 absorbance units,

The sequence described above was repeated for each wavelength region of interest and for each sample. A complete spectrum was assembled by combining the data from across the spectral region of interest,

2.2 LABORATORY SCALE-PHOTOTHERMAL DETOXIFICATION SYSTEM

Referring to the general schematic of the LS-PDU shown in Figure 1.4, operation of this system began with checking the gas supply pressure and making sure the supply valves were fully open, A nominally slow flow rate of dry nitrogen gas was set through the cold trap to make sure this component was dry before the nitrogen gas chiller was filled with liquid nitrogen coolant. Next, the GC/FID and GC/MS data systems were turned on and the GC/MS data system configured to autotune the quadrupole mass spectrometer. Normally, the LS-PDU was left pressurized with approximately 5 psig helium from previous runs in what is referred to as an idle mode. If this was not the case, the system was flushed with helium, the system vent closed, and the system pressure set to approximately 5 psig. With the LS-PDU pressurized with approximately 5 psig of helium an auto-tune was performed according to the manufacturer's specifications.

While the auto-tune procedure was executing, the ambient conditions (temperature and pressure) were recorded on a daily log and a stock sample for the day was prepared. This stock sample was prepared by injecting a predetermined volume of the liquid phase sample into a glass sampling vessel which had been cleaned, evacuated, and filled with air from the same

compressed air cylinder used for the LS-PDU reactor carrier gas. The internal volume of these gas sampling vessels had been previously measured by water displacement and recorded on each vessel. The sample injected into the glass vessel was allowed to evaporate resulting in a gas-phase sample of known concentration.

While the sample was evaporating in the sampling bulb, the temperature of the inlet chamber, exhaust line, and cold trap enclosure were set. These were typically initially set at 300°C from previous operations in an idle mode similar to that described for the HTAS. The temperature of the cold trap enclosure (the temperature controlled compartment which houses the cold trap) was nominally set at 350°C to prevent cold spots in the lines leading to and from the trap. The temperature sensors (type K thermocouples) and readouts (dedicated thermocouple readers) were calibrated using an NIST traceable thermocouple calibrator (Omega Model CL23A). The temperature of the reactor vessel was considered critical, so a calibration table was assembled to assist in setting the actual reactor temperature. Furthermore, the measurement of the reactor temperature was repeated 5 times to ensure the precision (2% RSD) and accuracy (+/- 5°K absolute difference) was met. The inlet chamber, exhaust line, and cold trap enclosure temperatures were considered noncritical so the indicated temperature was used. Since the LS-PDU could not be operated at a temperature of less that 300°C due to the heat input from the illumination system, the inlet, reactor, and exhaust line temperatures were set to this value. The cold trap enclosure temperature was set slightly warmer to approximately 350°C to promote rapid heating of the trap itself as described below.

At this point the results from the auto-tune procedure were available and the procedure complete. The system exhaust vent was opened to depressurize the system and the inlet gasses switched from helium to air. While the system was being purged with air the coolant reservoir was filled with liquid nitrogen and the cold trap cooled to approximately 20°C to condition the carrier gas for measuring the system flow rate.

With the system temperatures set, the flow rate of air through the reactor was set to give a mean residence time of 10 sec. The flow rate of gas through the system was measured at the system exhaust vent using a soap film flow meter (Alltech Model 4045). The indicated volume of this device was measured by water displacement using volumetric flasks (0.05% accuracy)

and found to be within the accuracy of the measurement, therefore the indicated volume was taken as the actual volume. The timer used to make the flow measurement was checked against time signals from WWV, the NIST broadcast time standard, and was found to be accurate to within 0.005 sec and precise to within 0.084% RSD. The flow through the test cell was measured 5 times to insure it was within the acceptance criteria of +/- 0.2 ml/s of the desired value and 5% RSD.

If the current test was a photothermal run, the xenon arc lamp (Spectral Energy Model SS-1000x) was ignited and the lamp current set to 40 amps. With a lamp current of 40 amps the lamp potential was nominally 24 Volts, giving an overall lamp energy of 960 Watts. The illumination system was allowed to stabilize for two minutes and the lamp current and voltage checked to ensure that they were at expected values and stable.

The coolant level in the cold trap reservoir was checked and refilled with liquid nitrogen, if necessary. The flow of nitrogen gas to the cold trap was then increased, reducing the temperature to below -160°C.

Once the cold trap temperature was stable (approximately 2 minutes) a predetermined volume of stock sample (typically 200 µl) was injected into the LS-PDU at a controlled rate using a syringe pump (Sage Instruments Model 341B). The flow rate of sample into the LS-PDU was determined by measuring the time required for the syringe plunger to admit a predetermined volume. This measurement was repeated 5 times to insure the acceptance criteria of 5% RSD and +/-1 ppm absolute difference in concentration was met. As the sample was being admitted to the reactor, the system conditions (temperatures, lamp current, lamp voltage, etc.) were monitored to ensure they were stable.

After all the sample had been introduced to the system the syringe was removed and a brief period of time allowed to pass (typically 2 minutes) to ensure all of the sample had passed through the reactor and cold trap. If the current test was a photothermal run the lamp was switched on at this time.

At this point the reactor phase of the run was complete and the analysis phase was ready to begin. Specifically, the system gases were switched from air to helium in preparation of

running the gas chromatograph. While the system purge was being conducted the GC/FID and GC/MS data systems are configured to perform the analysis. Furthermore, the GC/MS workstation was set to control the temperature pragram of the GC oven and the oven was cooled to its initial temperature. Once the GC oven was stable at it's initial temperature the system exhaust port was closed, the system pressurized to approximately 5 psig, the GC/FID and GC/MS data acquisition programs placed in acquire mode, and the cold trap coolant turned off, The cold trap would *then* rapidly heat to 350°C (approximately 3 minutes) releasing the collected products into the GC for analysis,

The analytical subsystem of the LS-PDU was a Hewlett-Packard Model 5890 GC main frame fitted with dual columns and detectors, and a heated split/splitless interface to the cold trap. The GC/FID channel was fitted with a 328 µm x 15 m fused silica column coated with a 0.25 µm dimethylpolysiloxane stationary phase (J&W Scientific DB-1). Similarly, the GC/MS channel was fitted with a 200 µm x 20 m fused silica column also coated with a 0.40 µm dimethylpolysiloxane stationary phase. Furthermore, the split/splitless interface was operated in a split mode using a 320 µm x 1 m split restrictor. The temperature program consisted of a 2 minute bold at -80°C (time zero was taken as the moment the coolant to the cold trap was switched off) followed by heating at 10°C/min to 0°C, then 15°C/min to 260°C. The temperature was held at 260°C for 5 minutes or until all solute peaks were observed on the GC/MS trace (which lagged, the GC/FID trace by about 3 minutes), which ever was longer. This combination of GC columns and temperature program was found to be suitable for all the organic compounds used in this program. The GC/MS channel used a Hewlett-Packard Model 5970A Mass Selective Detector (MSD) operating in a scanning mode. The mass range was scanned from 35 to 350 atomic mass units (AMU).

Quantitative results for parent compounds were recorded as fraction remaining by normalizing the integrated GC/FID peak areas with data obtained under non-destructive conditions (i.e., 300°C thermal exposures). Peaks were identified by relative ~tention time (GC/FID and GC/MS) and mass spectral identification (GC/MS). In the case of parent species identification was made using the GC/MS data system's mass spectral library. The identity of products were assigned by a combination of the mass spectral library identification followed by

confirmation using analytical standards. GC/FID response factors were determined by analyzing known quantities of standards. Typical GC/FID response factors are ***shown*** in Figure 2.1. These data, for trichloroethylene, illustrate that the LS-PDU was a very linear system with respect to the quantitative transport of material.

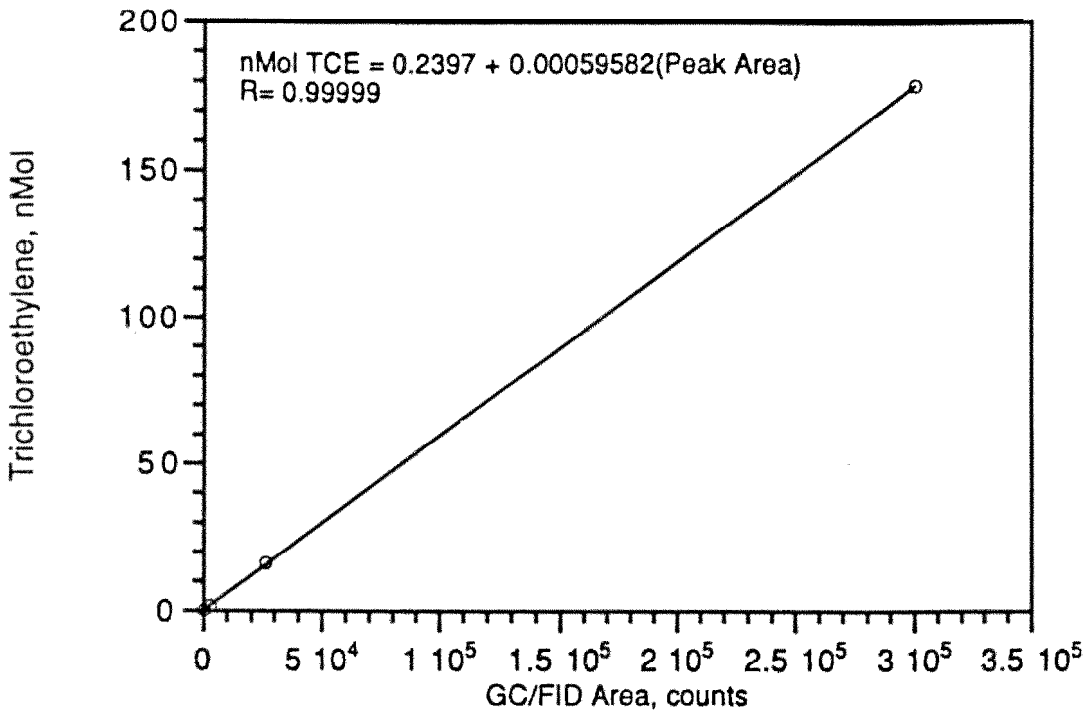

Figure 2.1. GC/FID calibration curve for trichloroethylene illustrating the linearity of the quantitative transport through the LS-PDU.

The overall procedure described above was conducted twice for each temperature and exposure condition (thermal and photothermal) to ensure that the acceptance criteria of 5% RSD and +/-0.01% absolute difference. The data for fraction remaining reported in the following sections represent the average value of two runs.

2.3 LS-PDU CARBON AND CHLORINE BALANCES

On the outset of this program it was anticipated that carbon and chlorine balances would be conducted on the LS-PDU. Unfortunately, difficulties were encountered which prevented conclusive results from being obtained from these efforts.

In the case of chlorine, it was assumed that the major products of HCl (melting point -114°C) and Cl_2 (melting point -101°C) would be quantitatively captured by the LS-PDU's cold trap and analyzed by the GC/MS channel (the GC/FID channel would not respond to inorganic gases). In practice this proved to be correct. Indeed HCl and Cl_2 were the sole chlorinated products observed in the GC/MS traces at high temperatures where the GC/FID traces showed all organic species had been destroyed. Unfortunately, attempts to obtain GC/MS response factors were unsuccessful, so the amount of HCl and Cl_2 produced could not be quantified. Specifically, it was observed that the sample handling equipment (e.g., syringe needles, sample bulbs, and septa) were rapidly and heavily corroded while attempting to prepare analytical standards of HCl and Cl_2 from bottled gasses and it was found that it was not possible to prepare a reliable calibrant for either gas.

The difficulties with the carbon balance was of a different nature. In this case it was not possible to use the LS-PDU's cold trapping system as it was not capable of quantitatively capturing CO (melting point -205°C). The trap was easily capable of capturing CO_2 (melting point -56°C) and indeed a large CO_2 peak was observed in all GC/MS analysis (the GC/FID channel would not respond to CO or CO_2). However, since the reaction atmosphere (dry air) contained CO_2 it was not possible to distinguish CO_2 produced as a product versus CO_2 from the atmosphere.

In an effort to overcome the problems associated with CO and CO_2 analysis an alternative technique was developed. Specifically, during tests in which analysis of CO and CO_2 were to be conducted the cold trap on the LS-PDU was maintained at 350°C instead of the customary -160°C. In this condition materials would flow through the trap and exit the system through the exhaust port. To collect these materials a 1 L Tedlar sample bag was attached to this port during the sample introduction phase of a run conducted for the sole purpose of obtaining

carbon balance data. Prior to each test the sample bag was evacuated and the sample collection time was carefully controlled to ensure consistency in the collected sample volume. After the sample collection was complete, the contents of the bag were analyzed for light gases using an isothermal, packed column gas chromatograph fitted with a thennoconductivity detector (TCD).

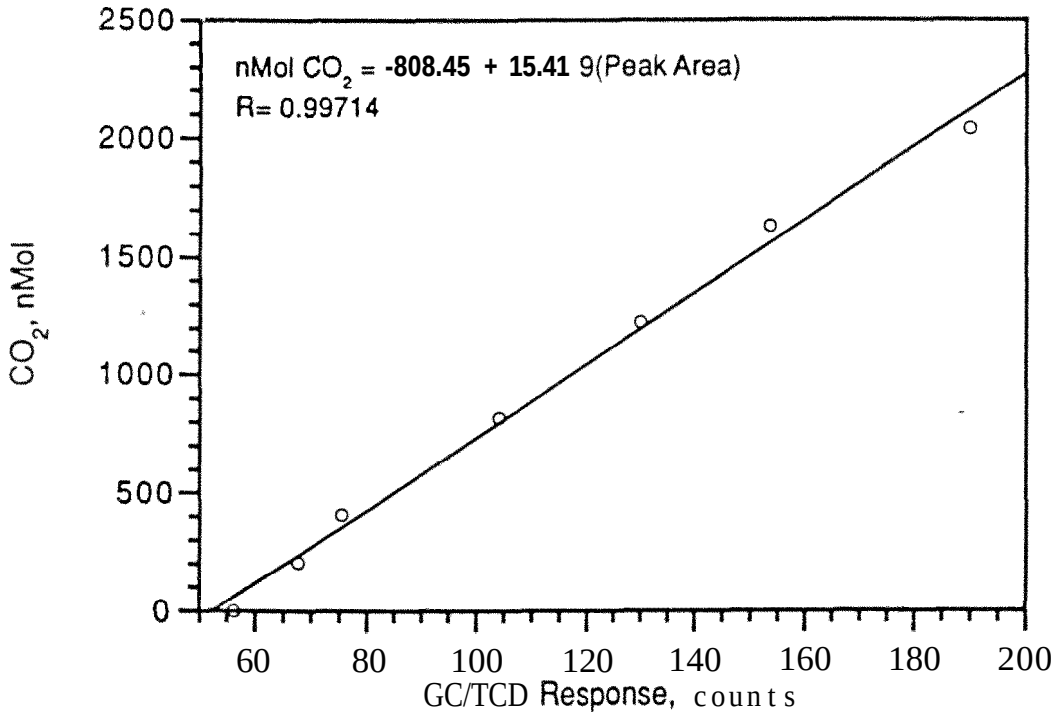

Figure 2.2. GC/TCD calibration curve for CO_2 using the discontinuous technique of collecting the LS-PDU effluent in a Tedlar sample bag for analysis with a stand-alone gas chromatograph.

Prior to conducting the carbon balance tests, the sample collection and GC/TCD system was calibrated by injecting known amounts of CO and CO_2 into the LS-PDU and collecting samples of the exhaust and analyzing them as described above. The results are summarized in Figures 2.2 and 2.3 for CO and CO_2, respectively (the volume of calibrant was measured under ambient conditions of 20°C and 745 mm Hg pressure). Note that the calibration curve for CO_2 has a negative intercept with the ordinate. This occurs because air is being used as the carrier gas in the LS-PDU which has approximately 330 ppm of CO_2. Therefore, CO_2 is present in the

Also, the GC/FID traces for light organic compounds (i.e. see 2-methyl-propane, melting point -160°C, in Figure 4.15) illustrate the ability of the LS-PDU to capture and analyze light organic compounds. These results suggest that no significant organic species remain unaccounted for in the effluent analysis.

Table 2.2
Carbon Balances From Thermal Exposures At 700°C For 10 sec In Air

Name	C_0[1]	CO[2]	CO_2[2]	%CO[3]	%CO_2[3]	%Total[4]
TCE	390	411	191	105	49.0	154
DCBz	10700	13200	2000	123	18.7	142
BTEX	435	397	154	91.3	35.4	127
TCDD	177	199	113	112	63.8	176

[1]Initial amount of organic carbon, units of 10^{-9} moles.
[2]Final amount of carbon observed as carbon monoxide or carbon dioxide, units of 10^{-9} moles.
[3]Mole percent carbon recovered as carbon monoxide or carbon dioxide.
[4]Total mole percent carbon recovered.

Table 2.3
Carbon Balances From Photothermal Exposures
With 17.6 W/cm^2 Xenon Arc Radiation At 700°C For 10 sec In Air

Name	C_0[1]	CO[2]	CO_2[2]	%CO[3]	%CO_2[3]	%Total[4]
TCE	390	392	195	101	50.0	151
DCBz	10700	14300	2100	134	19.6	154
BTEX	435	392	100	90	23.0	113
TCDD	177	197	77	111	43.5	154

[1]Initial amount of organic carbon, units of 10^{-9} moles.
[2]Final amount of carbon observed as carbon monoxide or carbon dioxide, units of 10^{-9} moles.
[3]Mole percent carbon recovered as carbon monoxide or carbon dioxide.
[4]Total mole percent carbon recovered.

Note that the carbon balance results do not suggest a bias in the LS-PDU data for organic species. The LS-PDU data for the conversion of parent species and the yield of organic products is conducted using a closed continuous process for which there is no opportunity for material loss. The likely source of error in the carbon balance tests is thought to be a combination of the discontinuous nature of the analysis and the small samples used. The problems with both the carbon and chlorine balances will be addressed in any future work by using a larger continuously fed reactor system which will permit the use of established methods for carbon and chlorine analysis.

2.4 LS-PDU ILLUMINATION SYSTEM

The radiant intensity impinging on the LS-PDU reactor vessel was measured by removing the illumination system from the instrument and characterizing the output from this unit. Specifically, a thermopile power meter (Scientech Model 362) was placed at an appropriate position with respect to the lamp to measure the radiation distribution impinging on the reactor vessel. The power meter was calibrated as per the manufacturer's specifications using an NIST traceable current source and voltage meter. Similarly, the spectral distribution of the illumination system was calibrated as per the manufacturer's procedure using a scanning monochrometer (Spex Model 1702/04) calibrated with a mercury vapor lamp. Following these measurements the illumination system was re-installed on the LS-PDU and aligned with the reactor.

SECTION 3

ABSORBANCE AS A FUNCTION OF TEMPERATURE

Reviewing the theoretical basis for the photothermal detoxification process discussed in Section 1 illustrates that knowledge of the absorption spectra of typical waste compounds is important to both the interpretation of data from laboratory scale reactors and to predicting the performance of large scale systems. For this reason spectroscopic data was obtained with the HTAS on a variety of test compounds ranging from simple hydrocarbons to complex PNAs. These data consisted primarily of the molar extinction spectrum measured at temperatures from 100 to 600°C. For the purposes of comparing the intensity of the overall UV absorption of the test compounds the relative oscillator strengths (the integrated molar extinction spectrum) were calculated at wavelengths greater than 230 nm (the onset of the LS-PDU xenon arc illumination system) and normalized by the value for benzene at 100°C.[8] These values are summarized in Table 3.1. Furthermore, the photon absorption rate constants for 18.1 W/cm2 of xenon arc radiation were calculated as summarized in Table 3.2. The emission spectrum for the LS-PDU's xenon arc source which was used in calculating the photon absorption rate constants is shown in Figure 3.1.

Table 3.1

Oscillator Strengths (λ>230 nm) Relative To Benzene At 100°C

Temp	Clfrm	Ctet	TCE	PCE	Bz	MCBz	DCBz	Tol	EthBz	Xyl	TCDD	89 Oct
100°C		0.0713	3.80		1.00							
200	0.0123	0.139	6.16	19.0	1.28	2.33	5.33	2.33	2.29	3.13		3.67
300	0.0314	0.246	8.47	24.1	1.46	2.89	7.26	2.59	2.57	3.62	366	4.35
400	0.0645	0.400	10.9	26.3	1.73	3.32	9.52	2.81	2.97	4.21	383	5.05
500	0.188	0.605	12.6	30.3	1.94	4.89	12.88	3.33	3.43	5.46	523	5.54
600		0.975	15.5	32.0	2.26	6.47	16.3	3.77	5.25	7.01		7.29

Table 3.2

Photon Absorption Rate Constants With 18.1 W/cm^2 Xenon Arc Radiation

Temp	Clfrm	Ctet	TCE	PCE	Bz	MCBz	DCBz	Tol	EthBz	Xylene	TCDD
100°C		9.20e-4	3.63e-2		3.81e-2						
200	1.24e-4	1.84e-3	7.72e-2	3.28e-1	5.16e-2	1.24e-1	2.62e-1	1.18e-1	1.14e-1	1.76e-1	
300	4.20e-4	3.71e-3	1.10e-1	5.12e-1	6.28e-2	1.49e-1	2.95e-1	1.36e-1	1.35e-1	2.04e-1	1.56e1
400	9.88e-4	7.68e-3	1.64e-1	6.00e-1	8.36e-2	1.64e-1	3.06e-1	1.51e-1	1.56e-1	2.25e-1	1.77e1
500	4.40e-3	1.23e-2	2.21e-1	8.12e-1	9.48e-2	2.14e-1	4.28e-1	1.77e-1	1.70e-1	2.68e-1	2.61e1
600		2.20e-2	3.02e-1	9.08e-1	1.16e-1	2.52e-1	5.00e-1	1.93e-1	2.53e-1	3.17e-1	

Key to abbreviations:

Clfrm	Chloroform
Ctet	Carbontetrachloride
TCE	Trichloroethylene
PCE	Tetrachloroethylene
Bz	Benzene
MCBz	Monochlorobenzene
DCBz	o-Dichlorobenzene
Tol	Toluene
EthBz	Ethyl Benzene
Xyl	m-Xylene
TCDD	1,2,3,4-Tetrachlorodibenzo-p-dioxin
89 Oct	89 Octane Gasoline

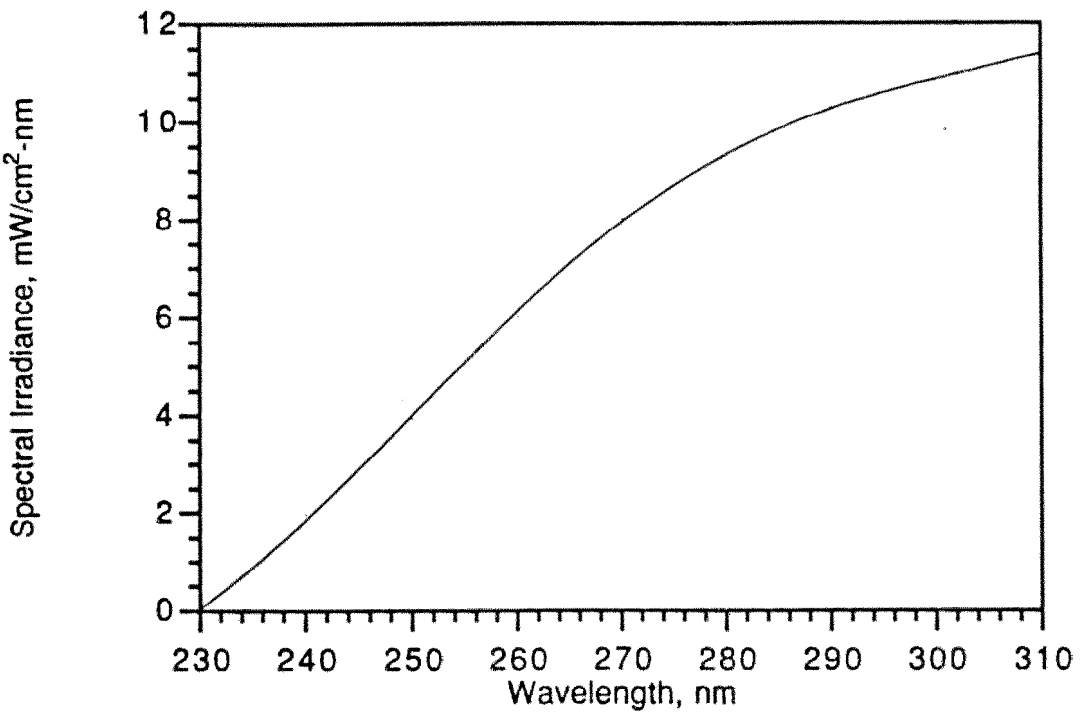

Figure 3.1. The spectral irradiance spectrum for the LS-PDU's xenon arc lamp showing the spectral distribution of radiation impinging on the reactor with an overall intensity of 18.1 W/cm^2.

3.1 HYDROCARBONS

The high temperature absorption spectra of n-hexane and iso-octane were taken from 100 to 600°C. These measurements showed that the test compounds were completely transparent at wavelengths between 190 and 320 nm. This suggests that a direct photothermal process using xenon or medium pressure mercury arc lamps may not be effective in treating aliphatic hydrocarbon wastes, However, these types of materials may prove treatable in the presence of other photosensitive wastes such as aromatic or halogenated hydrocarbons or through the use of photo-initiators such as hydrogen peroxide or ozone. Alternatively, other radiation sources (i.e. low pressure mercury, Xe_2 excimer, etc.) which emit mare far UV radiation (wavelengths shorter than 190 nm) than the xenon arc lamp used in the LS-PDU tests may prove effective.

3.2 CHLORINATED METHANES

The abso~tion spectrum of chloroform was obtained from 200 to 500°C (cf. Figure 3.2) and of carbon tetrachloride from 100 to 600°C (cf. Figure 3.3). The photon abso~tion rate data is summarized in Figure 3.4. The absorption spectra for these compounds show the increase in absorption intensity and red-shift with increasing temperature that is a common feature in this work, These dataillustrate that the chlorinated methanes are very weak absorbers of UV radiation. As summarized in Table 3.1, the relative oscillator strength far chloroform ranged from 0.0123 at 200°C to 0.188 at 500°C, and for carbon tetrachloride from 0.0713 at 100°C to 0,975 at 600°C. Similarly, the photon abso~tion rate constants for chloroform increased from 1.24×10^{-4} sec^{-1} at 200°C to 4.40×10^{-3} sec^{-1} at 500°C, and for carbon tetrachloride from 9.20×10^{-4} sec^{-1} at 100°C to 2.20×10^{-2} sec^{-1} at 600°C. Although the overall absorption is weak it is clear that the chlorine content had a significant impact on the strength of the absorption suggesting that larger chlorinated aliphatic compounds may be susceptible to the PDU process. Furthermore, the strength of the abso~tion band far both compounds increases with decreasing wavelength suggesting that these compounds may be effectively treated with radiation sources that reach further into the UV than the xenon arc source used here,

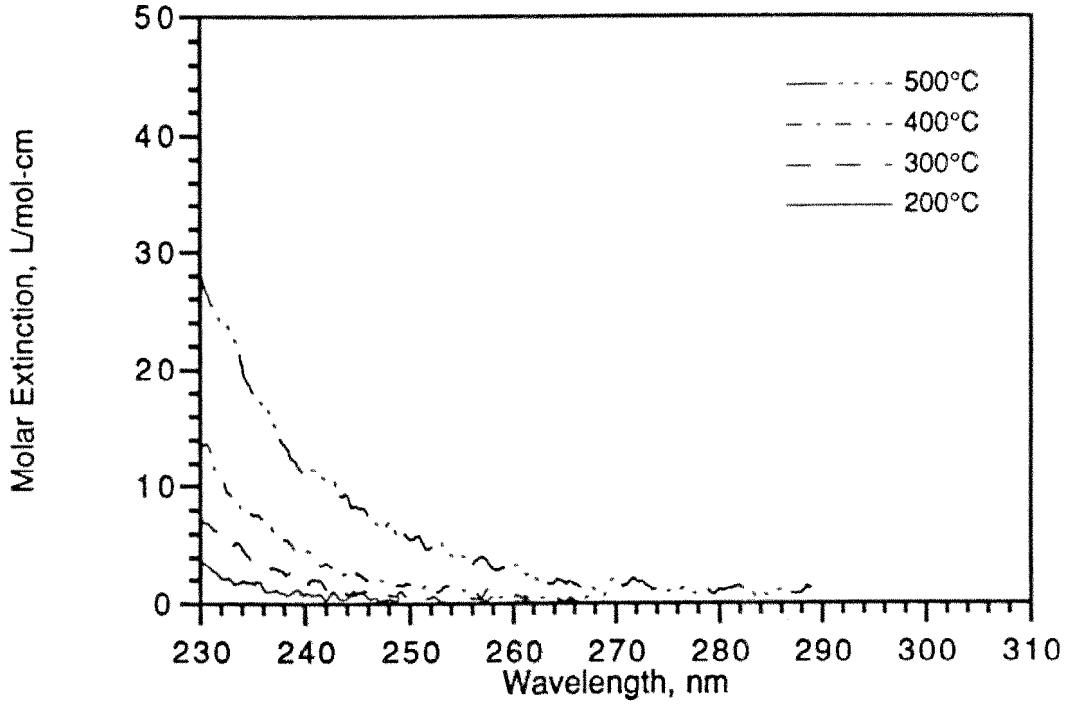

Figure 3.2. The gas-phase absorption spectra for chloroform at 200, 300, 400, and 500°C.

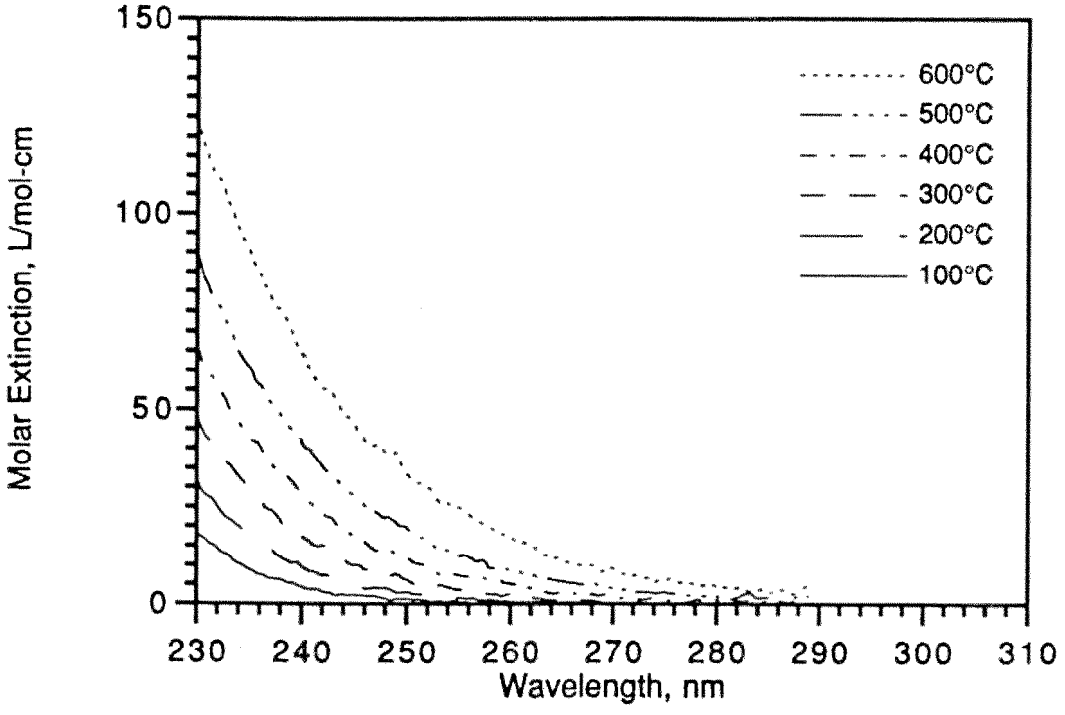

Figure 3.3. The gas-phase absorption spectra for carbon tetrachloride at 100, 200, 300, 400, 500, and 600°C.

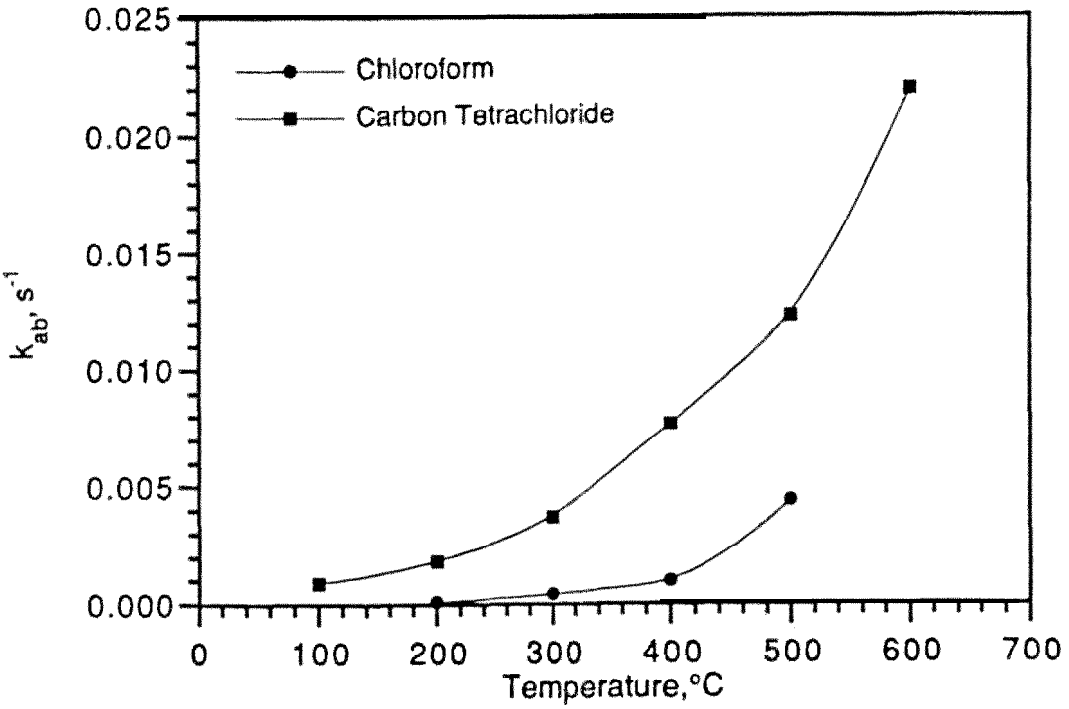

Figure 3.4. Summary of the photon absorption rate constants for chloroform and carbon tetrachloride showing the increase in the strength of absorption with temperature and chlorine substitution.

3.3 CHLORINATED ALKENES

The absorption spectra for trichloroethylene (100-600°C) and tetrachloroethylene (200-600°C) are summarized in Figures 3.5 and 3.6, respectively. The photon absorption rate constants are summarized in Figure 3.7. These data illustrate that the chloroalkenes are much more efficient absorbers of UV radiation than the chloromethanes. Indeed, the relative oscillator strengths given in Table 3.1 show that the chloroethenes are among the strongest UV absorbers studied in this program. Specifically, the relative oscillator strength for trichloroethylene (TCE) varied from 3.80 at 100°C to 15.5 at 600°C and from 19.0 at 200°C to 32.0 at 600°C for tetrachloroethylene (PCE). The photon absorption rate constant for TCE varied from 0.0363 sec^{-1} at 100°C to 0.302 sec^{-1} at 600°C and from 0.328 at 200°C to 0.908 at 600°C for PCE. Coupling of the non-

bonding electrons on the chlorine atoms with the $\pi^*<-\pi$ transition shifts the absorption towards the red as compared to hydrocarbons. This shifted predominantly $\pi^*<-\pi$ absorption renders these molecules susceptible to the PDU process as will be shown in Section 4. Unfortunately, the strength of the UV absorption rapidly fades at longer wavelengths suggesting that lamps which generate radiation deeper into the UV than standard xenon arc lamps may have a strong impact on the ability of the PDU to successfully treat these types of wastes.

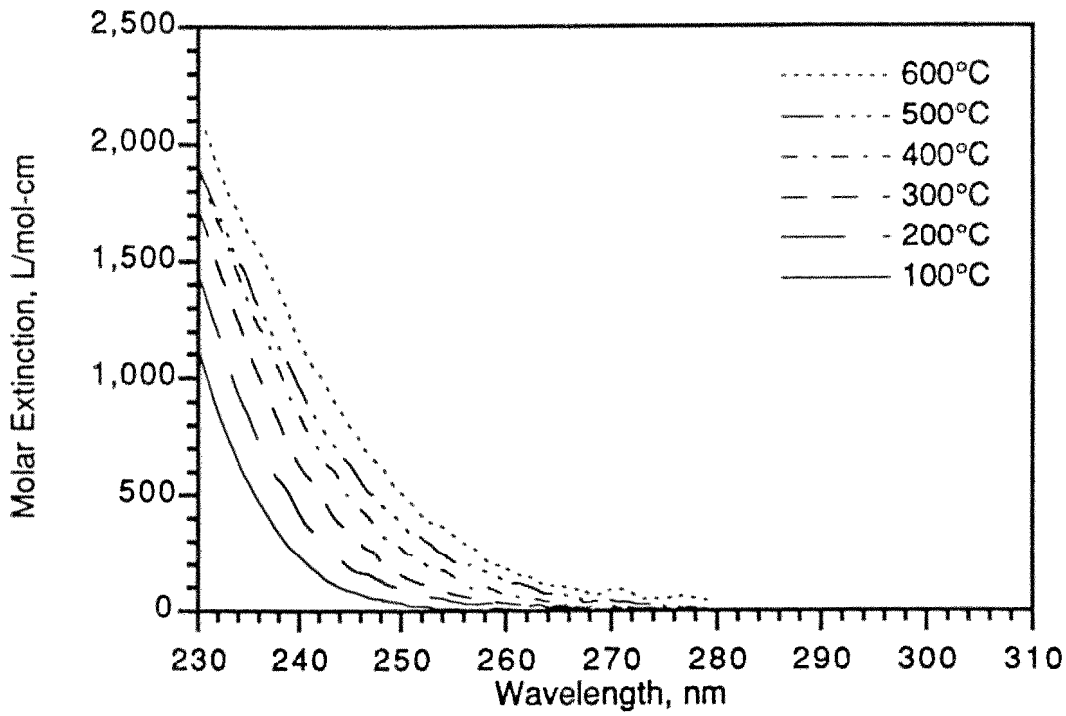

Figure 3.5. The gas-phase absorption spectra for trichloroethylene at 100, 200, 300, 400, 500, and 600°C.

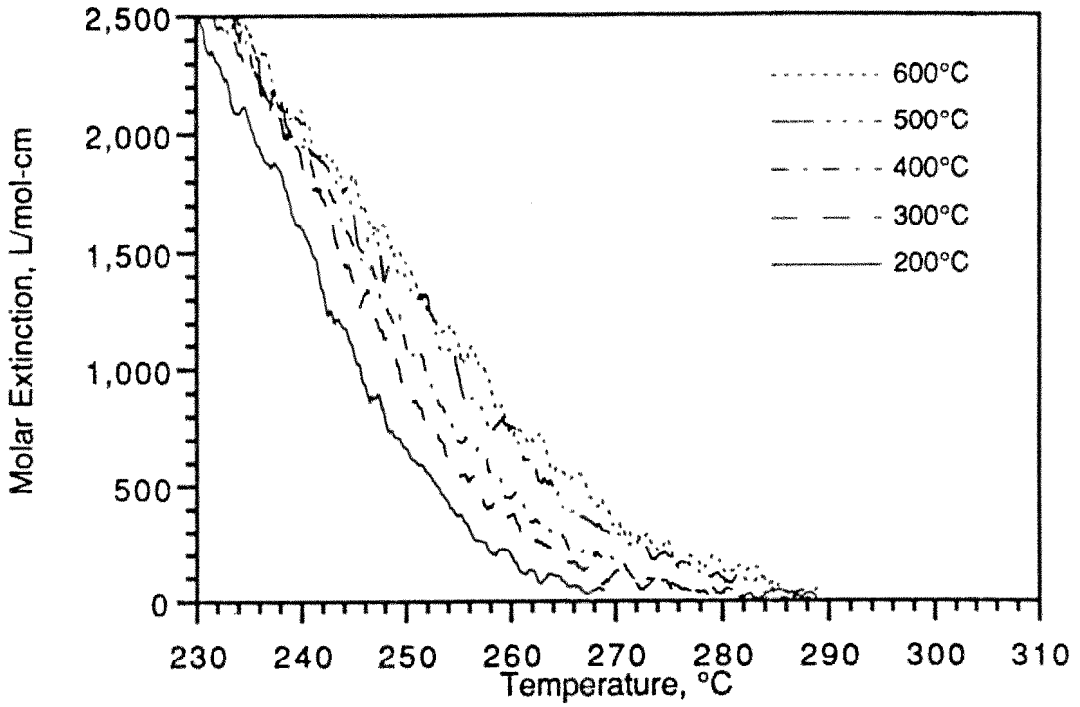

Figure 3.6. The gas-phase absorption spectra for tetrachloroethylene at 200, 300, 400, 500, and 600°C.

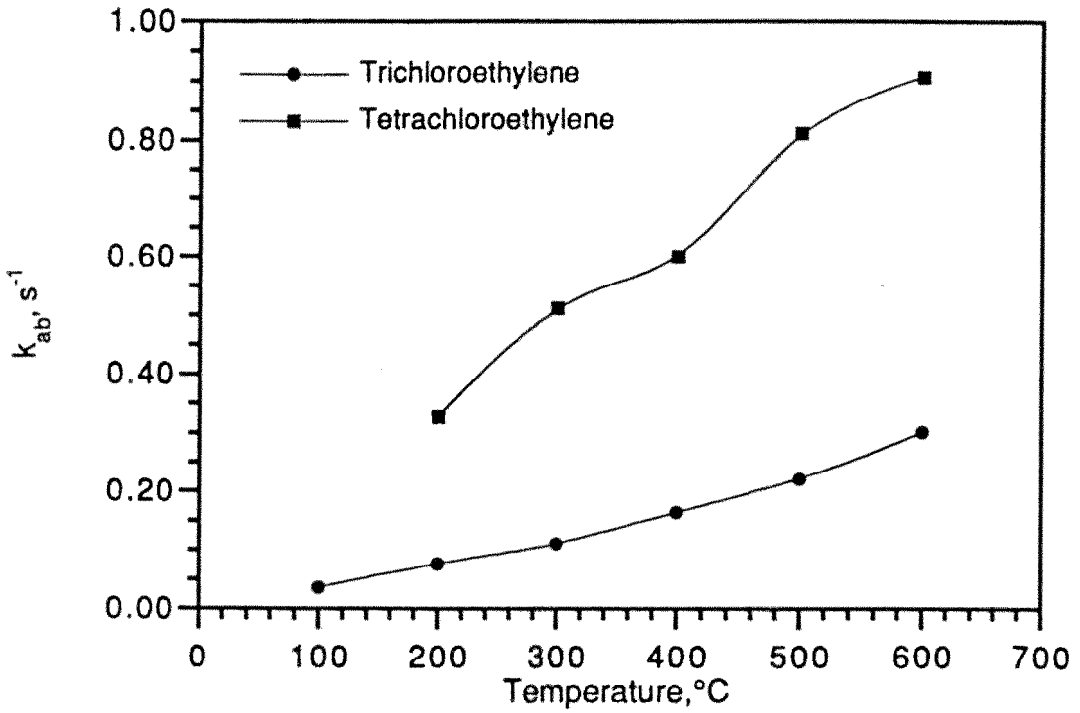

Figure 3.7. Summary of the photon absorption rate constants for trichloroethylene and tetrachloroethylene showing the increase in the strength of absorption with temperature and chlorine substitution.

3.4 AROMATICS AND ARENES

High temperature absorption spectra for benzene (100-600°C), toluene (200-600°C), ethyl benzene (200-600°C), and m-xylene (200-600°C) are summarized in Figures 3.8 through 3.11, respectively. The photon absorption rate constants are summarized in Figure 3.12. The relative oscillator strength (see Table 3.1) for benzene varied from 1.00 at 100°C (by definition) to 2.26 at 600°C, for toluene from 2.33 at 200°C to 3.77 at 600°C, for ethyl benzene from 2.29 at 200°C to 5.25 at 600°C, and for m-xylene from 3.13 at 200°C to 7.01 at 600°C. The photon absorption rate constant (see Table 3.2) for benzene varied from 0.0381 sec^{-1} at 100°C to 0.116 sec^{-1} at 600°C, for toluene from 0.118 sec^{-1} at 200°C to 0.193 sec^{-1} at 600°C, for ethyl benzene from 0.114 sec^{-1} at 200°C to 0.253 sec^{-1} at 600°C, and for m-xylene from 0.176 sec^{-1} at 200°C to 0.317 sec^{-1} at 600°C. These data suggest the alkane substitution had a significant impact on the strength of the UV absorption, though not as great as the effect from chlorine substitution. Furthermore, multiple substitution on the benzene ring had a larger impact on UV absorption than a single substitution of similar formula weight (e.g., ethyl benzene versus m-xylene) . In any event, these data suggest that the aromatic compounds as a class should be good candidates for PDU treatment.

3.5 CHLORINATED AROMATICS

High temperature absorption spectra for monochlorobenzene (MCBz, 100-600°C) and o-dichlorobenzene (DCBz, 100-600°C) are summarized in Figures 3.13 and 3.14, respectively. The photon absorption rate constants are shown in Figure 3.15. The photon absorption rate constants for benzene are included in Figure 3.15 for comparison. These data illustrate that the chlorinated aromatic compounds as a class are relatively strong absorbers of UV radiation, and that the strength of absorption rapidly increases with increasing chlorine content. Specifically, the relative oscillator strength (ca. Table 3.1) for MCBz varied from 2.33 at 200°C to 6.47 at 600°C, and for DCBz from 5.33 at 200°C to 16.3 at 600°C. Similarly, the photon absorption rate constant (ca. Table 3.2) for MCBz varied from 0.124 sec^{-1} at 200°C to 0.252 sec^{-1} at 600°C, and for DCBz from 0.262 sec^{-1} at 200°C to 0.500 sec^{-1} at 600°C. These data illustrate that chlorine

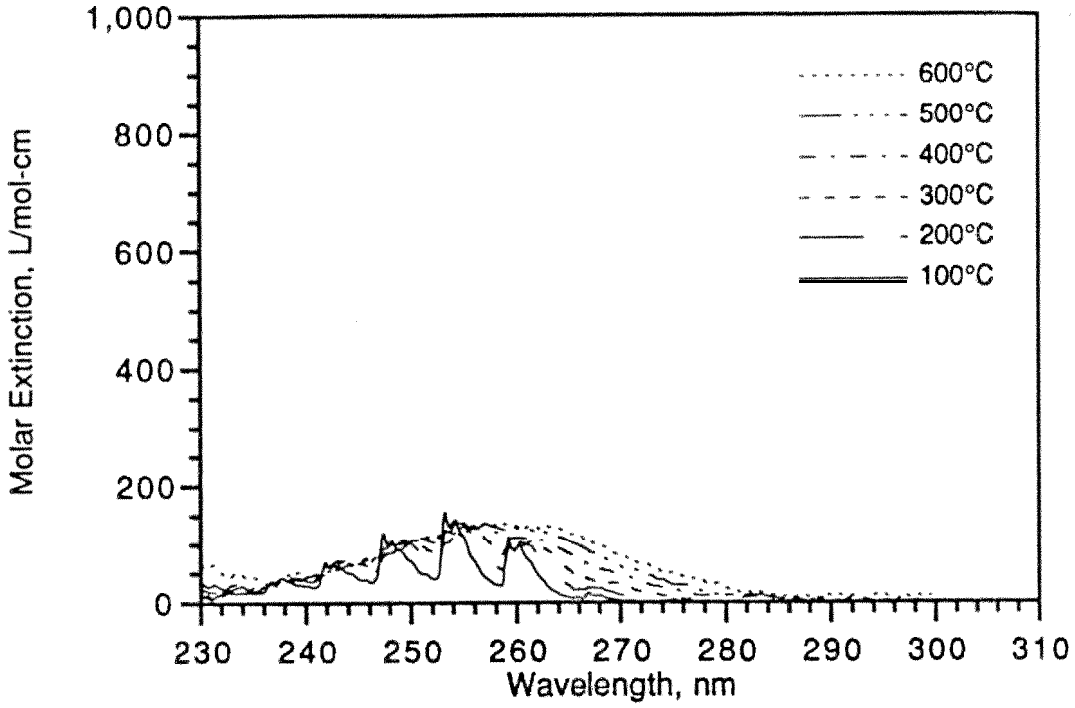

Figure 3.8. The gas-phase absorption spectra for benzene at 100, 200, 300, 400, 500, and 600°C.

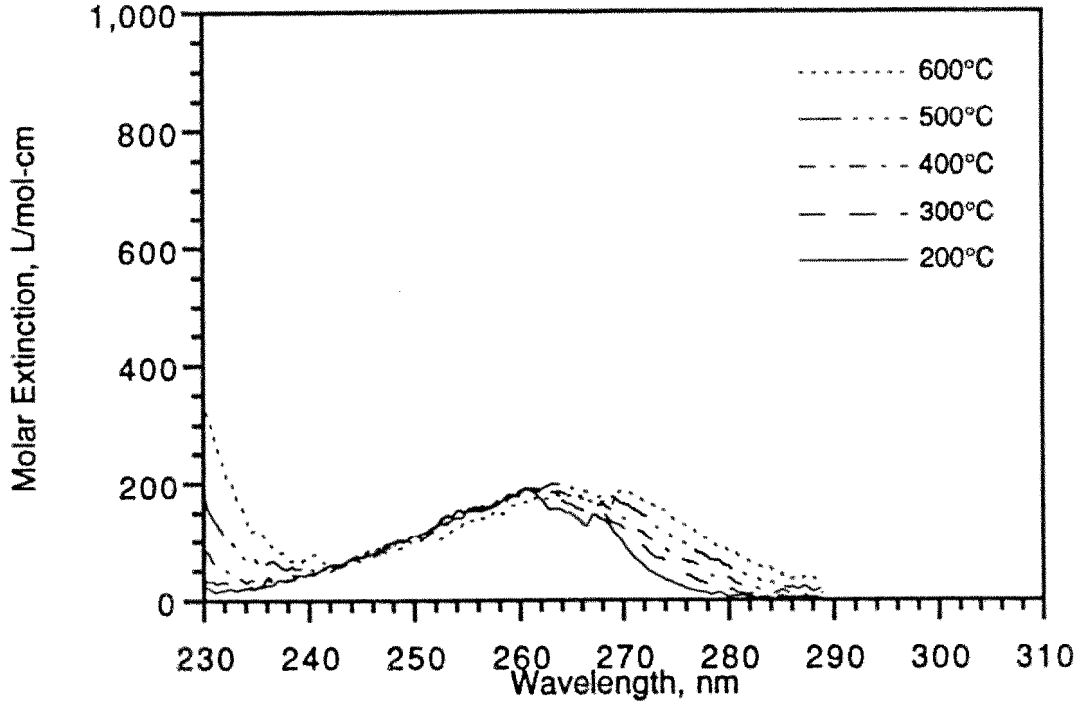

Figure 3.9. The gas-phase absorption spectra for toluene at 200, 300, 400, 500 and 600°C.

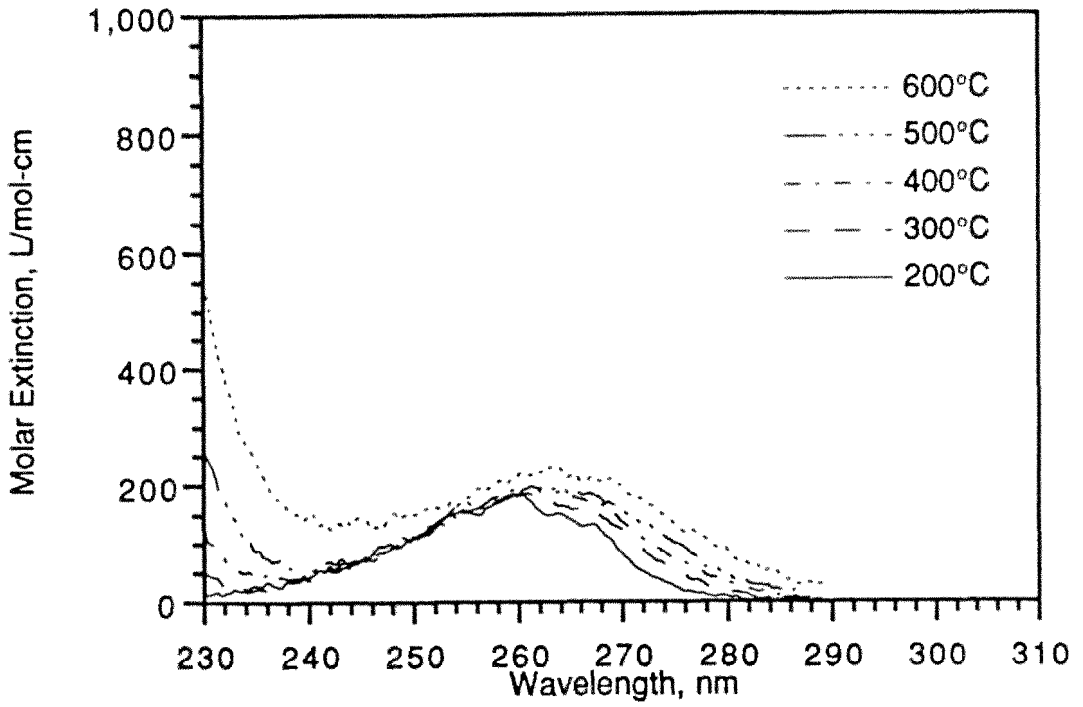

Figure 3.10. The gas-phase absorption spectra for ethyl benzene at 200, 300, 400, 500 and 600°C.

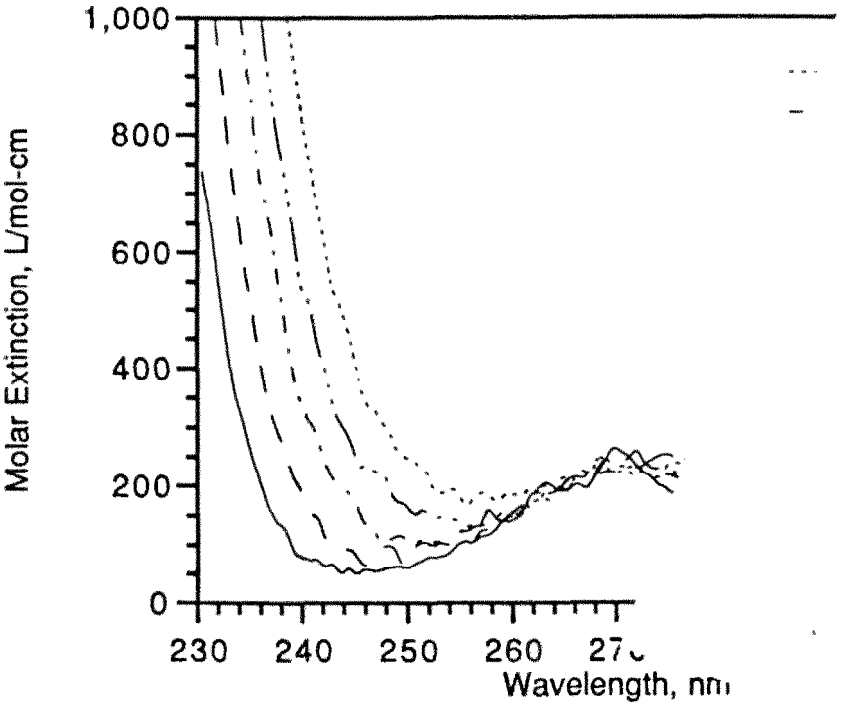

Figure 3.11. The gas-phase absorption spectra for m-xylene at 200, 300, 400, 500 and 600°C.

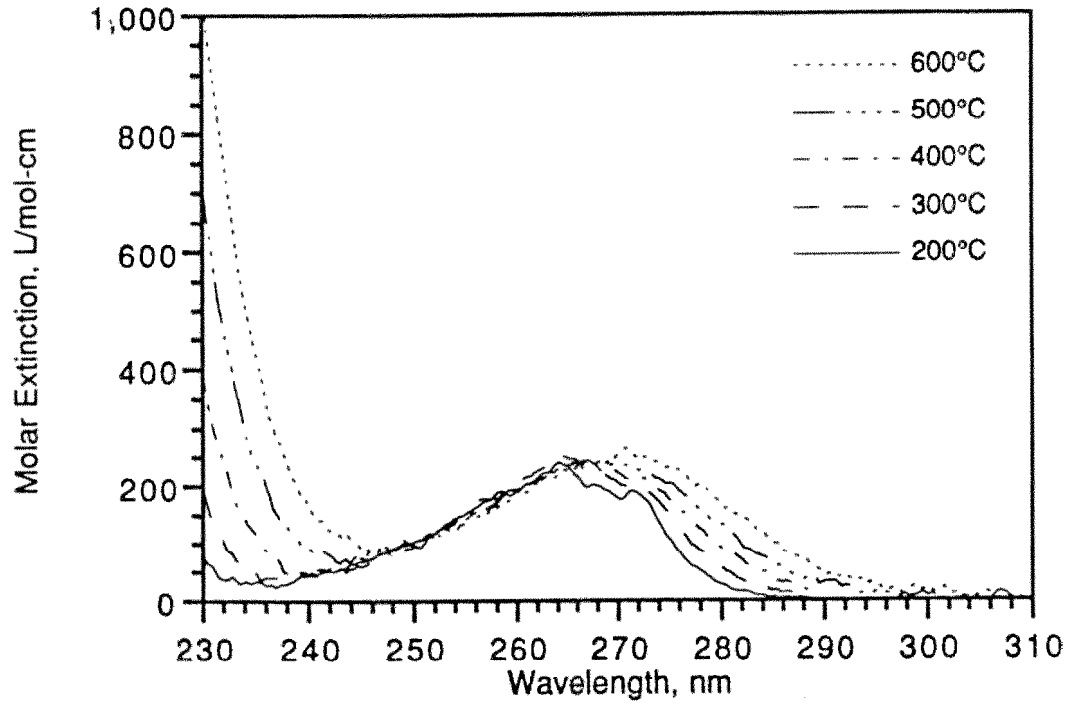

Figure 3.12. Summary of the photon absorption rate constants for benzene, toluene, ethyl benzene, and m-xylene showing the increase in the strength of absorption with temperature and the extent of alkane substitution.

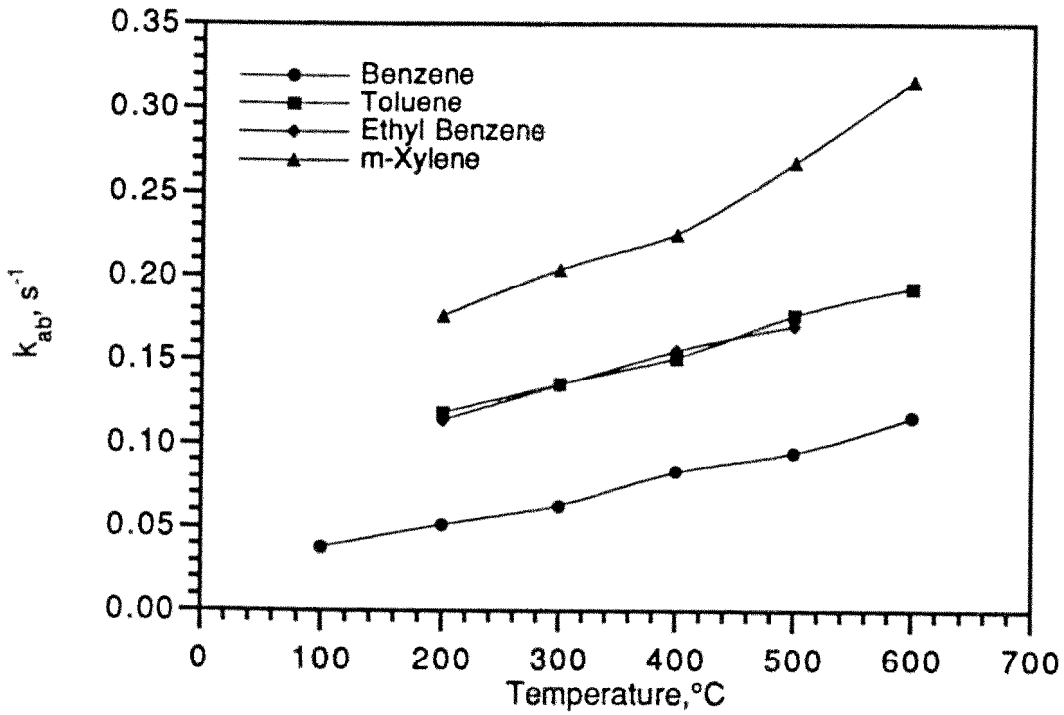

Figure 3.13. The gas-phase absorption spectra for monochlorobenzene at 200, 300, 400, 500 and 600°C.

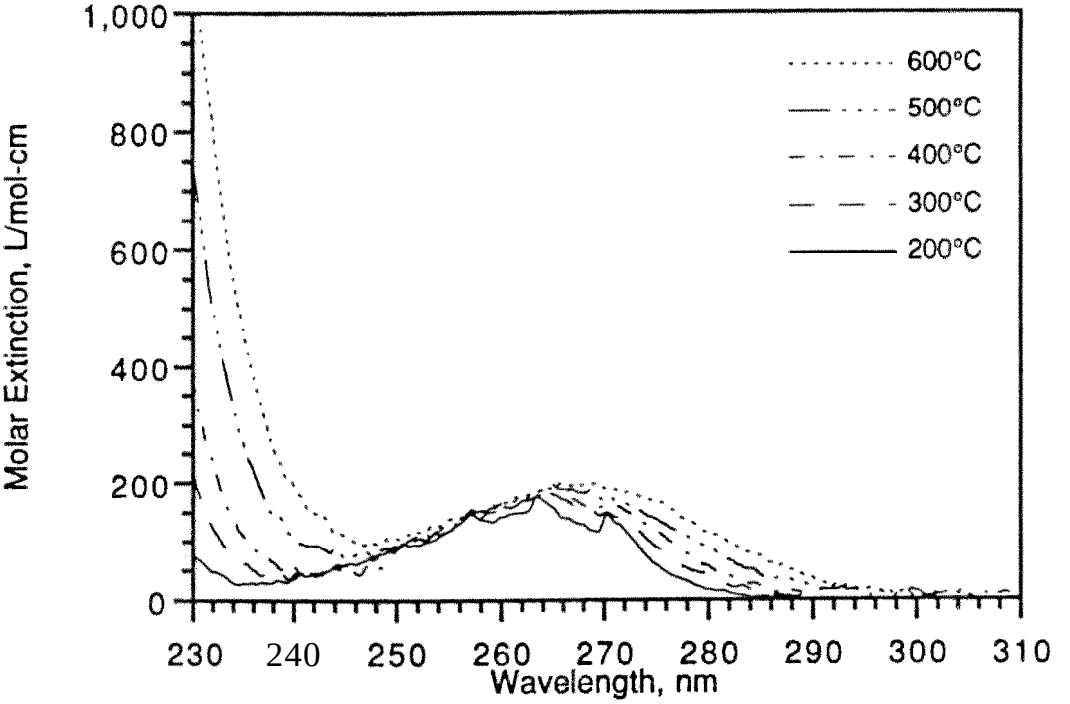

Figure 3.14. The gas-phase absorption spectra for o-dichlorobenzene at 200, 300, 400, 500 and 600°C.

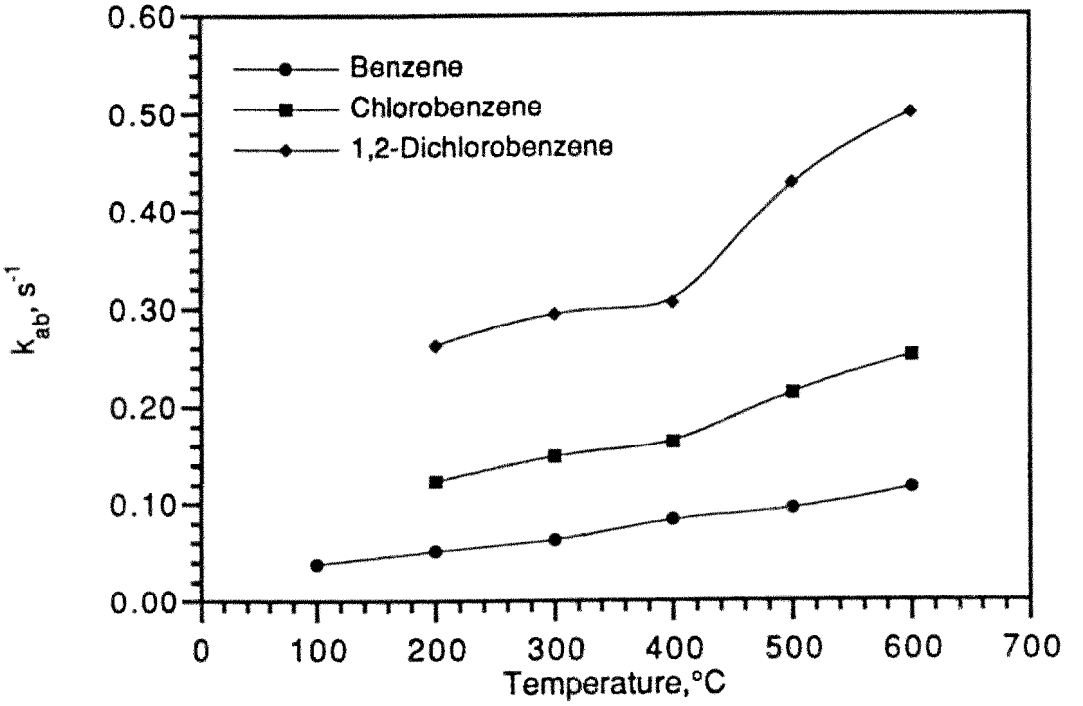

Figure 3.15. Summary of the photon absorption rate constants for monochlorobenzene and o-dichlorobenzene showing the increase in the strength of absorption with temperature and chlorine substitution.

substitution on the benzene ring shifted the onset of the intense S_2 absorption band (i.e., the strong absorption appearing at short wavelengths) to the red, a process further enhanced by increasing temperature. The intensity of this absorption at short wavelengths suggests once again that using illumination sources that provide radiation at wavelengths shorter than pravided by standard xenon arc lamps maysignificantly increase the potential performance of a PDU.

3.6 CHLORINATED DIBENZO-P-DIOXINS

The high temperature absorption spectra for 1,2,3,4-tetrachlorodibenzo-p-dioxin (TCDD) from 300 to 500°C are summarized in Figure 3.16 with the photon absorption rate constants shown in Figure 3.17, These Figures shows that TGDD is a verystrong absorber of UV radiation both in terms of absorption intensity and the breadth af the wavelength region of absorption, which reaches to relatively long wavelengths. The relative oscillator strength (ca. Table 3.1) varied from 366 at 300°C to 523 at 500°C while the photon absorption rate constant increased from 15.6 sec^{-1} at 300°C to 26.1sec^{-1} at 500°C. Comparing these values with those for the other test compounds shows that TCDD is the most intense absorber of UV radiation used in this program. The combination of the intense π^*<-n and π^*<-π transitions with the photochemical lability of carbon-chlorine bonds makes TCDD and related PNAs highly susceptible to the photothermal process.

3.7 GASOLINE

The absorption spectra for a commercial 89 octane unleaded gasoline (200-600°C) are shown in Figure 3.18. For the purposes of data reduction, this sample was assigned a mean molecular weight of 140 g/g-mol and a mean liquid phase density of 0.75 g/ml. Surprisingly, this sample proved to be a moderately strong absorber of UV radiation. As Figure 3.18 shows, this complex mixture exhibits an absorption spectrum with a strong aromatic character, though the transition between the S_1 and S_2 absorption bands is poorly defined compared to that of the spectra for other aromatic

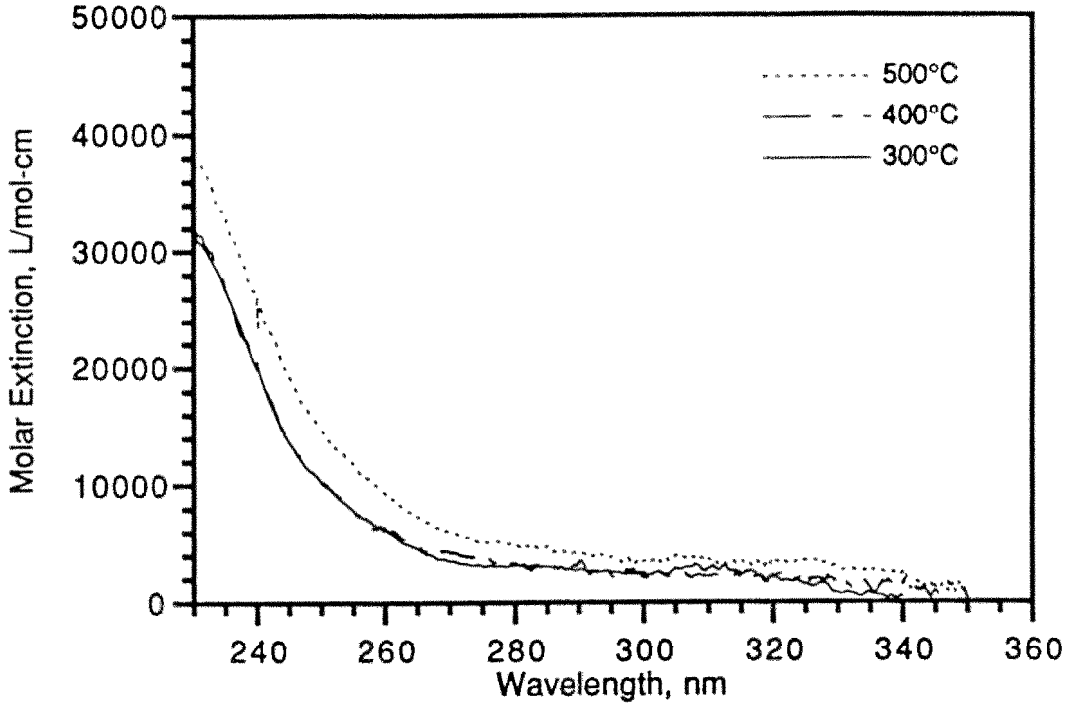

Figure 3.16. The gas-phase absorption spectra for 1,2,3,4-tetrachlorodibenzo-p-dioxin at 300, 400, and 500°C.

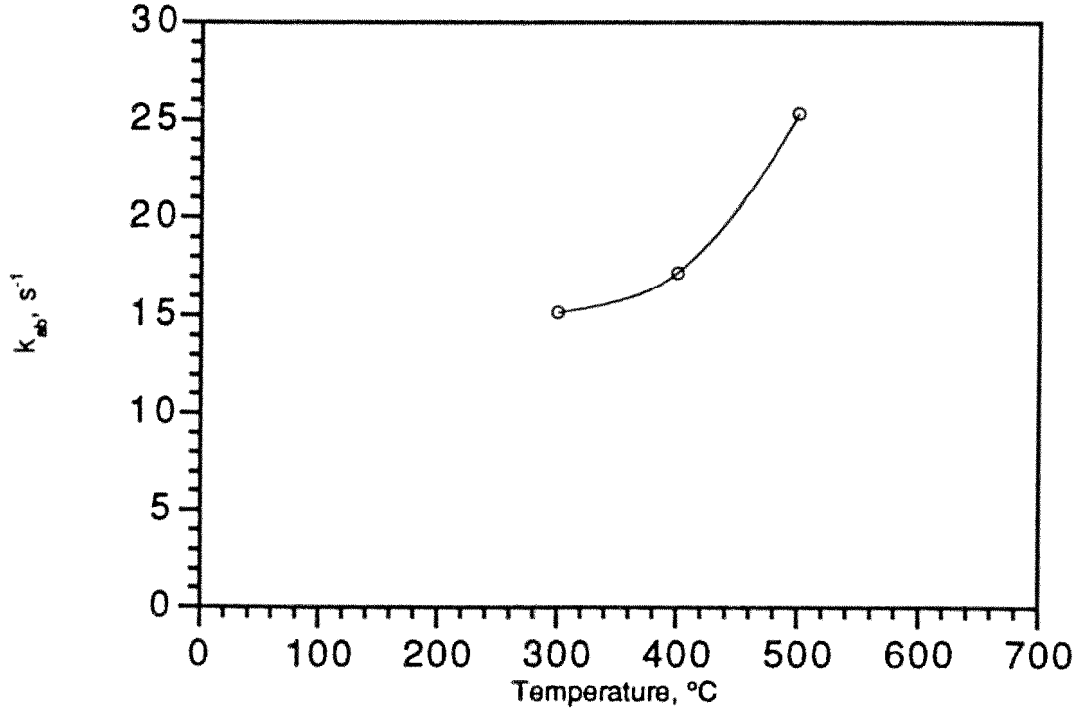

Figure 3.17. Summary of the photon absorption rate constants for 1,2,3,4-tetrachlorodibenzo-p-dioxin showing the increase in the strength of absorption with temperature.

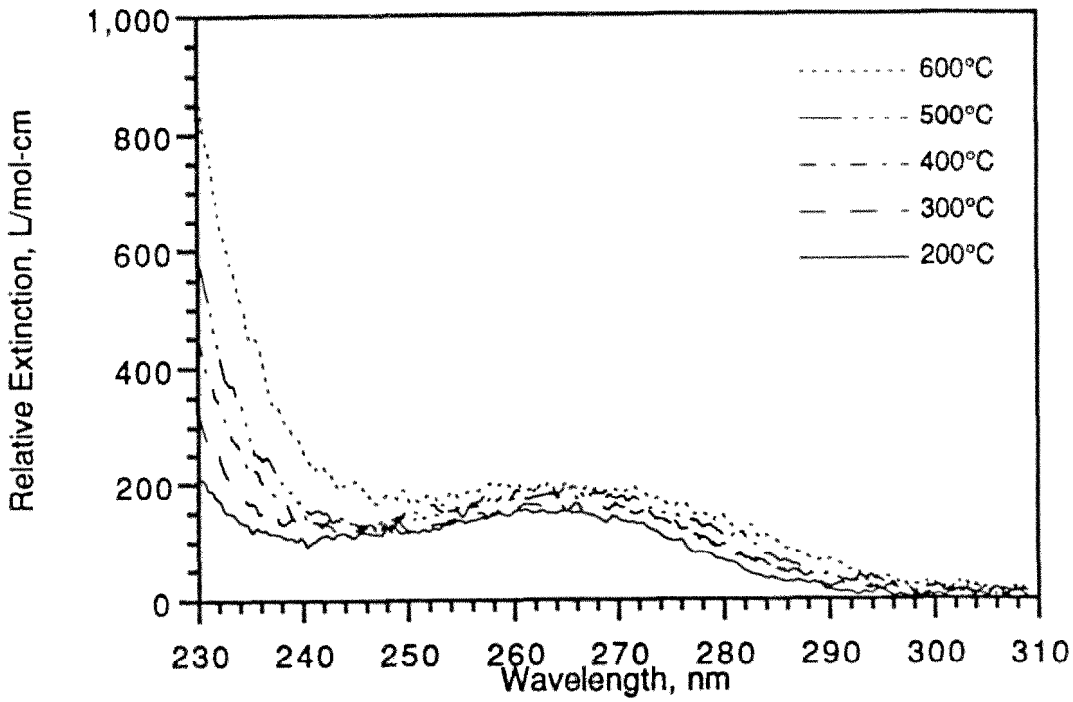

Figure 3.18. The gas-phase absorption spectra for gasoline using an assigned mean molecular weight of 140 g/g-mol and a liquid phase density of 0.75 g/ml at 200, 300, 400, 500, and 600°C.

compounds. The strength of absorption suggests that gasoline may be a candidate for PDU treatment.

3.8 SUMMARY

From the standpoint of absorption spectroscopy, several classes of compounds are suggested as good candidates for photothermal detoxification. Specifically, aromatic and arene compounds would generally be classified as good candidates based on their moderately strong absorption of UV radiation; chlorinated alkenes and aromatic compounds would be considered very good candidates; and, dioxins/furans and related PNAs may be very susceptible to the photothermal process. In contrast, systems composed exclusively of alkanes, even chlorinated alkanes, would likely pose a significant challenge to the photothermal process. However, it is possible that radiation sources with very short wavelength UV radiation (i.e., low-pressure mercury, Xe_2

excimer, etc.) may be able to address these materials. Finally, complex mixtures like gasoline may be considered treatable based on their spectroscopy, but the final degree of applicability may depend on which compounds in the mixture prove photo-active and how they interact with the other mixture components.

SECTION 4

LABORATORY-SCALE PHOTOTHERMAL DETOXIFICATION

The spectroscopic data discussed in Section 3 illustrated how the absorption of UV radiation of different classes of compounds behave as a function of temperature and provided the molar extinction information required as part of the PDU reactor performance model. In this Section the photothermal decomposition resulting from the absorption of UV radiation is discussed along with the thermal data needed to extract the fundamental kinetic and photochemical parameters needed to complete the reactor performance model.

Thermal and photothermal decomposition data has been obtained on six pure compounds and six mixtures of compounds with varying degrees of complexity. Specifically, data was obtained using the LS-PDU on chloroform, trichloroethylene (TCE), tetrachloroethylene(PCE), monochlorobenzene (MCBz), o-dichlorobenzene (DCBz), and 1,2,3,4-tetrachlorodibenzo-p-dioxin (TCDD). With respect to mixtures, tests were run with one formulation of benzene, toluene, ethyl benzene, and m-xylene (BTEX) and three variations of a mixture of TCE, DCBz, and water vapor. Tests were also run with gasoline and a trial mixture of benzene, hydrogen peroxide, and water vapor. The pure compounds were considered representative of chlorinated alkanes (chloroform) which weakly absorb ultraviolet radiation (UV), chlorinated alkenes (TCE, PCE) which absorb UV relatively well and represent a class of solvents commonly found in Super-fund sites, chlorinated aromatic compounds (MCBz, DCBz), and chlorinated dibenzo-p-dioxin compounds (TCDD) which are representative of the semi-volatile compounds which may be encountered in some Superfund remediation sites. The mixtures presented an opportunity to quickly assess the effectiveness of the photothermal process on several aromatics and arenes (BTEX), simulate the principal threats from an actual Superfund site (TCE/DCBz mixtures) for which data is available, and allow some very preliminary tests of a possible indirect photothermal process through the use of a photo-initiator (hydrogen peroxide). The overall

exposure conditions for each pure compound and mixture are summarized in Tables 4.1 and 4.2, respectively. The fraction remaining (where fr(n) is the fraction remaining with n W/cm2 radiation) for each compound and mixture is summarized in Tables 4.3 through 4.22. The photothermal quantum yields (the ratio of the rate of photochemical reaction to the rate of photon absorption) for the pure compounds are summarized in Table 4.23 and for the mixture components in Table 4.24. The pseudo first-order rate parameters for selected data sets are given in Table 4.25.

TABLE 4.1
Summary of LS-PDU Exposure Conditions[1] For
Samples Analyzed as Pure Compounds

Name	Initial Conc.[2]	Radiant Int.
Chloroform	2,650 ppm	17.6 W/cm^2
Trichloroethylene	157	18.1
Tetrachloroethylene	6.15	17.6
Monochlorobenzene	37.0	17.6
o-Dichlorobenzene	1,913	18.1
1,2,3,4-Tetrachlorodibenzo-p-dioxin	481	17.6

[1]All samples were run with a mean exposure time of 10 sec in dry air.
[2]Expressed at the initial conditions of 300°C and a mean atmospheric pressure of 745 torr.

4.1 ALKANES AND CHLORINATED ALKANES

It was anticipated that the most challenging class of wastes for the photothermal process would be those that either don't absorb UV radiation at all, or absorb it only weakly. Alkanes were considered examples of the former, and chlorinated alkanes examples of the later. For the purposes of this project chloroform and carbon tetrachloride were taken as example chlorinated alkanes and with hexane and iso-octane as example alkanes. High temperature absorption spectra (ca. Section 3) confirmed that the chloroalkanes were weak absorbers of the UV available in the LS-PDU, while the hydrocarbons were found to be non-absorbers.

TABLE 4.2
Summary of LS-PDU Exposure Conditions[1] For
Samples Analyzed as Mixtures

Name	Initial Conc.[2]	Radiant Int.
BTEX		
Benzene	11.4 ppm	17.6 W/cm^2
Toluene	9.62	17.6
Ethyl Benzene	8.32	17.6
m-Xylene	8.37	17.6
Gasoline[3]	15.4	17.6
TCE/DCBz/Water-1		
TCE	300	17.6
DCBz	5.19	17.6
Water	92.3	17.6
TCE/DCBz/Water-2		
TCE	5.29	17.6
DCBz	5.19	17.6
Water	92.3	17.6
TCE/DCBz/Water-3		
TCE	5.29	17.6
DCBz	5.19	17.6
Water	0	17.6
Benzene/Hydrogen peroxide		
Benzene (w/H_2O_2)	6.68	17.6
Hydrogen peroxide	14.4	17.6
Water	63.5	17.6
Benzene/Hydrogen peroxide-control		
Benzene (dry)	6.68	17.6
Hydrogen peroxide	0	17.6
Water	0	17.6

[1]All samples were run with a mean exposure time of 10 sec in dry air.
[2]Expressed at the initial conditions of 300°C and a mean atmospheric pressure of 745 torr.
[3]Taken as having a mean molecular weight of 140 g/g-mol and a liquid density of 0.75 g/ml

The thermal and photothermal data obtained on chloroform are summarized in Table 4.3 and Figure 4.1. These data illustrate that, as expected, this example compound does not respond favorably to the photothermal process using xenon arc illumination. These results are consistent with the weak rate of photon absorption by this compound. Indeed, calculations indicate that even if the photothermal quantum yield were unity, the result would be similar to that observed. Indirect evidence from the behavior of carbon tetrachloride, which was seen as a product from chloroform (ca. Section 5), suggests that this compound would likewise be unresponsive to the photothermal process using xenon arc radiation.

Table 4.3

Summary of LS-PDU Results For Chloroform
Exposed 10 sec in Air to 0 and 17.6 W/cm^2 Xenon Arc Radiation

Temperature	fr(0)	fr(17.6)
300°C	100%	100%
400	100	97.4
500	59.1	60.6
550	1.89	1.95
600	0.115	0.00735

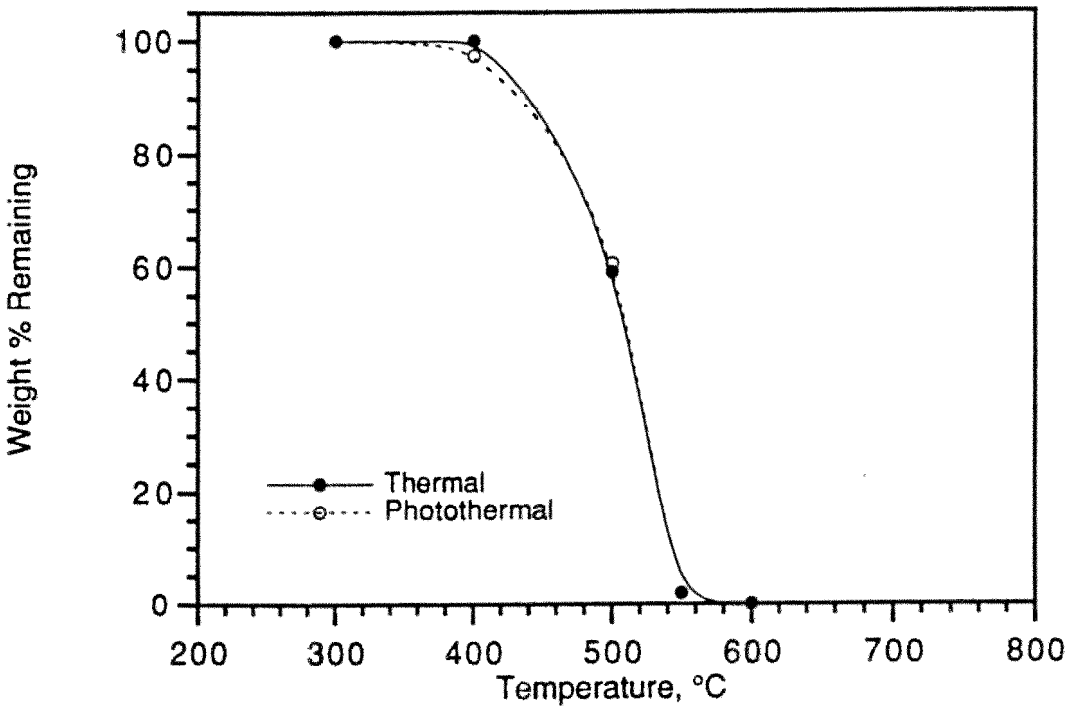

Figure 4.1. Summary of thermal and photothermal data for chloroform exposed to 0 and 17.6 W/cm^2 of xenon arc radiation for 10 sec in air.

Given the lack of response from chloroform (as a parent compound) and carbon tetrachloride (as a product from chloroform), thermal and photothermal tests with the alkanes were not conducted. These results suggest the photothermal process would not be generally effective in destroying weakly, or non-absorbing compounds. Possible mechanisms for addressing these compounds may include using radiation sources which emit shorter wavelengths than the xenon arc lamp used here, or utilizing UV light combined with photo-initiators such as hydrogen peroxide or ozone.

4.2 CHLORINATED ALKENES

Certainly an important class of compounds often found in Superfund sites are the chlorinated alkenes. Indeed, perhaps the most pervasive contaminant observed in these sites is TCE. As discussed in Section 3, the alkenes are of interest photochemically because of the spectroscopic properties resulting from the π electron structure of the double bond and the potentially high photo-reactivity of these compounds. These characteristics are further enhanced by the presence of heteroatoms within the target molecule and the spectroscopic data presented in Section 3 confirmed that these molecules are reasonably efficient absorbers of UV radiation.

The LS-PDU results for TCE and PCE are summarized in Tables 4.4 and 4.5, and in Figures 4.2 and 4.3, respectively. The photothermal quantum yields are summarized in Figure 4.4. These data clearly show that the chloroalkenes do indeed efficiently decompose through a photothermal process. Specifically, both compounds showed significant conversion at 300°C, the lowest temperature at which the LS-PDU could be operated with the xenon arc illumination system. At this temperature 12.2% of the TCE was destroyed and 36.6% of the PCE. In both examples the onset of thermal decomposition began at about 500°C where the photothermal process was destroying 57.3% of the TCE and 67.9% of the PCE. These examples illustrate that the photothermal process can destroy chloroalkenes at temperatures where no thermal destruction occurs.

Table 4.4

Summary of LS-PDU Results For Trichloroethylene
Exposed 10 sec in Air to 0 and 18.1 W/cm^2 Xenon Arc Radiation

Temperature	fr(0)	fr(18.1)
300°C	100%	87.8%
400	100	70.1
500	100	42.7
550	79.4	18.7
600	27.0	6.90
650	1.13	0.238
700	0.0697	

Table 4.5

Summary of LS-PDU Results For Tetrachloroethylene
Exposed 10 sec in Air to 0 and 17.6 W/cm^2 Xenon Arc Radiation

Temperature	fr(0)	fr(17.6)
300°C	100%	63.4%
400	100	47.8
500	97.1	32.1
600	79.9	19.0

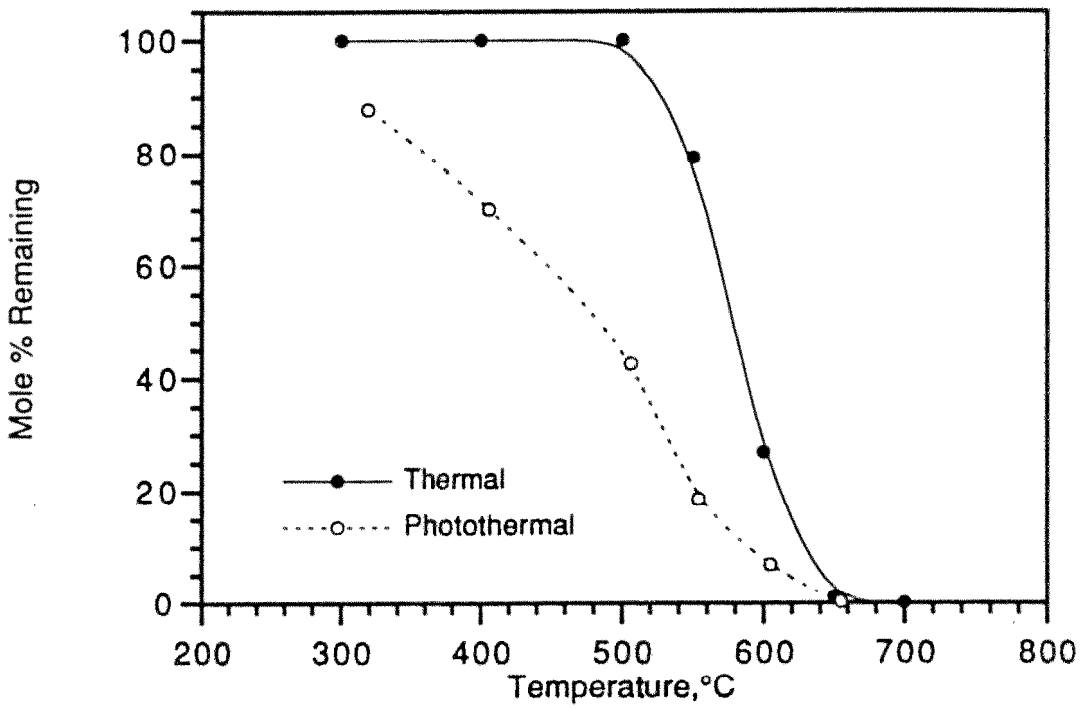

Figure 4.2. Summary of thermal and photothermal data for trichloroethylene exposed to 0 and 18.1 W/cm^2 of xenon arc radiation for 10 sec in air.

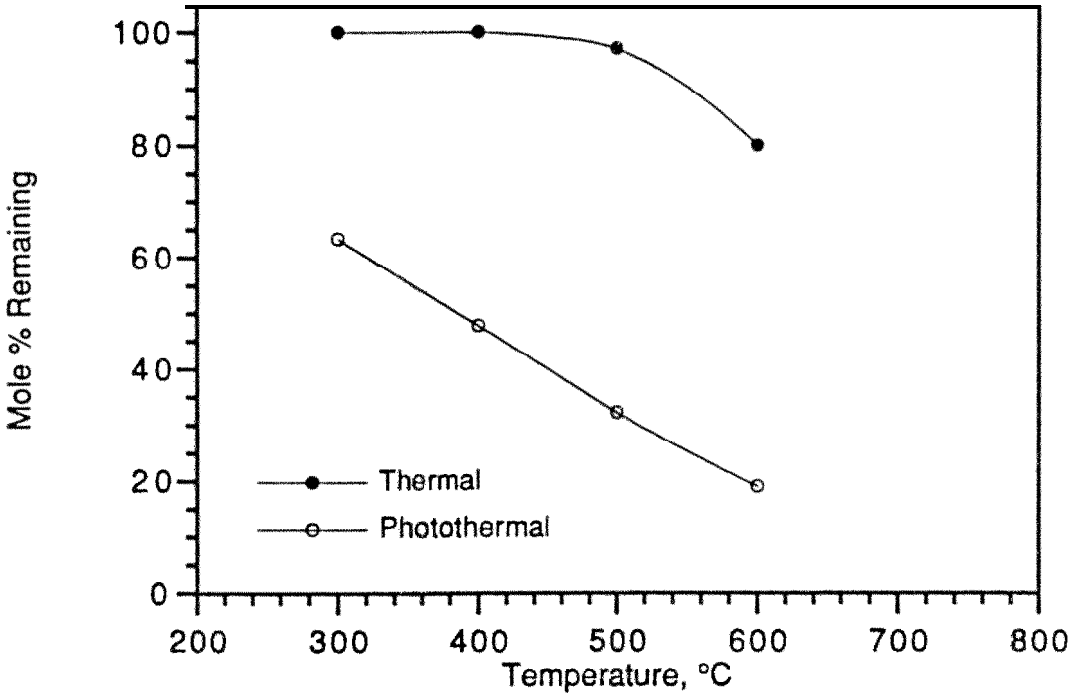

Figure 4.3. Summary of thermal and photothermal data for tetrachloroethylene exposed to 0 and 17.6 W/cm^2 of xenon arc radiation for 10 sec in air.

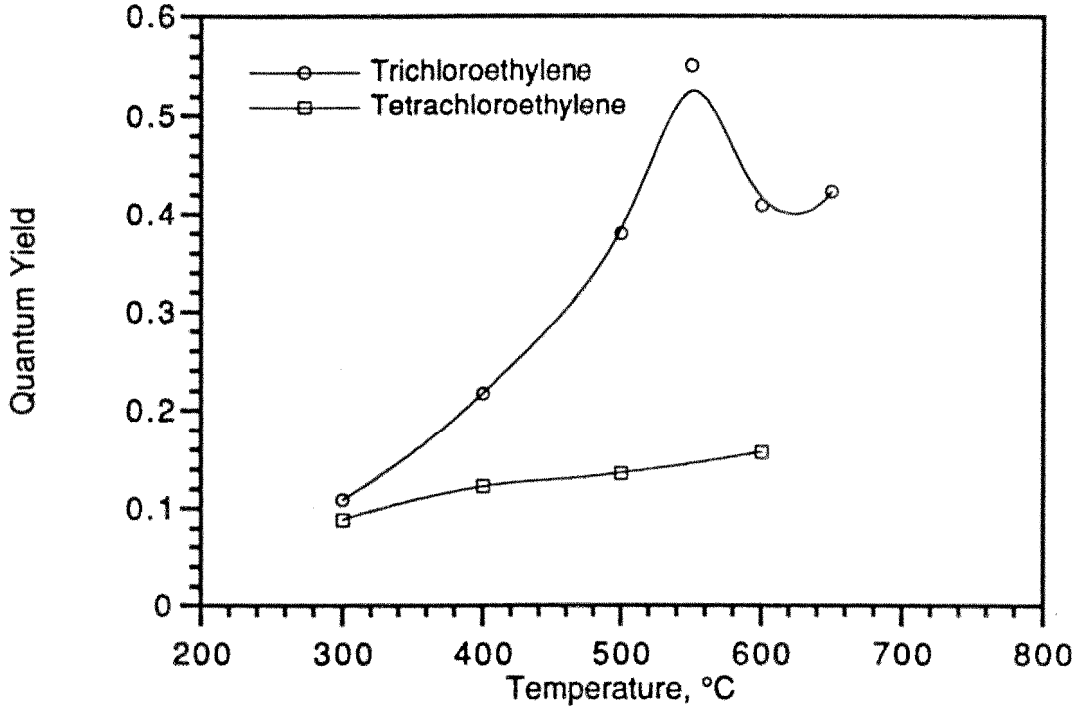

Figure 4.4. Summary of the photothermal quantum yields for trichloroethylene and tetrachloroethylene.

The photothermal quantum yields summarized in Figure 4.4 illustrate that the quantum yield (and hence the relative rate of excited state destruction) increases throughout the temperature range studied. This demonstrates that the rate of reaction from the excited state is being thermally accelerated as expected. Interestingly, even though the LS-PDU data clearly shows a greater photothermal conversion for PCE than TCE, it has a lower quantum yield. For example, at 600°C 27.0% of the TCE remained thermally versus 6.90% photothermally giving a ratio of thermal-to-photothermal of 3.91 and a quantum yield of 0.409 as compared to 79.9% of the PCE remaining thermally versus 19.0% photothermally giving a ratio of 4.21 but a quantum yield of only 0.158. This suggests that the competing process of deactivation of the excited state may be more efficient for PCE than for TCE. This is consistent with spectroscopic theory in that as the allowedness of the $S_0 \rightarrow S_1$ transition increases, so does the allowedness of the reverse process.[6]

One characteristic of the data shown here, and in other data sets in this Section, that should be discussed is the apparent convergence of the thermal and photothermal data at high temperatures. This apparent behavior is in part a consequence of how the data is presented. Specially, at high temperatures both data sets are approaching a fraction remaining of zero, however close examination of the data shows the photothermal data always remains below the thermal. For example, in the case of TCE, 1.13% of the parent compound remains following a thermal exposure at 650°C, while only 0.238% remains photothermally. The four fold better performance of the photothermal process is significant, but appears small on the Figure. Furthermore, these results merely serve to illustrate that the exposure conditions used in the laboratory may be inappropriate for the actual processing of this material. The important feature in these data is they demonstrate the photothermal process is capable of destroying these materials and the extent of difference between the thermal and photothermal data is sufficient to obtain the fundamental data needed to design a prototype photothermal system.

4.3 AROMATICS AND ARENES

To quickly assess the effectiveness of the photothermal process on aromatics and arenes the thermal and photothermal destruction of benzene, toluene, ethyl benzene, and m-xylene were obtained in a mixture referred to as BTEX. Although some interaction between the mixture

components is likely, it is felt this will provide the most time effective means of determining if a direct photothermal process is appropriate for these types of compounds.

The LS-PDU data for the thermal and photothermal decomposition of the individual components of BTEX are summarized in Tables 4.6 through 4.9 and Figures 4.5 through 4.8. The photothermal quantum yields are summarized in Figure 4.9. Comparing these data shows that benzene was the most thermally stable component of the mixture followed by toluene, ethyl benzene, and m-xylene. Furthermore, ethyl benzene and m-xylene showed nearly identical decomposition behavior. The increase in photothermal destruction efficiency follows a similar pattern. Specifically, benzene was the least affected by the xenon arc radiation, followed by toluene and ethyl benzene and m-xylene with the latter two showing the largest (and similar) photothermal effect. These data show that the aromatic compounds as a class are fair candidates for photothermal processing, though caution would have to be taken with benzene due to it's relatively high photothermal stability. Certainly a treatability study would be in order prior to processing a waste with a significant concentration of benzene. Furthermore, as suggested above, using an illumination system which delivers radiation deeper in the UV than the xenon arc system used here should improve the performance of a photothermal system.

Table 4.6
Summary of LS-PDU Results For the Benzene Component of BTEX
Exposed 10 sec in Air to 0 and 17.6 W/cm^2 Xenon Arc Radiation

Temperature	fr(0)	fr(17.6)
300°C	100%	99.7%
400	100	99.5
500	98.3	96.0
550	98.3	91.1
600	83.7	64.9
650	30.4	24.3
700	0.998	0.998

Table 4.7

Summary of LS-PDU Results For the Toluene Component of BTEX
Exposed 10 sec in Air to 0 and 17.6 W/cm^2 Xenon Arc Radiation

Temperature	fr(0)	fr(17.6)
300°C	100%	96.6%
400	100	97.0
500	93.9	88.0
550	94.1	74.3
600	53.5	24.8
650	4.95	2.80
700		

Table 4.8

Summary of LS-PDU Results For the Ethyl Benzene Component of BTEX
Exposed 10 sec in Air to 0 and 17.6 W/cm^2 Xenon Arc Radiation

Temperature	fr(0)	fr(17.6)
300°C	100%	91.7%
400	100	90.8
500	89.3	77.9
550	85.7	53.2
600	32.2	9.12
650	1.09	0.452
700		

Table 4.9

Summary of LS-PDU Results For the m-Xylene Component of BTEX
Exposed 10 sec in Air to 0 and 17.6 W/cm^2 Xenon Arc Radiation

Temperature		fr(17.6)
300°C	100%	90.8%
400	100	89.3
500	88.5	76.2
550	83.8	49.7
600	29.1	7.51
650	0.838	0.361
700		

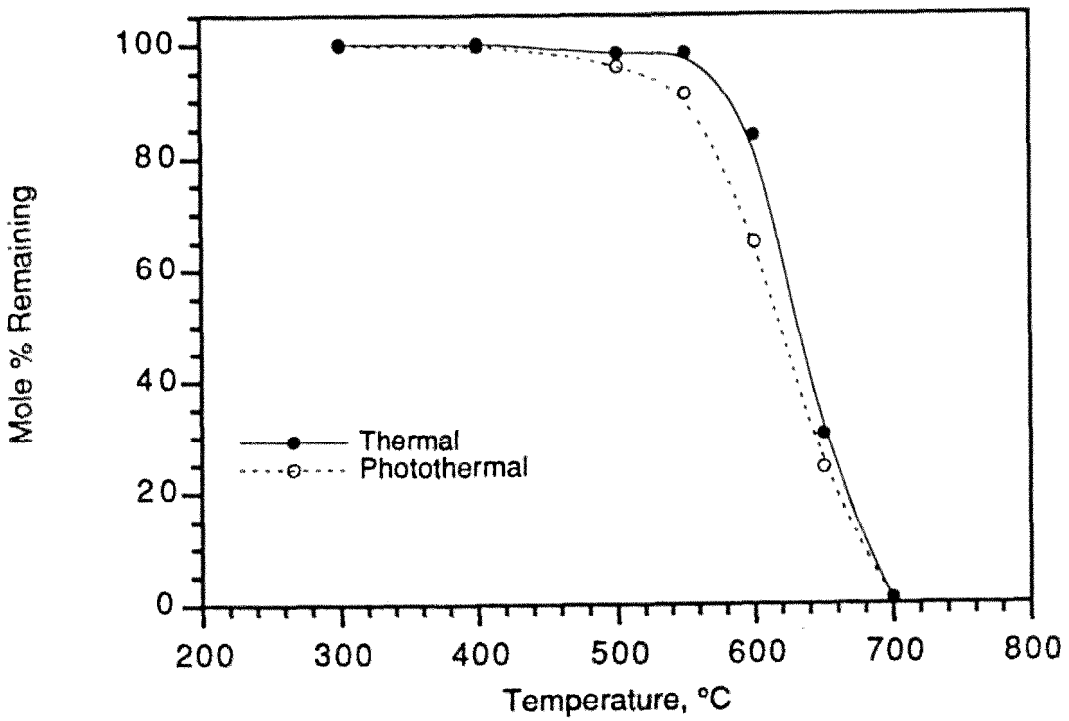

Figure 4.5. Summary of thermal and photothermal data for the benzene component of BTEX exposed to 0 and 17.6 W/cm^2 of xenon arc radiation for 10 sec in air.

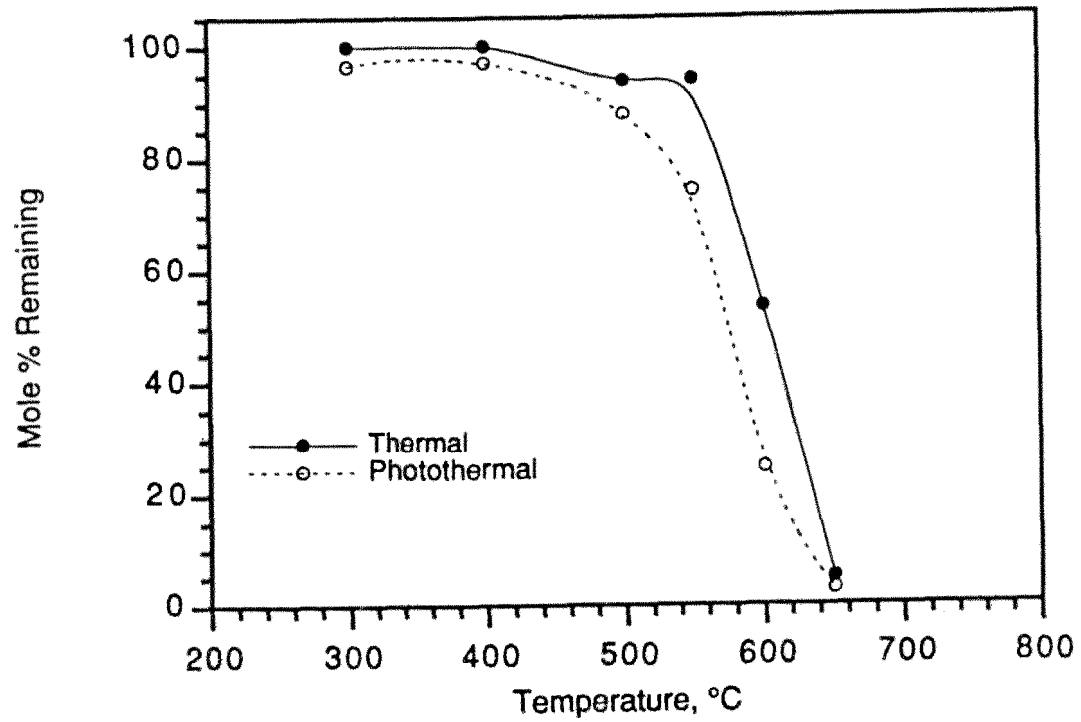

Figure 4.6. Summary of thermal and photothermal data for the toluene component of BTEX exposed to 0 and 17.6 W/cm^2 of xenon arc radiation for 10 sec in air.

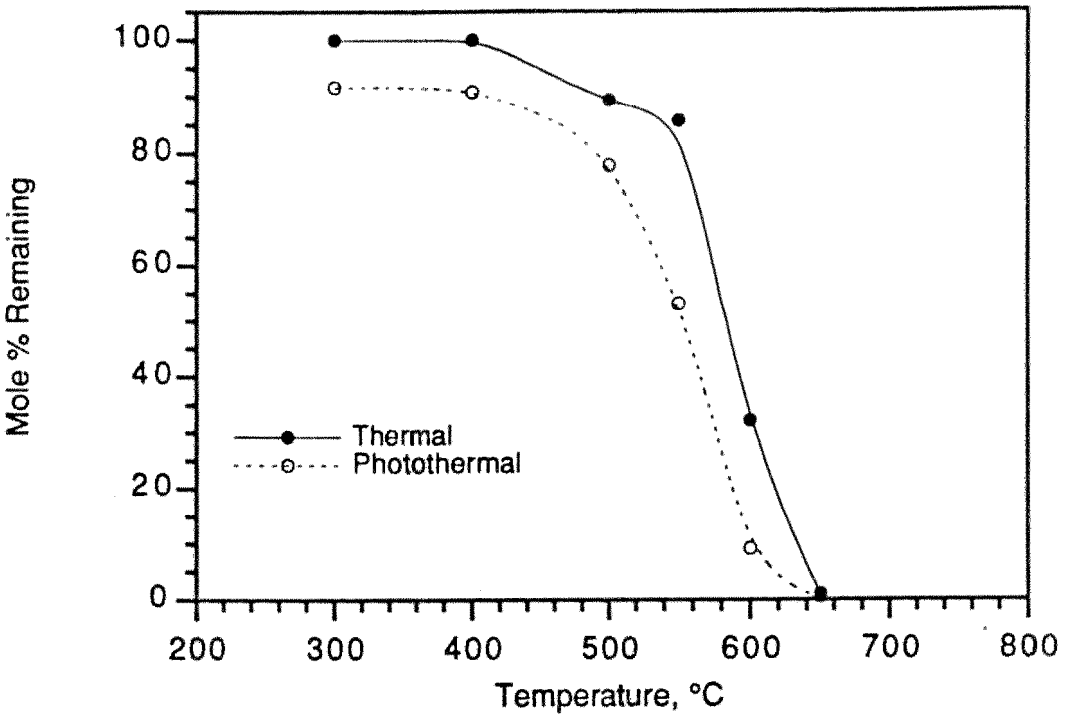

Figure 4.7. Summary of thermal and photothermal data for the ethyl benzene component of BTEX exposed to 0 and 17.6 W/cm^2 of xenon arc radiation for 10 sec in air.

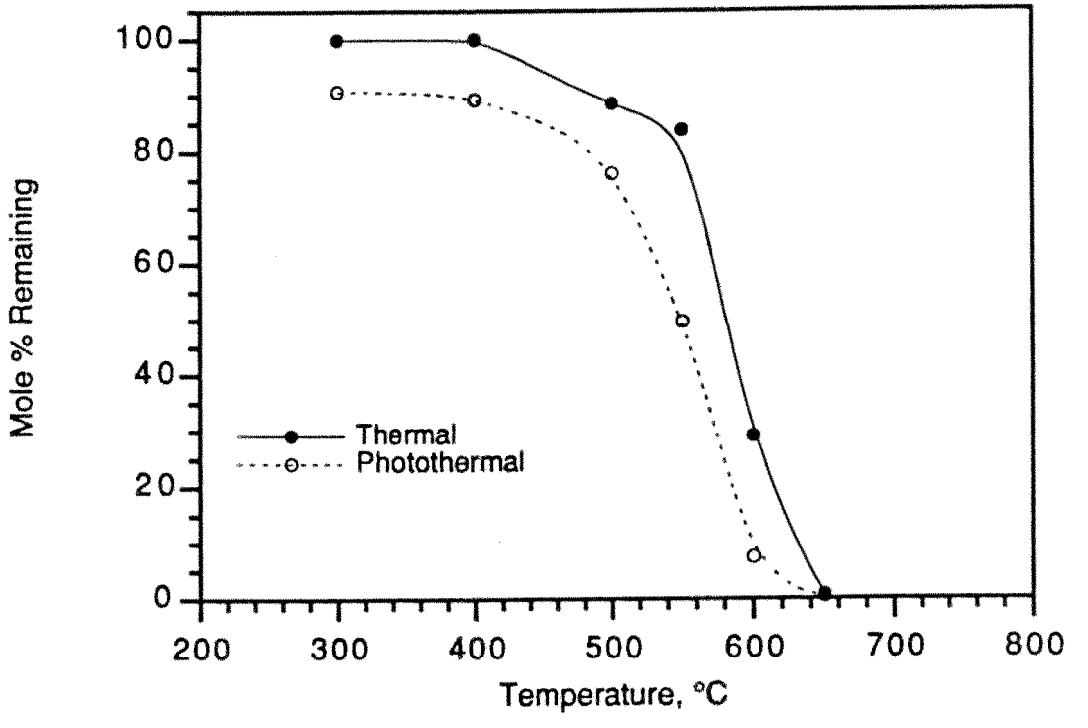

Figure 4.8. Summary of thermal and photothermal data for the m-xylene component of BTEX exposed to 0 and 17.6 W/cm^2 of xenon arc radiation for 10 sec in air.

Interestingly, the quantum yields for the BTEX components shown in Figure 4.9 are nearly constant at temperatures below 500°C, followed by a rapid rise to a maximum at approximately 600°C. This clearly suggests an optimal temperature for processing these types of materials of 600°C to maximize the destruction via photothermal pathways. It is also interesting to note that while the photothermal conversion of ethyl benzene and m-xylene were nearly identical (ca. Figures 4.7 and 4.8), the quantum yield for m-xylene is significantly lower than for ethyl benzene. This result is a consequence of m-xylene having a higher photon absorption rate constant (ca. Table 3.2), but not a higher rate of conversion than ethyl benzene. As in the case of TCE and PCE, this result points to a difference in the competing processes of excited state deactivation.

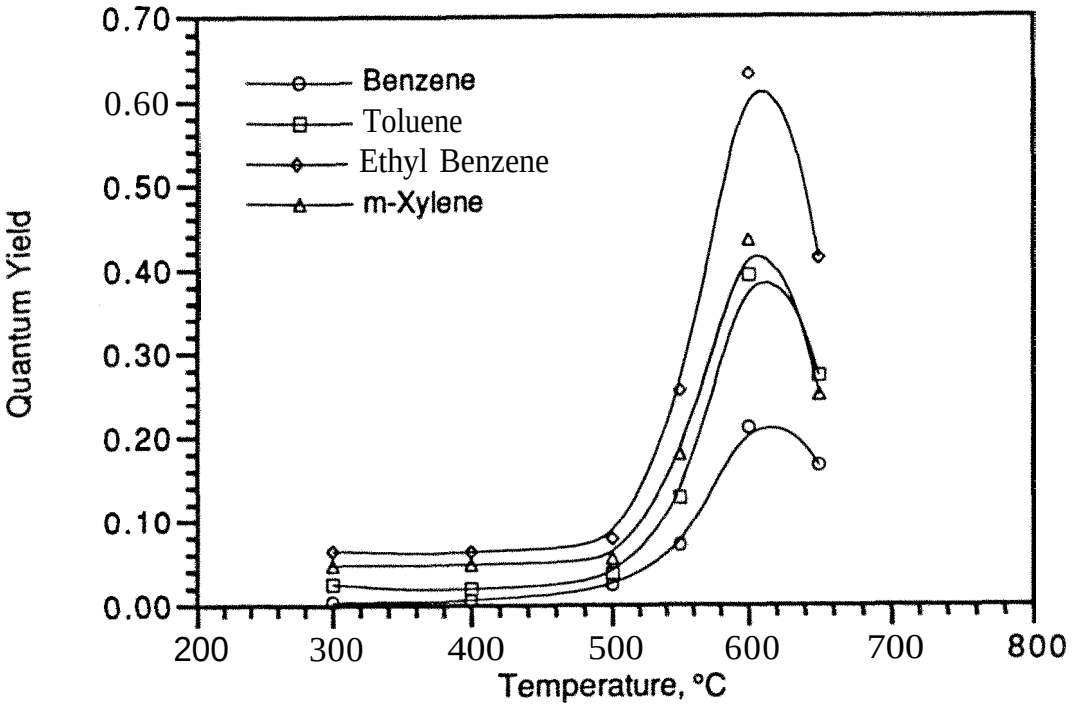

Figure 4.9. Summary of the photothermal quantum yields for components of BTEX.

4.4 CHLORINATED AROMATICS

The data described above illustrated that aromatic hydrocarbons can be destroyed by the photothermal process. Furthermore, the data presented above for the chloroalkenes suggests that molecules which contain relatively heavy heteroatoms may be particularly susceptible to the photothermal process. These two types of compounds are brought together in the chlorinated aromatics which are an important class of compounds which form the basic building blocks for larger, more complex materials such as the highly toxic PNAs

The two example chlorinated aromatic compounds selected for this program where MCBz and DCBz. The LS-PDU data for these materials are summarized in Tables 4.10 and 4.11, and Figures 4.10 and 4.11, respectively. The photothermal quantum yields are summarized in Figure 4.12. As with the chloroalkenes the photothermal effect is clearly evident with a significant level of photothermal destruction occurring at temperatures where no measurable thermal destruction is taking place. In the case of MCBz the onset of thermal conversion occurs at approximately 500°C whereas the photothermal process has destroyed 25.9% of the feed by this point. Similarly, for the case of DCBz the onset of thermal destruction occurs at about 600°C at which point the photothermal process has destroyed 53.4% of the feed material. Clearly the photothermal process is effective in destroying chlorinated aromatic materials. Furthermore, the data suggest that the extent of conversion increases with chlorine content, which is the opposite of the thermal response. Specifically, the thermal stability of a waste typically increases with chlorine content, whereas the photothermal stability is seen to decrease. This suggests the photothermal process will be particularly effective in destroying wastes with high chlorine contents or contain other heavy components.

Table 4.10

Summary of LS-PDU Results For Monochlorobenzene
Exposed 10 sec in Air to 0 and 17.6 W/cm* Xenon Arc Radiation

Temperature		fr(17.6)
300°C	100%	85.3%
400	100	83.6
500	99.7	74.1
600	94.4	62.6

Table 4.11

Summary of LS-PDU Results For o-Dichlorobenzene
Exposed 10 sec in Air to 0 and 18.1 W/cm^2 Xenon Arc Radiation

Temperature	fr(0)	fr(17.6)
300°C	100%	71.3%
400	100	69.6
500	100	66.3
600	100	46.6
625	87.8	
650	67.8	27.0
675	33.5	5.84
700	0.406	0.0397

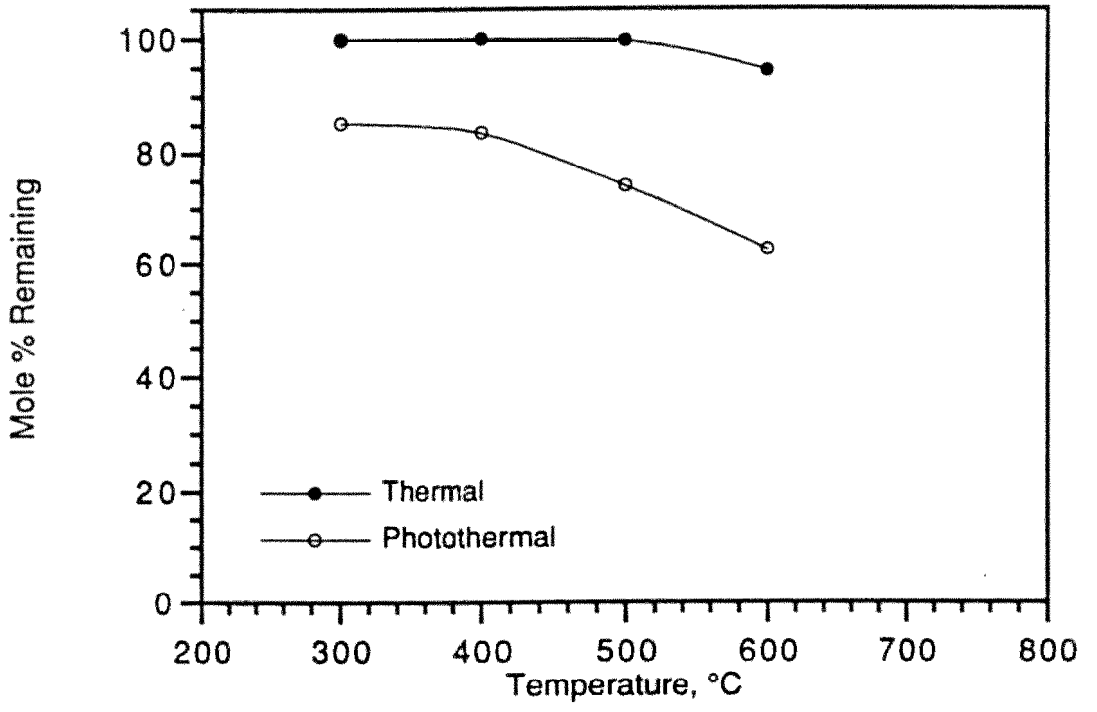

Figure 4.10. Summary of thermal and photothermal data for monochlorobenzene exposed to 0 and 17.6 W/cm^2 of xenon arc radiation for 10 sec in air.

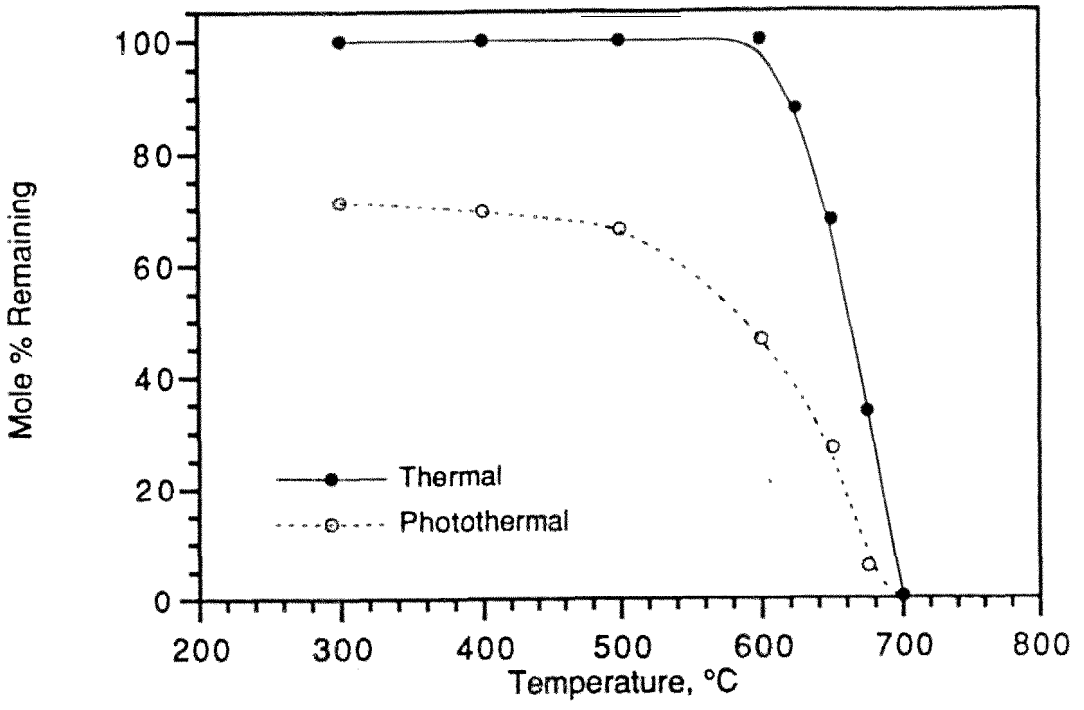

Figure 4.11. Summary of thermal and photothermal data for o-dichlorobenzene exposed to 0 and 17.6 W/cm^2 of xenon arc radiation for 10 sec in air.

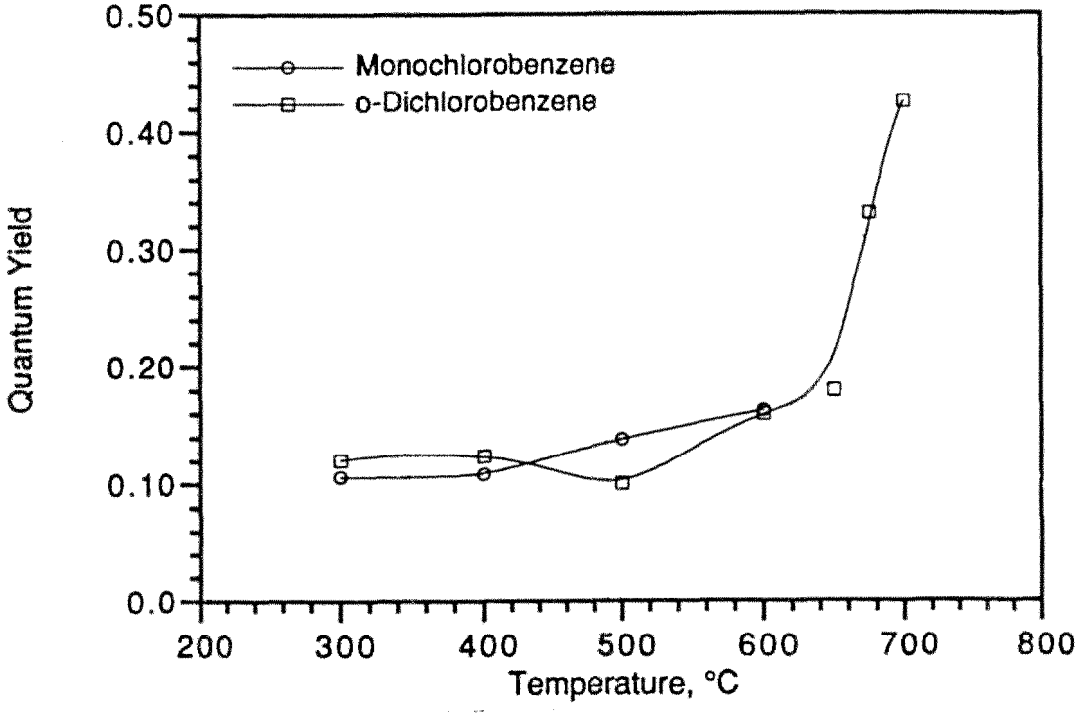

Figure 4.12. Summary of the photothermal quantum yields for monochlorobenzene and o-dichlorobenzene.

The photothermal quantum yields summarized in Figure 4.12 show that for this example the quantum yield of MCBz and DCBz are approximately equivalent at temperatures to 600°C. Furthermore, as in the case of the BTEX components, a rapid rise in quantum yields is observed at higher temperatures, though in this case a maximum is not present. This suggests the: photothermal conversion of these materials would benefit from operating at relatively high temperatures.

4.5 CHLORINATED DIBENZO-P-DIOXINS

Although perhaps not as numerous as other types of sites, locations contaminated with high molecular weight chlorinated materials such as polychlorinated biphenyls (PCBs), dibenzofurans (PCDFs), and dibenzo-p-dioxins (PCDDs) are af concern because of their high toxicity. Furthermore, the relatively high thermal stability and the requirement for exceptionally efficient destruction of these types of compounds makes it difficult to destroy them by conventional thermal means. Conceptually, these types of compounds should be readily treatable via the photothermal process as they include the structural and compositional characteristics that should render them very susceptible to the photothermal destruction. Specifically, PCBs, PCDDs, PCDFs, and PNAs generally include a basic aromatic structure which absorbs UV photons at relatively long wavelengths as well as numerous heteroatom substitutions which. combine ta give a molecule that absorbs WV radiation very efficiently and should be photo-active.

The results of thermal and photothermal tests with TCDD are summarized in Table 4.12 and Figure 4.13, with the quantum yield shown in Figure4.14. In this case the onset of thermal decomposition was observed at 400°C at which point the photothermal process was destroying 98.69% of the feed. The extent of performance superiority of the photothermal process is maintained throughout the temperature range studied with the level of improvement increasing from approximately 72 fold at 400°C to over 1,200 fold (64.6% destroyed thermally versus 99.97 15% destroyed photothermally) at 600°C. This clearly shows the photothermal process is well suited for destroying these types of wastes.

Table 4.12

Summary of LS-PDU Results For 1,2,3,4-Tetrachlorodibenzo-p-dioxin
Exposed 10 sec in Air to 0 and 17.6 W/cm^2 Xenon Arc Radiation

Temperature	fr(0)	fr(17.6)
300°C	100%	3.59%
400	94.1	1.31
500	83.0	0.394
600	35.4	0.0285
650	3.92	
700	0.242	

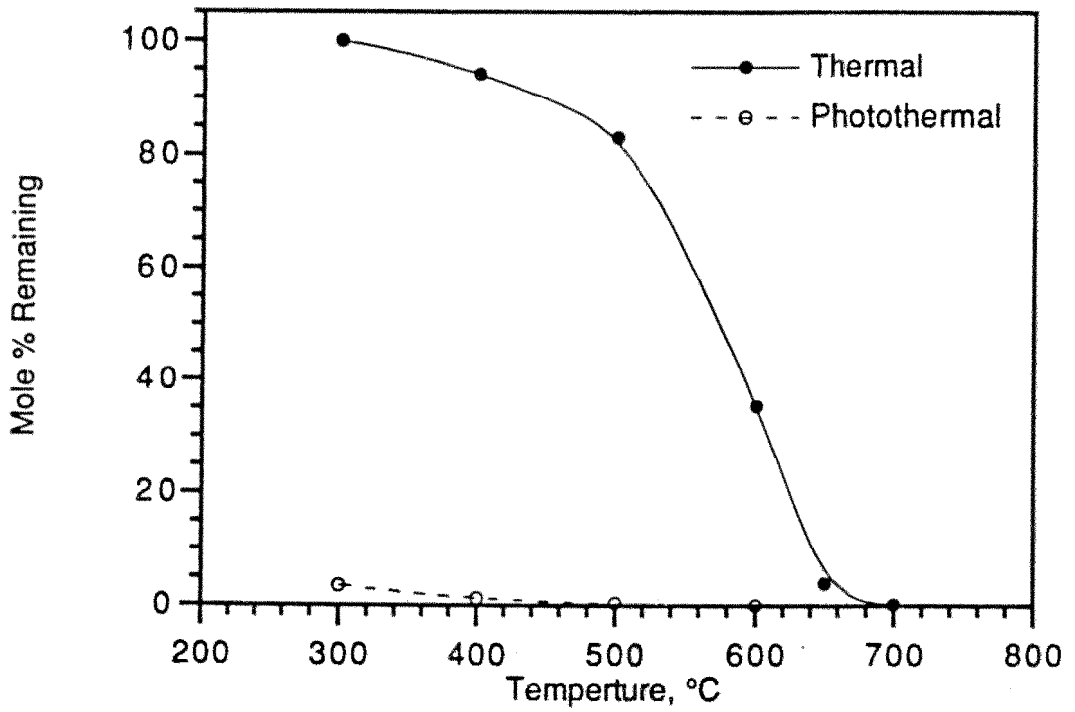

Figure 4.13. Summary of thermal and photothermal data for 1,2,3,4-tetrachlorodibenzo-p-dioxin exposed to 0 and 17.6 W/cm^2 of xenon arc radiation for 10 sec in air.

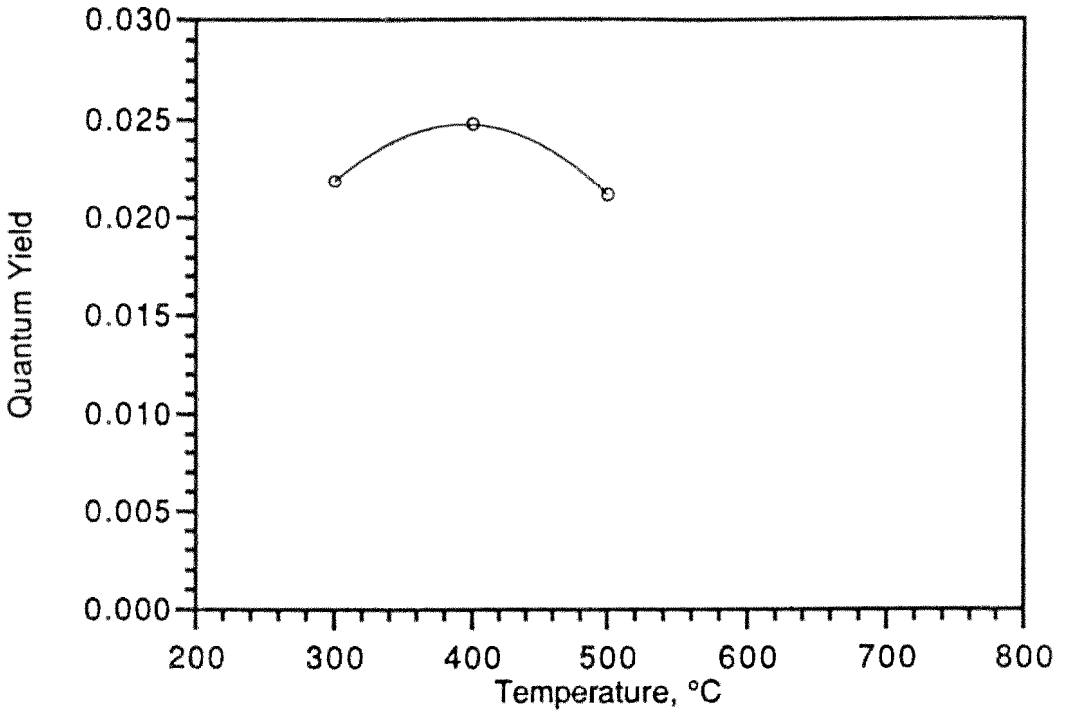

Figure 4.14. Summary of the photothermal quantum yields for 1,2,3,4-tetrachlorodibenzo-p-dioxin.

The photothermal quantum yield data summarized in Figure 4.14 shows that over the limited span for which data is available the quantum yield peaked at 400°C though it varied over a narrow range. The interesting feature in this data is the low value of the quantum yield of approximately 0.024. This shows that this material is relatively photochemically inactive. However, this relative inactivity is offset by the strength of the absorption as shown by the photon absorption rate constants listed in Table 3.2. Once again, this result is consistent with spectroscopic theory which predicts shorter excited state lifetimes, and therefore less time for decomposition to occur, for chemicals with strong absorption coefficients.

4.6 GASOLINE

The last sample tested as part of the initial evaluation process consisted of a commercial grade automobile fuel (89 octane unleaded gasoline) to determine if the photothermal process would be applicable to sites contaminated with this type of material. The complexity of this sample is illustrated by the GC/FID trace shown in Figure 4.15. This data is from a non-

destructive thermal exposure (300°C for 10 sec in air). Detailed inspection of this trace reveals over 150 individual components. The selected peaks (identifications assigned by mass spectra) show that the mixture is dominated by alkanes with some significant amounts of aromatic compounds, most notably toluene and xylenes, at the high molecular weight end of the chromatogram.

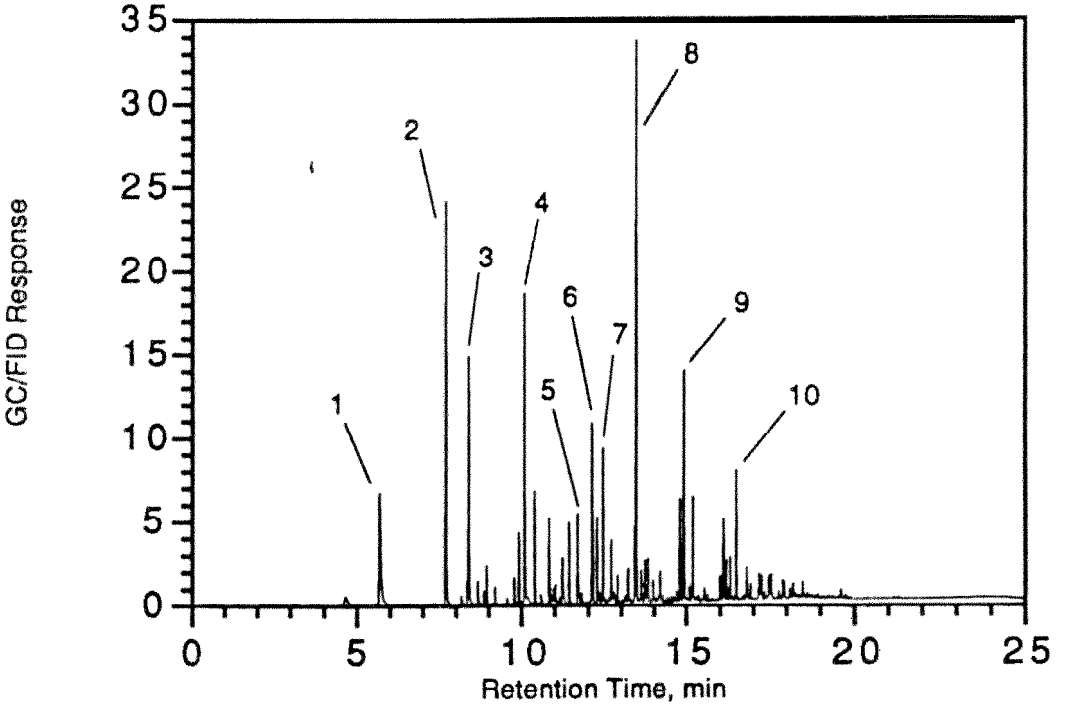

Figure 4.15. Example GC/FID chromatogram of gasoline exposed to non-destructive conditions (300°C for 10 sec in air) illustrating the complex nature of this sample. Peaks identified by GS/MS library searches include;

1) 2-Methyl-propane
2) 2-Methyl-butane
3) 2,3-Dimethyl-butane
4) 2-Methyl-pentane
5) Benzene
6) 2,3-Dimethyl-pentane
7) 2,2,4-Trimethyl-pentane
8) Toluene
9) o-Xylene
10) 1,2,4-Trimethyl-benzene

The overall thermal and photothermal decomposition of the sample is summarized in Table 4.13 and Figure 4.16. This data shows the weight percent remaining taken as the sum of all the integrated GC/FID peak areas in the chromatograms from each run. This data suggests a small amount of photothermal conversion at low temperatures (i.e., 300°C) that remains constant until the onset of thermal decomposition at approximately 500°C. Above this temperature the thermal and photothermal curves are essentially identical.

Table 4.13

Summary of LS-PDU Results For Gasoline
Exposed 10 sec in Air to 0 and17.6 W/cm^2 Xenon Arc Radiation

Temperature	fr(0)	fr(17.6)
300°C	100%	90.5%
500	93.3	89.0
600	22.3	21.5
700	0.385	0.341

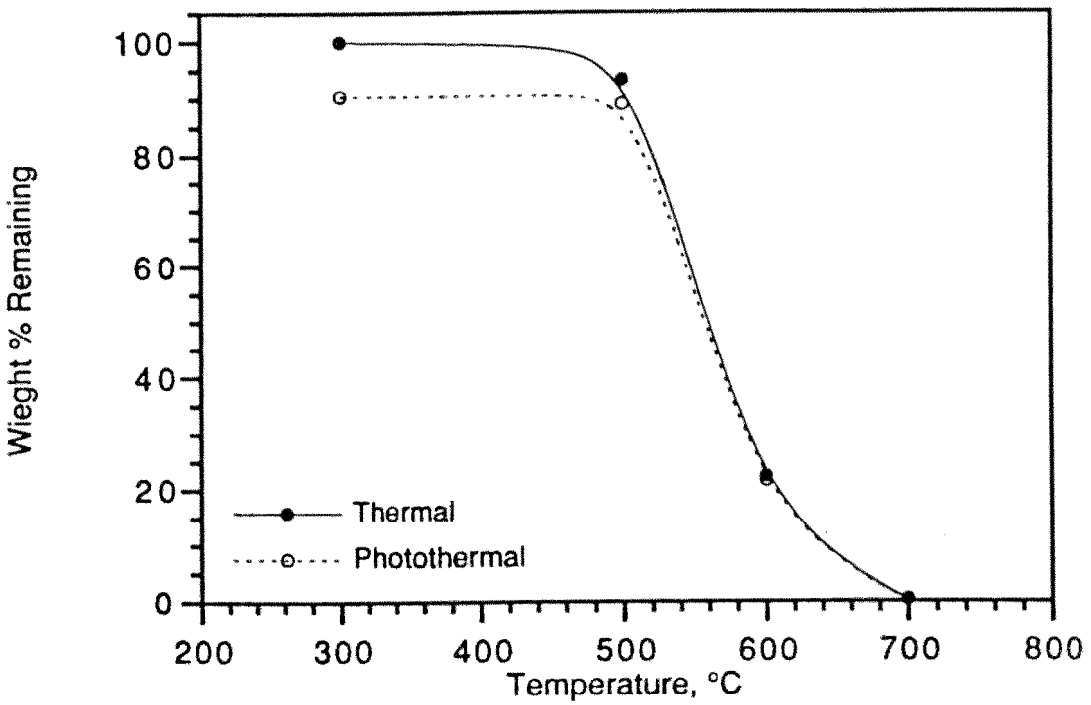

Figure 4.16. Overall decomposition (sum of all integrated GC/FID peaks) for gasoline exposed to 0 and 17.6 W/cm^2 of xenon arc radiation for 10 sec in air.

An alternative analysis of the data from this complex sample is shown in Figure 4.17, which summarizes the number of peaks observed in each chromatographic trace. This data

suggests an overall simplification of the sample as the photothermal chromatograms consistently contained fewer peaks than the thermal. However, since the photothermal conversion data does not show a significant improvement in reactor performance the peaks affected by the photothermal exposure must be small. Again, the overall thermal and photothermal system performance is roughly equivalent.

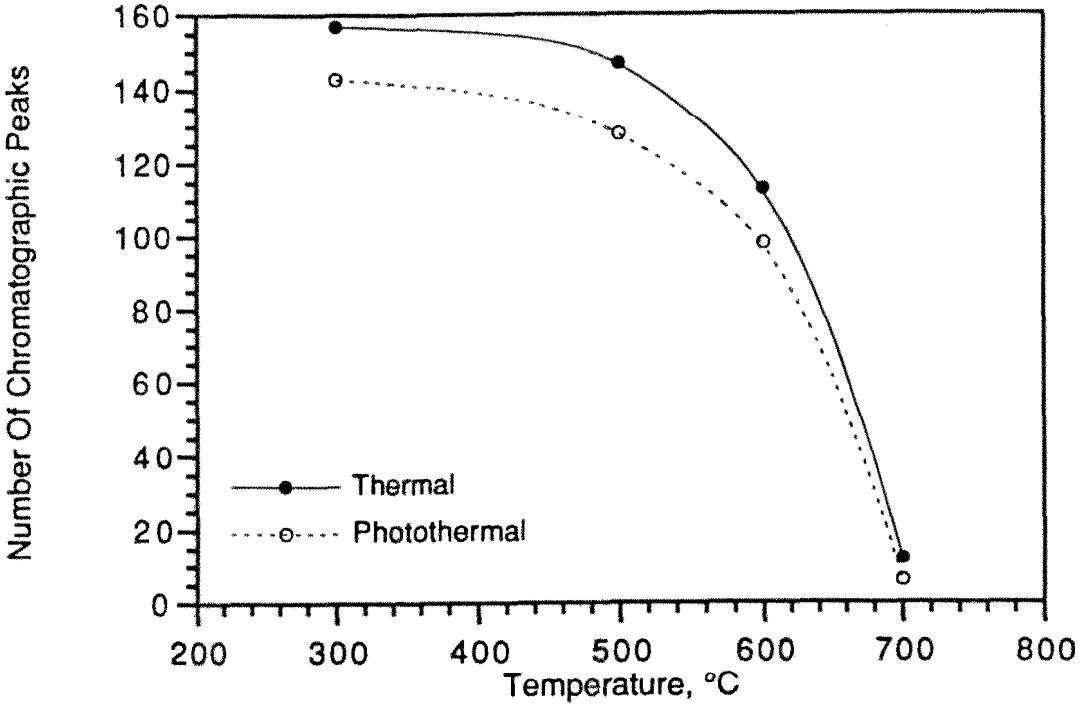

Figure 4.17. Summary of the number of GC/FID peaks observed from the analysis of gasoline exposed to 0 and 17.6 W/cm^2 of xenon arc radiation for 10 sec in air.

Similar behavior is observed when individual components are examined, such as methyl butane and toluene as shown in Figures 4.18 and 4.19, respectively. Specifically, little photothermal effect is observed in the major aliphatic and aromatic components. This suggests that the small differences in the overall reactor performance lies in the impact on minor components.

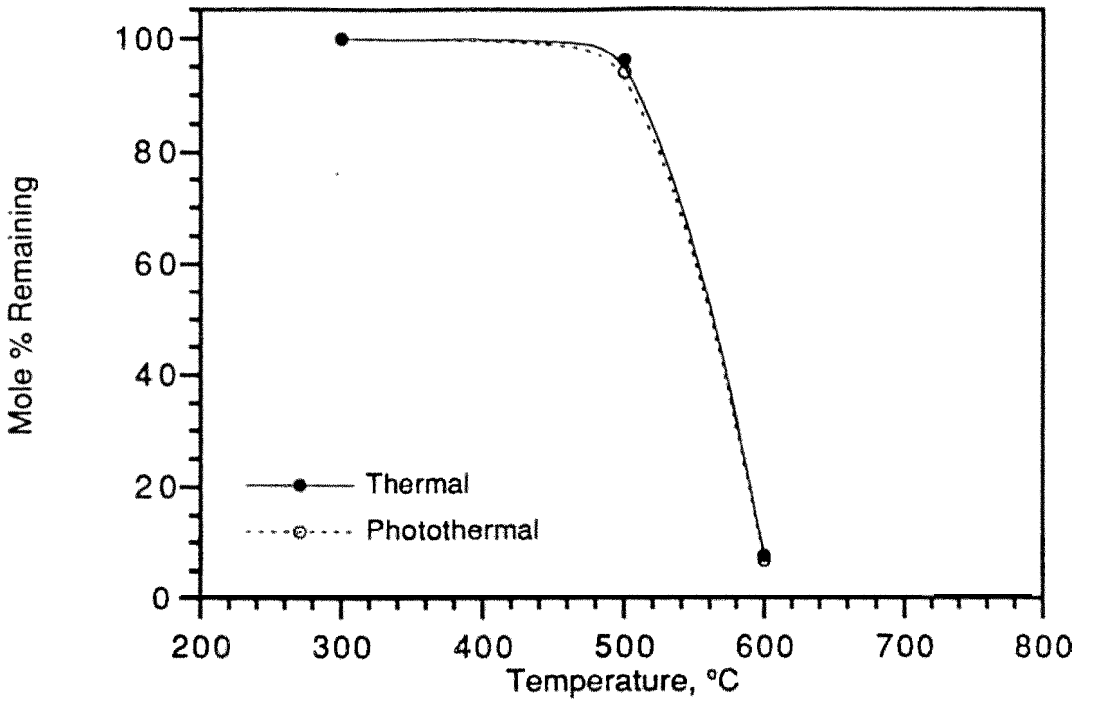

Figure 4.18. Summary of the decomposition of the 2-methyl butane (identification assigned by GC/MS spectral library) component of gasoline exposed to 0 and 17.6 W/cm^2 of xenon arc radiation for 10 sec in air.

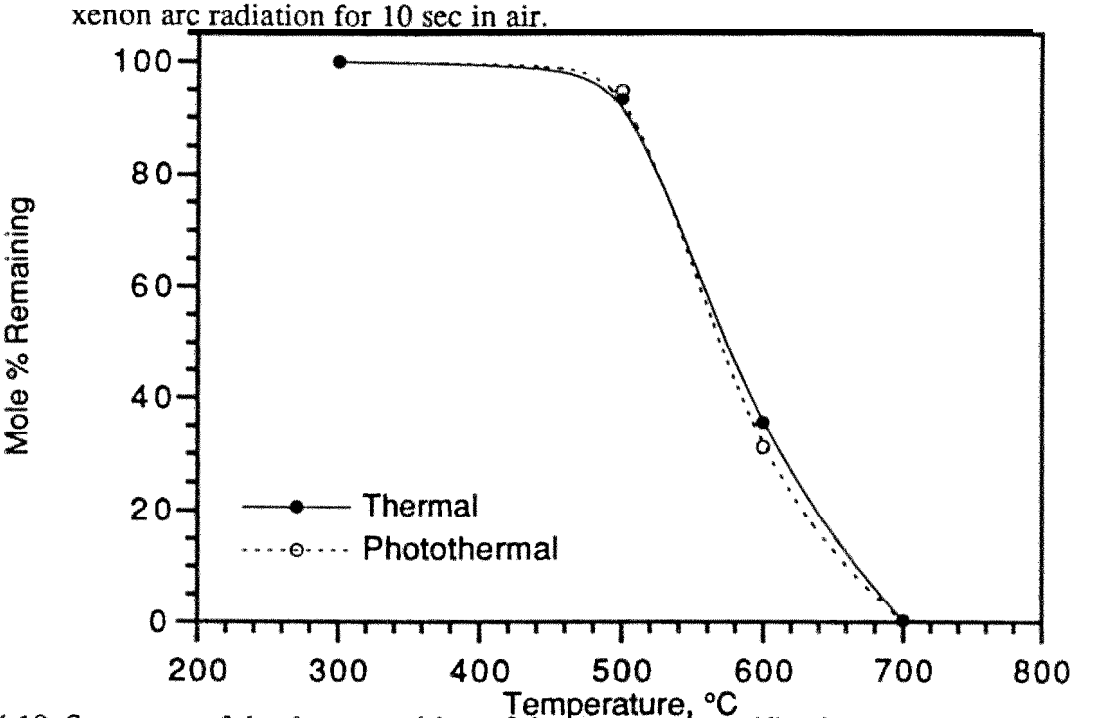

Figure 4.19. Summary of the decomposition of the toluene (identification assigned by GC/MS spectral library) component of gasoline exposed to 0 and 17.6 W/cm^2 of xenon arc radiation for 10 sec in air.

In summary then, this data shows that the direct photothermal process would not be a good candidate for treating fuel spill sites. However, using radiation sources other than xenon arc (i.e., mercury vapor) or an indirect process using a powerful oxidizer like hydroxyl radicals from the photo-dissociation of hydrogen peroxide may be worth pursuing.

4.7 MIXTURES OF TCE, DCBz, AND WATER VAPOR

In addition to the complex gasoline sample described above, data was obtained on a simpler mixture consisting of TCE, DCBz, and water vapor. This mixture was selected to simulate the principal threats from a site located in western Nevada for which we had actual field data on the contaminant levels and identities and which was being considered for cleanup by soil vapor extraction (SVE). A summary of the contaminants and relative concentrations are summarized in Table 4.14. This information shows that the principal threats are from TCE and dichlorobenzenes. Two test mixtures were formulated to simulate the relative concentrations of TCE:

1) at the start of the SVE operation where it was assumed the components would be in relatively high concentration, and

2) later where the concentration of TCE would be reduced relative to the DCBz as DCBz's lower vapor pressure would result in it's slower removal.

A third mixture was formulated without water vapor to determine if this component had any measurable effect on the system performance.

Mixture #I

As shown in Table 4.2 (which summarizes the initial concentrations of mixture components), the first test mixture was composed of a TCE:Water:DCBz ratio of approximately 60:20:1 indicating the initial draw from the site would be mostly a TCE/water mixture with a trace of DCBz. The test results for TCE and DCBz components are summarized in Tables 4.15 and 4.16, and Figures 4.20 and 4.21, respectively. The photothermal quantum yields are summarized in Figure 4.22.

Table 4.14

Summary Of Contaminants At An Example Site In Western Nevada

Compound	Mean Soil Conc. (mg/kg)
Phenol	0.87
Chloroform	1.2
P,P-DDD	1.9
P.P-DDT	3.4
Bis(2-rthylhexyl)phthalate	4.9
2,4-Dimethylphenol	5.5
Ethyl Benzene	6.5
2-Methylnaphthalene	11
Naphthalene	11
Methylene Chloride	17
Chlorobenzene	21
Toluene	23
1,2,4-Trichlorobenzene	23
Xylenes	30
Trichloroethylene	280
Dichlorobenzenes	747

Table 4.15

Summary of LS-PDU Results For the Trichloroethylene Component of Mix #1
Exposed 10 sec in Air to 0 and 17.6 W/cm^2 Xenon Arc Radiation

Temperature	fr(0)	fr(17.6)
300°C	100%	82.0%
400	100	60.9
500	70.6	19.5
550	35.1	7.68
600	5.58	1.61
650	0.339	0.0962
700	0.0385	

Table 4.16

Summary of LS-PDU Results For the o-Dichlorobenzene Component of Mix #1
Exposed 10 sec in Air to 0 and 17.6 W/cm^2 Xenon Arc Radiation

Temperature	fr(0)	fr(17.6)
300°C	100%	63.1%
400	100	49.1
500	67.0	7.41
550	28.4	6.40
600	15.9	4.26
650	8.14	3.12
700	1.69	0.921

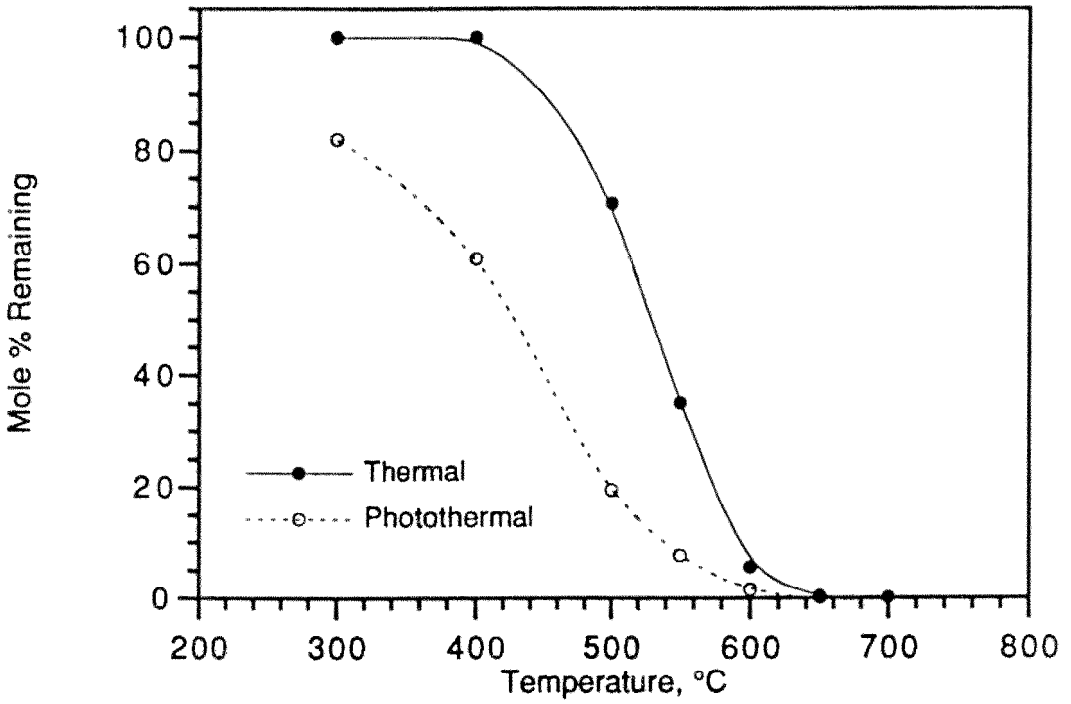

Figure 4.20. Summary of thermal and photothermal data for the trichloroethylene component of a TCE:Water:DCBz (60:20:1) mixture exposed to 0 and 17.6 W/cm^2 of xenon arc radiation for 10 sec in air.

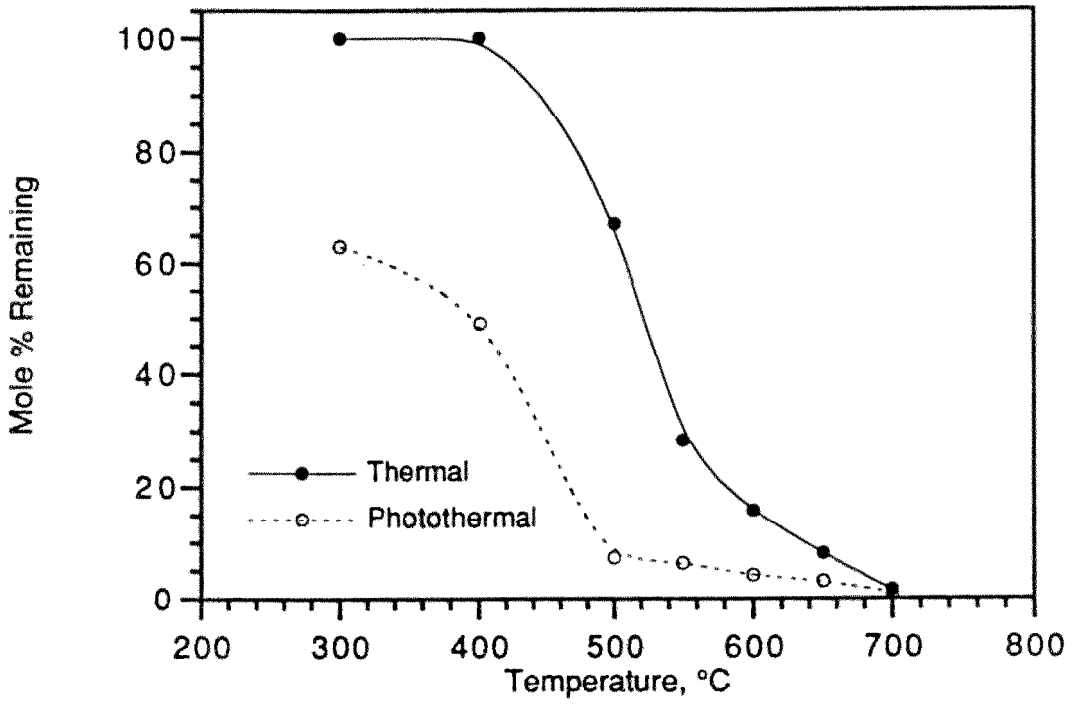

Figure 4.21. Summary of thermal and photothermal data for the o-dichlorobenzene component of a TCE:Water:DCBz (60:20:1) mixture exposed to 0 and 17.6 W/cm^2 of xenon arc radiation for 10 sec in air.

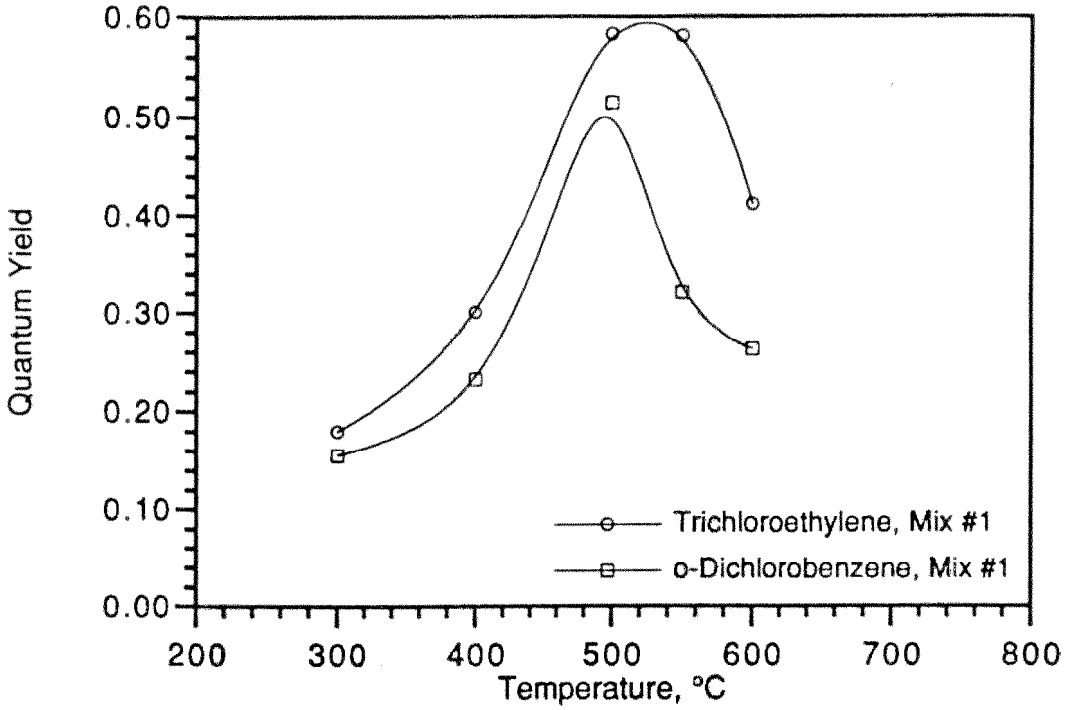

Figure 4.22. Summary of the photothermal quantum yields for the trichloroethylene and o-dichlorobenzene components of a TCE:Water:DCBz (60:20:1) mixture.

Comparing the data in Figures 4.20 and 4.21 shows a significant improvement in reactor performance operating in a photothermal versus thermal mode. Specifically, for both components the onset of thermal decomposition occurs at approximately 400°C whereas the photothermal process has destroyed 39.1% of the TCE and 50.9% of the DCBz. It is interesting to note that the onset of thermal decomposition of the TCE and DCBz when tested as pure compounds did not occur until approximately 500 and 600°C, respectively, indicating the thermal stability of the mixture components were reduced compared to their stability when tested as pure components. This type of behavior has been reported previously from studies of thermal decomposition and has been attributed to interaction between the parent species and reactive radicals formed from the decomposition of the mixture components. [10] Similar behavior is seen in the photothermal data suggesting a similar mechanism is occurring in this environment as well. Another interesting feature is seen in the DCBz data, where the apparent stability of material increases following an initial rapid rate of decomposition. Reviewing prior data with TCE tested as a pure compound (Section 4.2) revealed that this sample produces DCBz as a PIC in very low yields (<1%). Therefore, what is being observed here in the mixture data is

the initial destruction of the DCBz parent at low temperatures, followed by its appearance as a PIC from the reaction of TCE. Although the absolute yield of DCBz from TCE is quite small, it is significant compared to the amount of DCBz in the system. In any event, these data clearly show that the photo-thermal process should be able to readily destroy this mixture under the appropriate conditions.

Comparing the photothermal quantum yield data in Figure 4.22 with that for the pure compound in Figures 4.4 (TCE) and 4.12 (DCBz) shows that an overall increase in the quantum yield is observed illustrating the interaction of the mixture components increased the overall rate of photothermal decomposition. It should be noted that the decline in the DCBz quantum yield is a result of the production of this compound as a PIC from TCE which had the effect of reducing the overall destruction rate on this component. Even with this effect, the quantum yield for DCBz in the mixture exceeded that for DCBz as a pure compound.

Mixture #2

As shown in Table 4.2, the TCE:Water:DCBz ratio in the second test mixture was approximately 1:20:1. The results from the tests with this sample are summarized in Tables 4.17 and 4.18 and Figures 4.23 and 4.24 for TCE and DCBz, respectively. The photothermal quantum yields are summarized in Figure 4.25. Once again we find a comparatively early onset of thermal decomposition at approximately 400°C where the photothermal process has destroyed 26.5% of the TCE and 40.8% of the DCBz. Although the extent of photothermal conversion is not as great as in the first formulation, it is certainly significant and this mixture would still be considered an excellent candidate for photothermal destruction.

Table 4.17

Summary of LS-PDU Results For the Trichloroethylene Component of Mix #2
Exposed 10 sec in Air to 0 and 17.6 W/cm^2 Xenon Arc Radiation

Temperature		fr(17.6)
300°C	100%	88.0%
400	100	73.5
500	95.4	56.0
600	68.8	32.7
650	44.0	
700	3.92	0.648

Table 4.18

Summary of LS-PDU Results For the o-Dichlorobenzene Component of Mix #2
Exposed 10 sec in Air to 0 and 17.6 W/cm^2 Xenon Arc Radiation

Temperature	fr(0)	fr(17.6)
300°C	100%	69.2%
400	100	59.2
500	90.2	46.3
600	77.2	31.8
650	48.9	
700	5.11	0.949

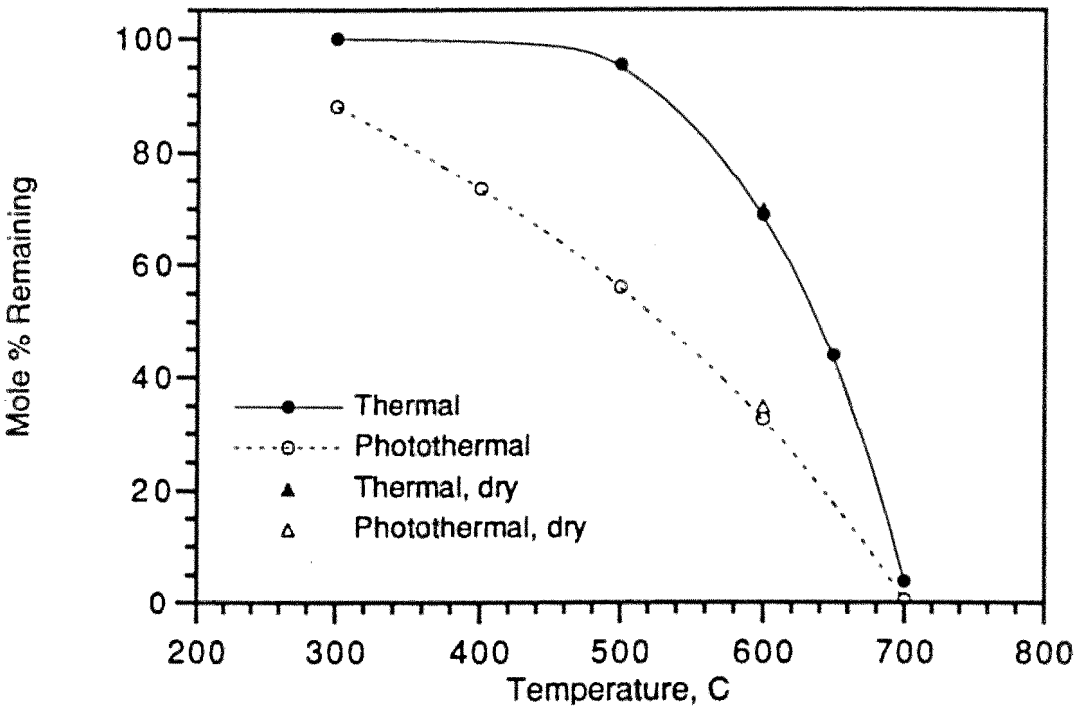

Figure 4.23. Summary of thermal and photothermal data for the trichloroethylene component of a TCE:Water:DCBz (1:20:1) mixture exposed to 0 and 17.6 W/cm^2 of xenon arc radiation for 10 sec in air. Data for the same mixture run without water (1:0:1) is also shown.

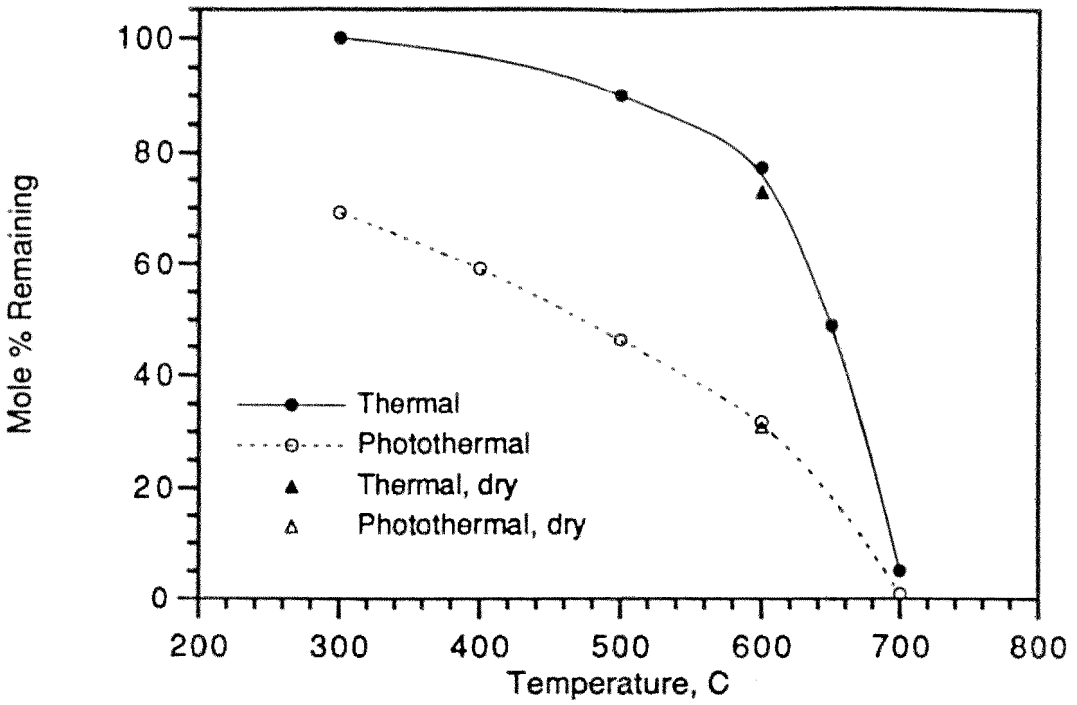

Figure 4.24. Summary of thermal and photothermal data for the o-dichlorobenzene component of a TCE:Water:DCBz (1:20:1) mixture exposed to 0 and 17.6 W/cm^2 of xenon arc radiation for 10 sec in air. Data for the same mixture run without water (1:0:1) is also shown.

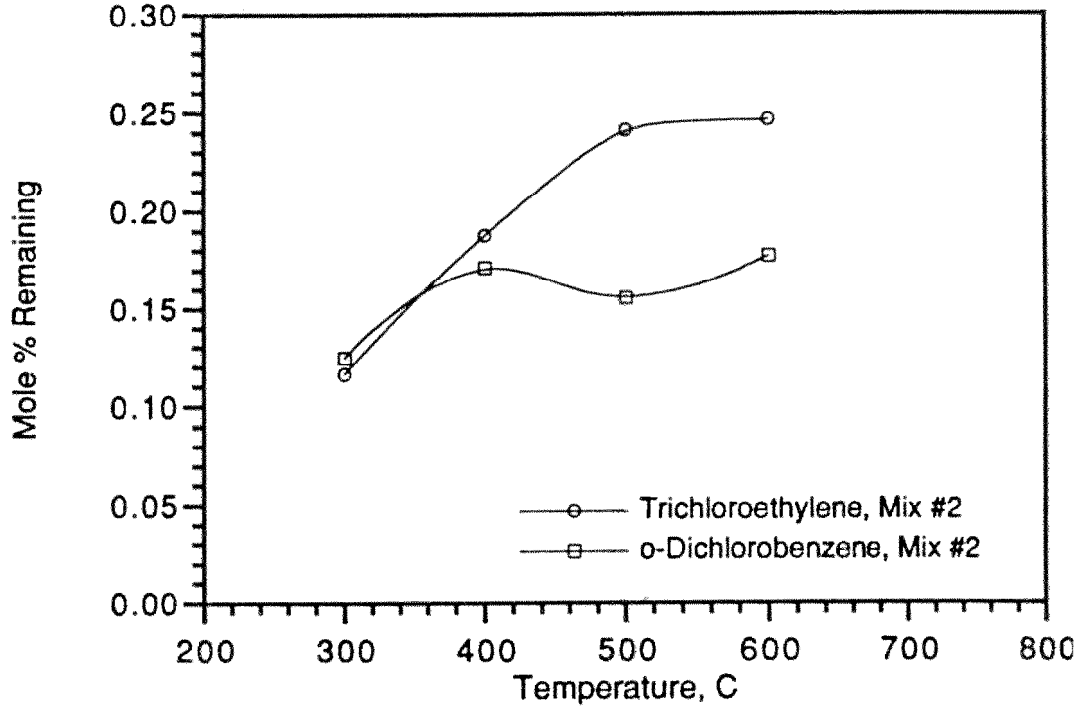

Figure 4.25. Summary of the photothermal quantum yields for the trichloroethylene and o-dichlorobenzene components of a TCE:Water:DCBz (1:20:1) mixture.

In contrast to Mixture #l, the quantum yield data for this formulation summarized in Figure 4.25 shows the quantum yield for DCBz is slightly higher in the mixture than the pure compound (ca. Figure 4.12) and that for TCE is somewhat lower (ca. Figure 4.4). These tests clearly illustrate that the behavior of mixtures can differ markedly from pure compound performance. Our experience has been that overall mixtures tend to be less stable than pure components, though this is not always the case. This emphasizes the need for feasibility studies to be a part of any scale-up plan

Mixture #3

A brief set of tests were conducted with a formulation identical to Mixture #2 except the water component was withheld giving a TCE:Water:DCBz ratio of approximately 1:0:l. It was hypothetically considered that the water vapor might be participating in the photothermal decomposition process in some indirect way such as acting as a radical scavenger or possibly reacting with ozone (which may have been formed photochemically in the reactor) to form hydroxyl radicals. The results from these tests for TCE and DCBz are summarized in Tables 4.19 and 4.20, and included in Figures 4.23 and 4.24, respectively. These data illustrate that the water vapor had essentially no effect on the thermal or photothermal process.

Table 4.19

Summary of LS-PDU Results For the Trichloroethylene Component of Mix #3
Exposed 10 sec in Air to 0 and 17.6 W/cm^2 Xenon Arc Radiation

Temperature	fr(0)	fr(17.6)
300°C	100%	
600	69.8	35.0%

Table 4.20

Summary of LS-PDU Results For the o-Dichlorobenzene Component of Mix #3
Exposed 10 sec in Air to 0 and 17.6 W/cm^2 Xenon Arc Radiation

Temperature	fr(0)	fr(17.6)
300°C	100%	
600	72.8	31.0%

4.8 BENZENE AND HYDROGEN PEROXIDE

A brief series of tests were performed with a mixture of benzene, hydrogen peroxide, and water vapor to determine if the photo-dissociation of hydrogen peroxide to hydroxyl radicals could provide a mechanism of photothermally destroying compounds through an indirect photothermal process. As shown in Table 4.2 the benzene:hydrogen peroxide:water ratio was approximately 1:3:13. Furthermore, control tests were conducted with an identical sample of benzene without hydrogen peroxide or water vapor.

The data for the hydrogen peroxide and control tests are summarized in Tables 4.21 and 4.22, respectively, and in Figure 4.26 with the quantum yield surnmarized in Figure 4.27. As these data illustrate, essentially no effect was observed in either the thermal or photothermal destruction of benzene. This was a rather surprising result in that the photochemical dissociation of hydrogen peroxide is a common process for decontaminating dilute aqueous waste streams. Thermal degradation of the hydrogen peroxide was considered unlikely as the control test was nearly identical to the mixture test. An examination of the UV absorption spectrum perhaps explains these results. As the spectrum in Figure 4.28 for hydrogen peroxide in water at 20°C shows this sample is an exceptionally weak absorber in the wavelength region of xenon arc emission (i.e., wavelengths greater than 230 nm). Indeed, it's nearly an order of magnitude weaker than chloroform (ca. Figure 3.1). Therefore, even if the quantum yield for the photo-dissociation of hydrogen peroxide were unity, the rate of reaction would be too slow to show significant conversion of benzene on the time scale used here. This problem may be overcome using other photo-initiators, radiation sources which reach further into the UV, or both.

Table 4.21

Summary of LS-PDU Results For Benzene in the Presence of Hydrogen Peroxide
Exposed 10 sec in Air to 0 and 17.6 W/cm^2 Xenon Arc Radiation

Temperature	fr(0)	fr(17.6)
300°C	100%	99.7%
400	100	
500	99.3	97.0
600	89.7	85.7
650	48.5	41.7
700	8.63	7.48

Table 4.22

Summary of LS-PDU Results For Benzene in the Absence of Hydrogen Peroxide Exposed 10 sec in Air to 0 and 17.6 W/cm^2 Xenon Arc Radiation

Temperature	fr(0)	fr(17.6)
300°C	100%	
650	48.4	41.5%

The quantum yield data for the benzene component of this mixture shown in Figure 4.27 illustrates the quantum yield for benzene is quite small, though it rapidly increases with temperature. Given that the conversion of benzene in the control sample was nearly identical to the mixture sample the results for the photothermal conversion and quantum yield reflect those for pure benzene.

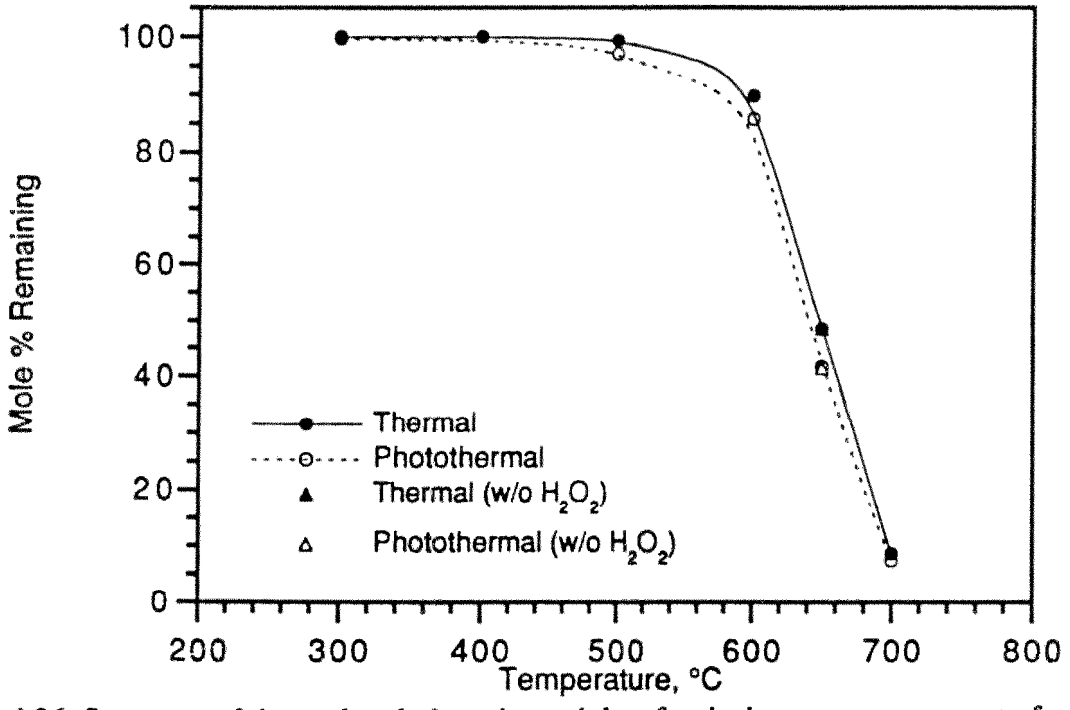

Figure 4.26. Summary of thermal and photothermal data for the benzene component of a Bz:H_2O_2:Water (1:3:13) mixture exposed to 0 and 17.6 W/cm^2 of xenon arc radiation for 10 sec in air. Data for the same mixture run without hydrogen peroxide or water (1:0:0) is also shown.

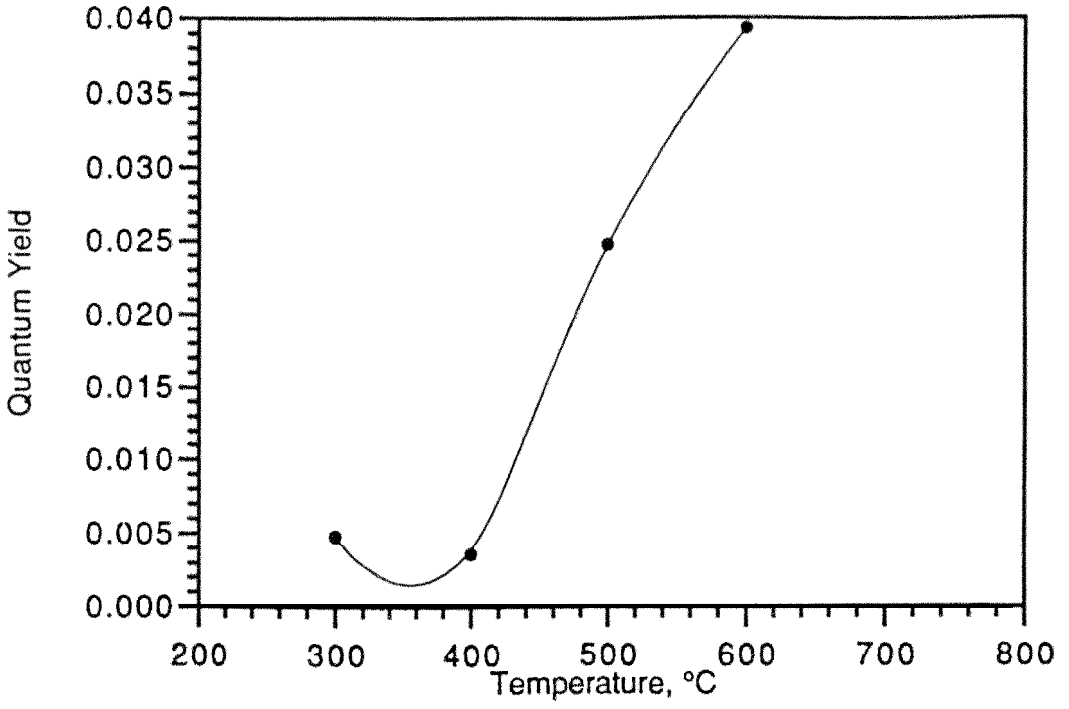

Figure 4.27. Summary of the photothermal quantum yields for the benzene component of a Bz:H_2O_2:Water (1:3:13) mixture.

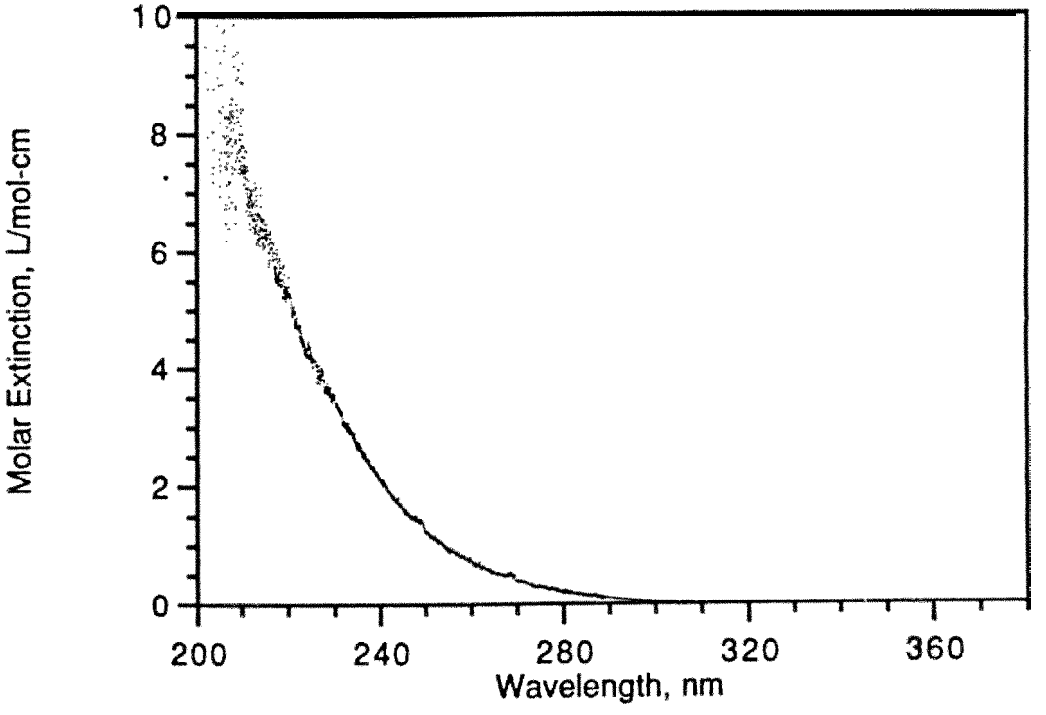

Figure 4.28. Absorption spectrum for hydrogen peroxide in water (referenced against water) at 20°C illustrating that this compound is a very weak absorber of UV radiation.

Table 4.23

Summary Of Photothermal Quantum Yields
For Samples Tested As Pure Compounds

Temp	TCE	PCE	MCBz	DCBz	TCDD
300°C	0.109	0.089	0.107	0.121	0.0219
400	0.217	0.123	0.109	0.125	0.0248
500	0.380	0.136	0.139	0.101	0.0212
550	0.551	---	---	---	---
600	0.409	0.158	0.163	0.160	---
650	0.423	---	---	0.180	---
675	---	---	---	0.330	---
700	---	---	---	0.426	---

Key to abbreviations; TCE Trichloroethylene
PCE Tetrachloroethylene
MCBz Monochlorobenzene
DCBz o-Dichlorobenzene
TCDD 1,2,3,4-Tetrachlorodibenzo-p-dioxin

Table 4.24

Summary Of Photothermal Quantum Yields
For Samples Tested As Mixtures

Temp	Bz	Tol	Eth Bz	Xyl	TCE #1	TCE #2	DCBz #1	DCBz #2
300°C	0.00482	0.0257	0.0652	0.0479	0.181	0.116	0.156	0.125
400	0.00646	0.0200	0.0635	0.0486	0.301	0.188	0.232	0.171
500	0.0245	0.0376	0.0785	0.0556	0.583	0.241	0.514	0.156
550	0.0705	0.129	0.256	0.180	0.581	---	0.322	---
600	0.211	0.393	0.634	0.435	0.412	0.246	0.263	0.177
650	0.167	0.274	0.413	0.252	---	---	---	---

Key to abbreviations; Bz Bezene component of BTEX
Tol Toluene component of BTEX
Eth Bz Ethyl benzene component of BTEX
Xyl m-Xylene component of BTEX
TCE #1 Trichloroethylene in mixture #1
DCBz #1 o-Dichlorobenzene in mixture #1
TCE #2 Trichloroethylene in mixture #2
DCBz #2 o-Dichlorobenzene in mixture #2

Table 4.25

Summary of Pseudo First-Order Thermal Oxidation Kinetic Parameters
Measured For The Test Compounds Used In This Project

Name	Frequency Factor	Activation Energy
Chloroform	4.30×10^{9} sec^{-1}	38.4 kcal/mol
Carbon Tetrachloride[1]	2.88×10^{5}	26.0
Trichloroethylene	2.40×10^{8}	37.0
Tetrachloroethylene[1]	2.57×10^{6}	33.0
Monochlorobenzene[1]	8.32×10^{4}	23.0
o-Dichlorobenzene	5.80×10^{18}	85.0
1,2,3,4-Tetrachlorodibenzo-p-dioxin	1.72×10^{4}	20.3
Benzene (BTEX)[2]	6.00×10^{9}	45.6
Ethyl Benzene (BTEX)[2]	1.61×10^{8}	36.6
Toluene (BTEX)[2]	3.36×10^{8}	38.9
m-Xylene (BTEX)[2]	1.49×10^{8}	36.3

[1]As sited in literature reference 5.
[2]As measured in a mixture of benzene, toluene, ethyl benzene, and m-xylene.

4.9 SUMMARY REMARKS

Overall, the breadth of applicability of the photothermal process illustrated by the LS-PDU results follows the same general order as the strength of UV absorption. If the pollutant absorbs the available UV radiation, the photothermal liability generally increases with chlorine substitution as well as the addition of other functional groups as demonstrated by the alkyl benzenes. These trends are in accord with accepted spectroscopic theory.

SECTION 5
PRODUCTS OF INCOMPLETE CONVERSION

An important aspect of any destruction process is its ability to convert the hazardous material to mineral products of complete conversion such as carbon dioxide, water vapor, and hydrogen chloride. Previous research on thermal destruction has shown that a common feature of the thermal decomposition of organic compounds is the production of organic products of incomplete conversion (PICs), or products of incomplete combustion as they are called in the incineration literature.[l0] Furthermore, it is frequently reported that conventional, low-temperature, direct photochemical processes produce complex mixtures of organic by-products in relatively high yields.[9] Therefore, it is important to demonstrate that the photothermal process is capable of completely mineralizing (convert to mineral products) the organic compounds of interest. In the course of obtaining the data discussed in Section 4, information was also collected on the formation of PICs from both the thermal and photothermal tests. Analysis of this data varied from general observations to detailed identification and quantification of individual PICs. This information is summarized in the paragraphs that follow grouped in a similar manner as the discussion in the previous sections.

5.1 ALKANES AND CHLORINATED ALKANES

As discussed above, the alkanes as a class are considered non-absorbing compounds, while the chlorinated alkanes as very weakly absorbing within the spectral range of xenon arc emission (i.e., wavelengths greater than 230nm). Photothermal destruction data for chloroform suggests that the rate of photon absorption for these compounds is so small that even if they had quantum yields of unity they would not respond well to the photothermal process using xenon arc radiation. For this reason only chloroform was examined as an example of this class, and an examination of the PICs from chloroform suggest a similar response for organic products.

Since chloroform was found to be a relatively poor responder to the photothermal process detailed quantification of products was not conducted. However, identifications were assigned using the mass spectral data and the relative yields calculated using the GC/FID response factor for chloroform. Furthermore, the relative yield for the product phosgene was calculated using the GC/MS response factor for chloroform. These data are summarized in Tables 5.1 and 5.2, and Figures 5.1 and 5.2, for the thermal and photothermal tests, respectively.

Table 5.1

Summary Of LS-PDU Data For Chloroform
Exposed For 10 sec In Air[1]

Temp(°C)	$CHCl_3$	$COCl_2$	CCl_4	C_2Cl_4	C_2HCl_5	C_2Cl_6
300	100	-	-	-	-	-
400	100	-	-	-	-	-
500	59.1	18.8	3.34	6.30	1.71	21.3
550	1.89	32.7	10.6	31.0	0.190	26.0
600	0.115	3.52	17.0	50.1	-	0.198

[1]Values are weight % remaining taken as $CHCl_3$. $COCl_2$ data is based on GC/MS data, all others are GC/FID; [Compound Response]/[$CHCl_3$ Response]$_0$x100%

Table 5.2

Summary Of LS-PDU Data For Chloroform Exposed
To 17.6 W/cm^2 Xenon Arc Radiation For 10 sec In Air[1]

Temp(°C)	$CHCl_3$	$COCl_2$	CCl_4	C_2Cl_4	C_2HCl_5	C_2Cl_6
300	100	-	-	-	-	-
400	97.4	-	-	-	0.0864	0.437
500	60.6	15.6	3.09	3.40	1.96	18.7
550	1.95	37.0	8.82	21.8	0.150	41.4
600	0.00735	5.45	18.9	20.9	-	0.258

[1]Values are weight % remaining taken as $CHCl_3$. $COCl_2$ data is based on GC/MS data, all others are GC/FID; [Compound Response]/[$CHCl_3$ Response]$_0$x100%

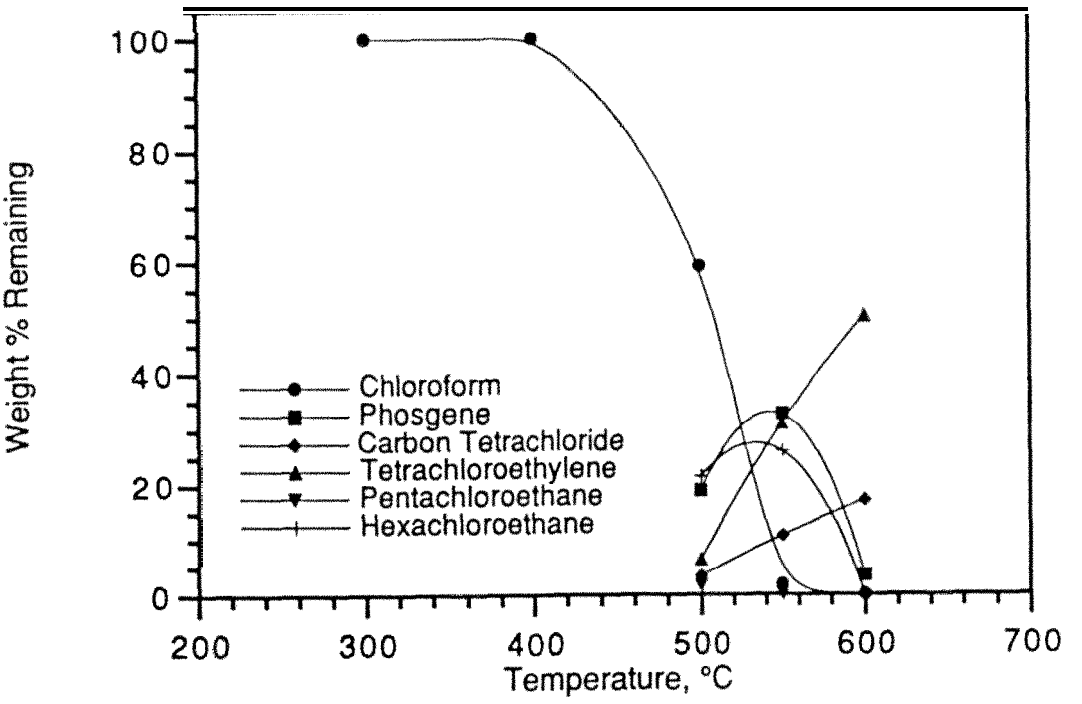

Figure 5.1. Summary of LS-PDU data far chloroform and its major PICs exposed for 10 sec in air. GC/FID response factors for all PICs except phosgene were taken as chloroform. Similarly, the GC/MS response factor for phosgene was taken as chloroform. Note the relative yields of tetrachloroethylene and carbon tetrachloride continue to increase at high temperature.

Reviewing the data presented in Tables 5.1 and 5.2, and Figures 5.1 and 5.2, shows similar behavior for most of the PICs from chloroform. Specifically, the PICs appear at the onset of decomposition (500°C thermally, and 400°C photothermally), reach a maximum yield at approximately 550°C, then quickly disappearing at higher temperatures. However, two PICs show a much different behavior. Specifically, in the thermal PICs tetrachloroethylene and carbon tetrachloride initially appear at much lower yields than the other PICs and continue to increase in yield even at high temperatures. This suggests these may in fact be PICs resulting, at least in part, from the decomposition of the other PICs. Interestingly, the yield of tetrachloroethylene is clearly suppressed at high temperature (i.e., 600°C), whereas the photothermal yield of carbon tetrachloride is not. This suggests that PICs may follow the same

trend observed in the conversion of the waste feed. Specifically, PICs which efficiently absorb UV radiation should be readily destroyed by the photothermal process while non-absorbing PICs may be more resistive to the process. Therefore, it would be unlikely to produce highly toxic, high molecular weight PICs (such as TCDD) from a photothermal system as these materials have been shown to be efficiently destroyed by the photothermal process.

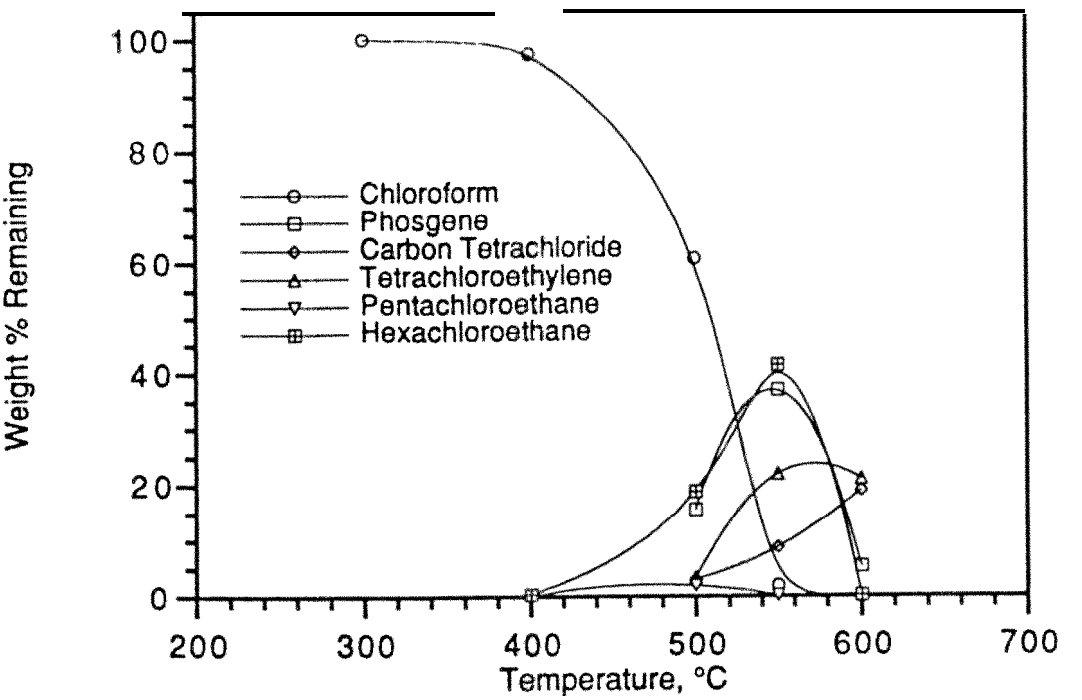

Figure 5.2. Summary of LS-PDU data for chloroform and its major PICs exposed to 17.6 W/cm^2 of xenon arc radiation for 10 sec in air. GC/FID response factors for all PICs except phosgene were taken as chloroform. Similarly, the GC/MS response factor for phosgene was taken as chloroform. Note the relative yield of tetrachloroethylene, which absorbs UV radiation, decreases at high temperature, while carbon tetrachloride, a weak UV absorber, continues to increase.

5.2 CHLORINATED ALKENES

In contrast to chloroform, which produced several major PICs, only two significant PICs were formed from the thermal and photothermal decomposition of trichloroethylene. Specifically, GC/FID analysis showed carbon tetrachloride as a major organic product, along

with phosgene as detected with the LS-PDU's GC/MS channel. In this case the yield of carbon tetrachloride was calibrated with an analytical standard. An attempt was made to calibrate the phosgene GC/MS response, but we were unable to establish a reproducible reference at the low concentrations required. These problems have been attributed to the high reactivity of this material with trace water present in the sample handling equipment. Note that the TCE data was taken prior to the chloroform data reported above for which an alternative semi-quantitative method for phosgene was used.

The mole % yield of carbon tetrachloride (normalized by the original amount of trichloroethylene) from the thermal and photothermal tests are summarized in Tables 5.3 and 5.4, and Figures 5.3 and 5.4, respectively. These data illustrate that the photothermal process produces this PIC in a yield comparable to the thermal process (18.9% versus 15.0%). This result is consistent with the results of the tests with chloroform described above. Specifically, the direct photolysis process may not be effective in suppressing PICs which do not efficiently absorb UV radiation. However, the data presented here shows that the photothermal process is capable of mineralizing this product at high temperatures, though this is likely due to thermal reactions.

Table 5.3

Summary Of LS-PDU Data For Trichloroethylene
Exposed For 10 sec In Air[1]

Temperature°C	Trichloroethylene	Carbon Tetrachloride
300	100	---
400	100	---
500	100	---
550	79.4	3.15
600	27.0	15.0
650	1.13	10.6
700	0.238	0.276

[1]Data are mole % remaining; [Compound]/[Trichloroethylene]$_0$x100%

Table 5.4

Summary Of LS-PDU Data For Trichloroethylene Exposed To 18.1 W/cm^2 Xenon Arc Radiation For 10 sec In Air[1]

Temperature,°C	Trichloroethylene	Carbon Tetrachloride
319	87.8	---
406	70.1	1.77
506	42.7	10.6
554	18.7	17.8
605	6.90	18.9
655	0.238	8.05

[1]Data are mole % remaining; [Compound]/[Trichloroethylene]$_0$x100%

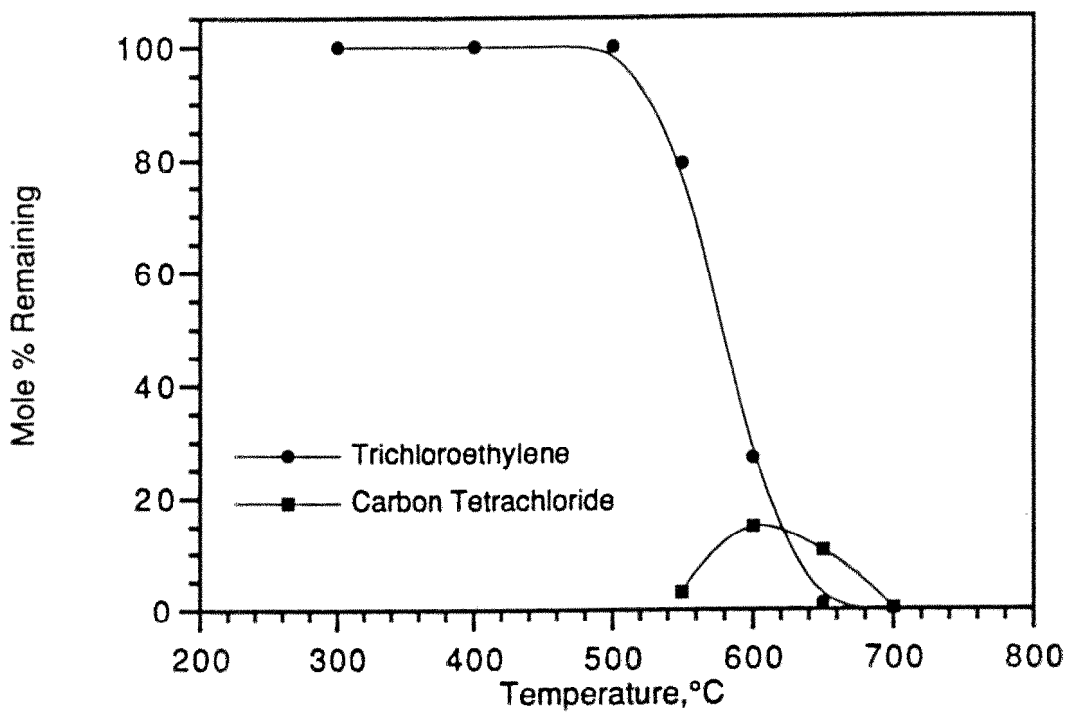

Figure 5.3. Summary of LS-PDU data for trichloroethylene and its major PIC exposed for 10 sec in air.

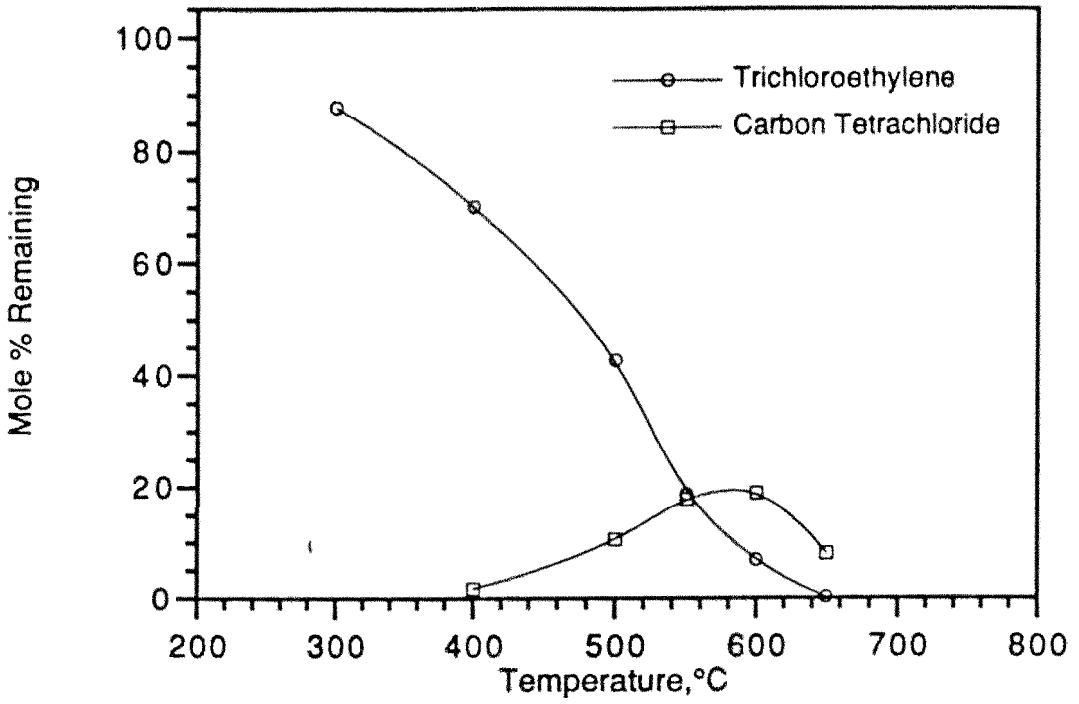

Figure 5.4. Summary of LS-PDU data for trichloroethylene and its major PIC exposed to 18.1 W/cm^2 of xenon arc radiation for 10 sec in air.

With respect to phosgene, although quantitative data is not available, qualitatively the results are similar to that for this PIC from chloroform. Specifically, the GC/MS data shows that phosgene is destroyed at high temperatures in a manner similar to the carbon tetrachloride.

It should be noted that PIC data was not obtained for tetrachloroethylene as this compound was run over a limited temperature range primarily to measure the photothermal quantum yield.

5.3 AROMATICS AND ARENES

During the period that the LS-PDU tests were being conducted on BTEX, the data system associated with the LS-PDU's GC/MS channel was not operating properly, so mass spectral information on PICs for this mixture are not available. However, general observations can be made by examining the GC/FID data from these tests. Example GC/FID traces from thermal exposures (300,600, and 700°C), and photothermal exposures (300,600, and 700°C) are shown in Figures 5.5 and 5.6, respectively.

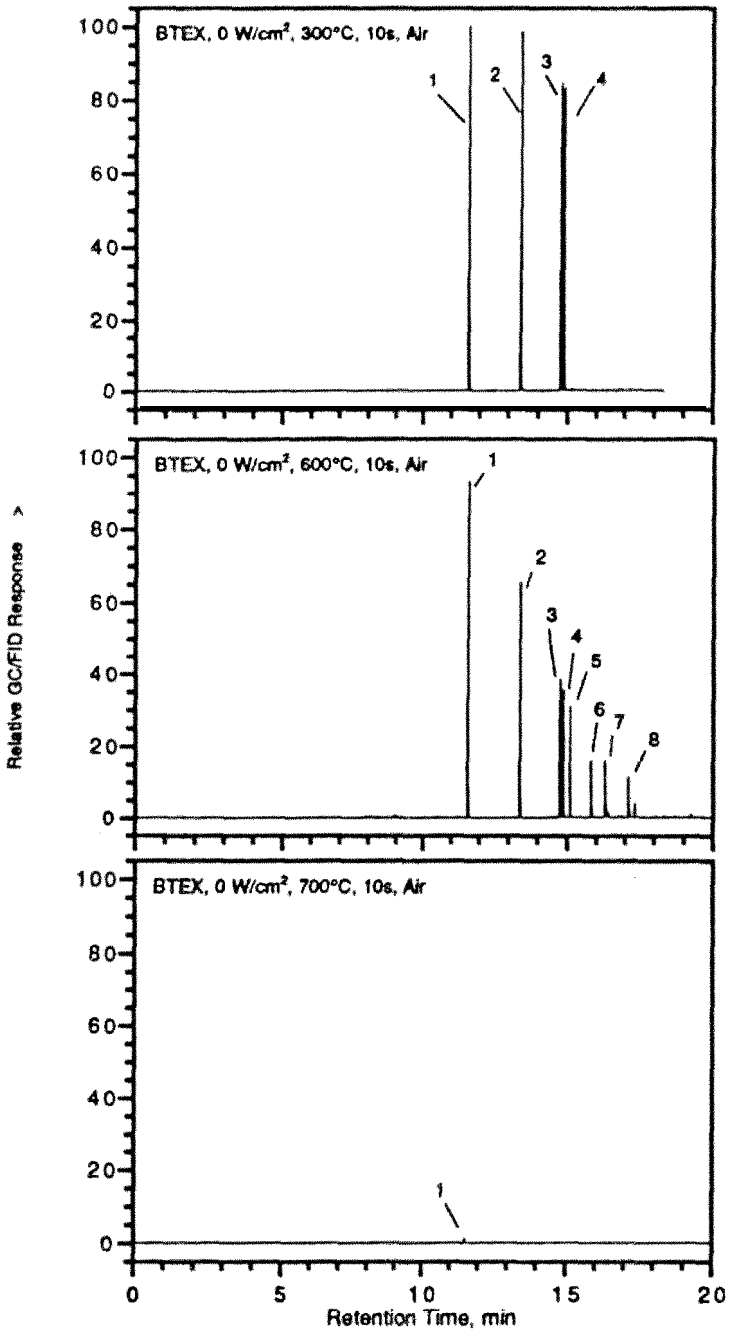

Figure 5.5. Example GC/FID chromatograms from BTEX exposed to 300, 600, and 700°C for 10 sec in air showing that benzene is the most stable component. 1) Benzene, 2) Toluene, 3) Ethyl Benzene, 4) m-Xylene, 5) PIC P1, 6) PIC P2, 7) PIC P3, 8) PIC P4.

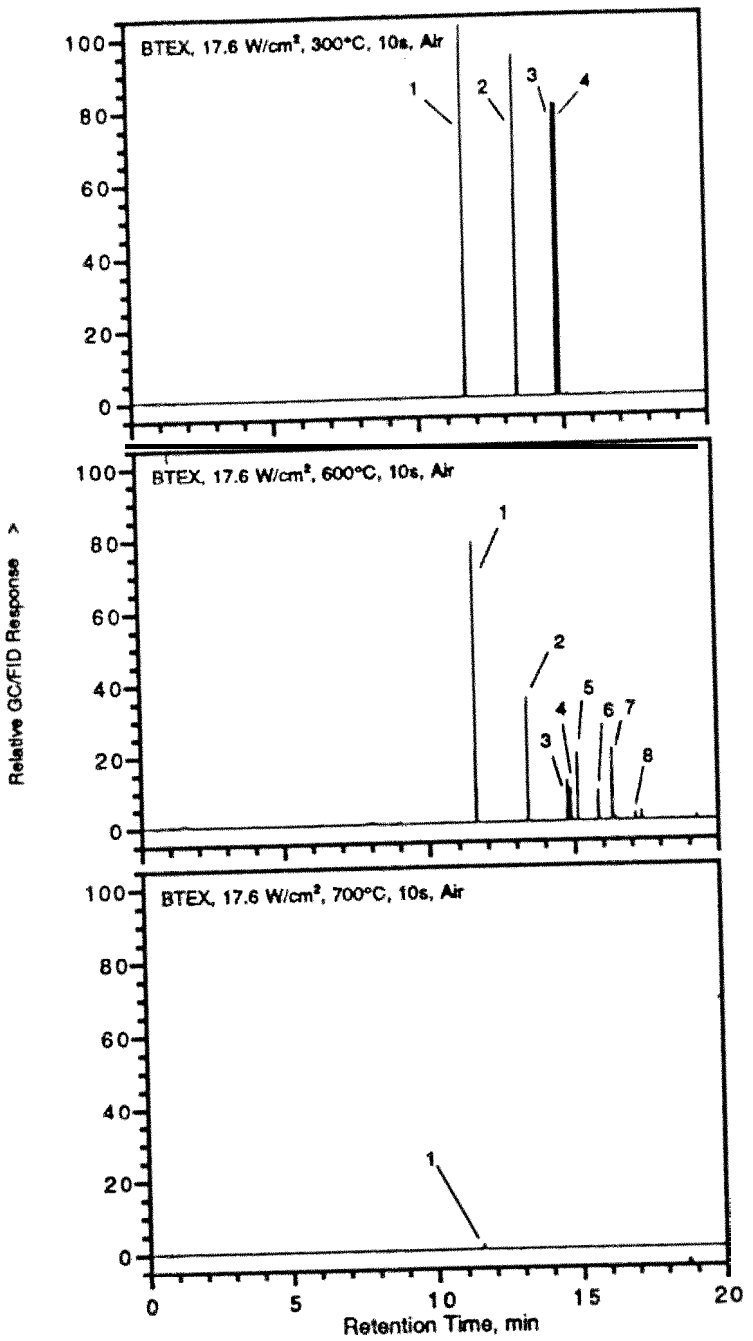

Figure 5.6. Example GC/FID chromatograms from BTEX exposed to 300, 600, and 700°C and 17.6 W/cm2 for 10 sec in air showing that benzene is the most stable component. 1) Benzene, 2) Toluene, 3) Ethyl Benzene, 4) m-Xylene, 5) PIC P1, 6) PIC P2, 7) PIC P3, 8) PIC P4.

These data illustrate that four relatively major (maximum yields on the order of 10%) organic products were formed. Furthermore, although specific identifications cannot be assigned to these PICs, labeled P1 through P4 in Figures 5.5 and 5.6, the chromatographic techniques used here (temperature-programmed using a non-polar liquid phase) suggests the molecular weight of these products increases in the order of P1 to P4, and that all are higher in molecular weight than the parent BTEX components. The general production and disappearance behavior of these PICs, taking their GC/FID response as benzene, are shown in Figures 5.7 and 5.8 for the thermal and photothermal tests, respectively. Comparing these figures shows behavior consistent with the discussion above. Specifically, the maximum PIC yields from the photothermal process are lower than for the thermal process, and the effect increases with molecular weight (i.e., the higher molecular weight PICs are destroyed or suppressed more efficiently than the lower molecular weight products). Furthermore, Figures 5.7 and 5.8 illustrate that the parent benzene component is far more stable than any of the organic PICs and should therefore serve as a suitable performance indicator for this mixture.

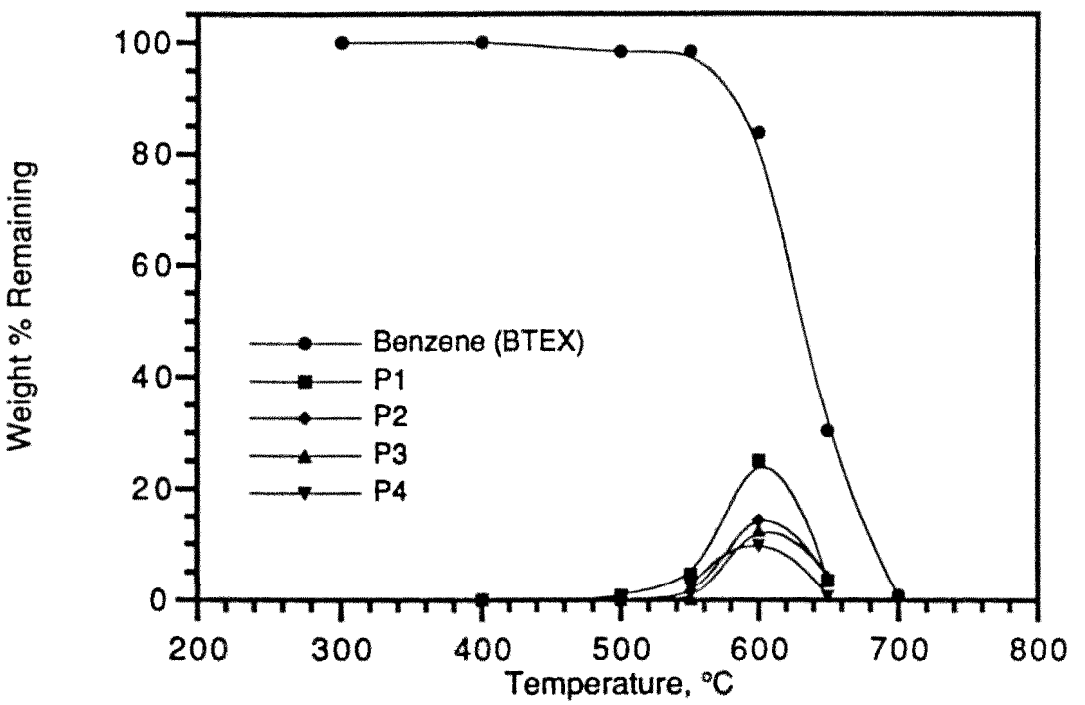

Figure 5.7. Summary of LS-PDU data for the benzene component of BTEX and the major PICs when BTEX is exposed for 10 sec in air. The data illustrates benzene is far more stable than any of the organic products. GC/FID response factors for all PICs were taken as benzene.

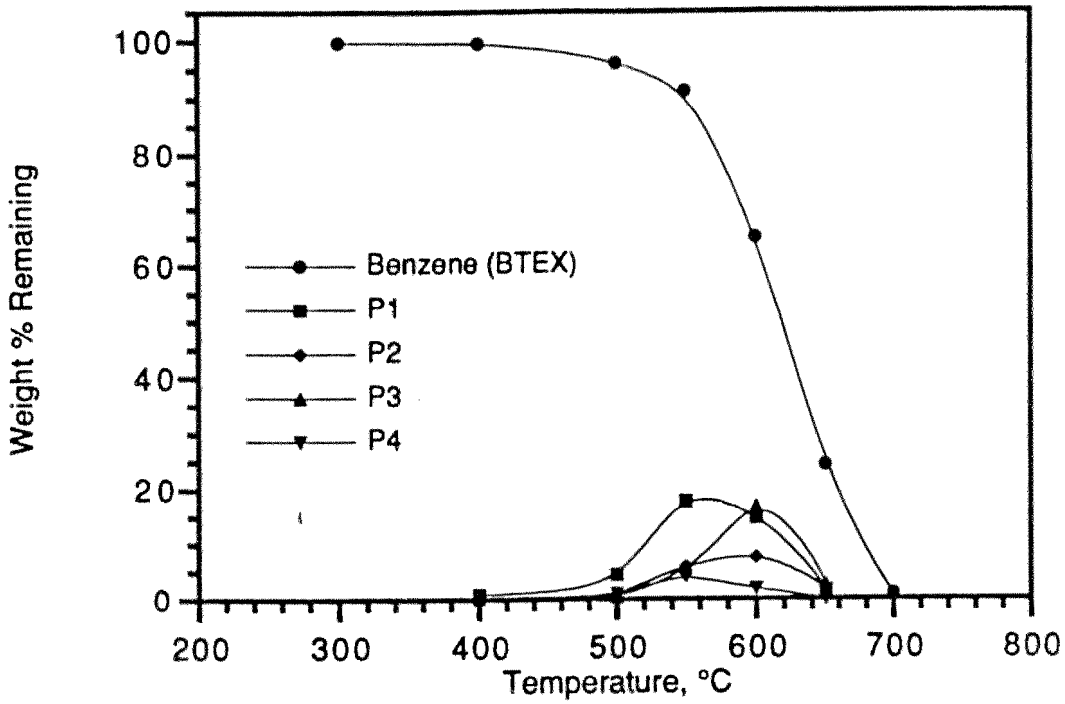

Figure 5.8. Summary of LS-PDU data for the benzene component of BTEX and the major PICs when BTEX is exposed to 17.6 W/cm^2 for 10 sec in air. The data illustrates benzene is far more stable than any of the organic products. GC/FID response factors for all PICs were taken as benzene.

5.4 CHLORINATED AROMATICS

The organic PIC data for o-dichlorobenzene is summarized in Tables 5.5 and 5.6, and in Figure 5.9 and 5.10 for the thermal and photothermal tests, respectively. These data illustrate that only two PICs, monochlorobenzene and 2-chlorophenol, where produced from this compound. Both of the observed products reached relatively small maximum yields under both thermal and photothermal conditions. Specifically, monochlorobenzene reached a maximum yield of approximately 1.05% (photothermal) and 1.07% (thermal), while 2-chlorophenol achieved a yield of 1.26% (photothermal) and 0.48% (thermal). Both products were efficiently destroyed at temperatures above 675°C.

As **in the case of tetrachloroethylene,** PIC data was not obtained for monochlorobenzene as this compound was run over a limited temperature range primarily to measure the photothermal quantum yield.

Table 5.5

Summary Of LS-PDU Data For o-Dichlorobenzene
Exposed For 10 sec InAir[1]

Temperature, °C	o-Dichlorobenzene	Chlorobenzene	2-Chlorophenol
300	100	---	---
400	100	---	---
500	100	0.0236	0.0509
600	100	0.116	0.167
625	87.8	0.3396	0.25 1
650	67.8	0.734	0.482
675	33.5	1.07	0.314
700	0.406	0.0142	---

[1]Data are mole % remaining; [Compound]/[o-Dichlorobenzene]$_0$x100%

Table 5.6

Summary Of LS-PDU Data For o-Dichlorobenzene Exposed
To 18.1 W/cm^2 Xenon Arc Radiation For 10 sec In Air[1]

Temperature, °C	o-Dichlorobenzene	Chlorobenzene	2-Chlorophenol
300	71.3	---	0.513
400	69.6	0.124	0.781
500	66.3	0.468	1.15
600	46.6	0.925	I.26
650	27.0	1.05	0.469
675	5.84	0.301	0.0480
700	0.0397	---	---

[1]Data are mole % remaining; [Compound]/[o-Dichlorobenzene]$_0$x100%

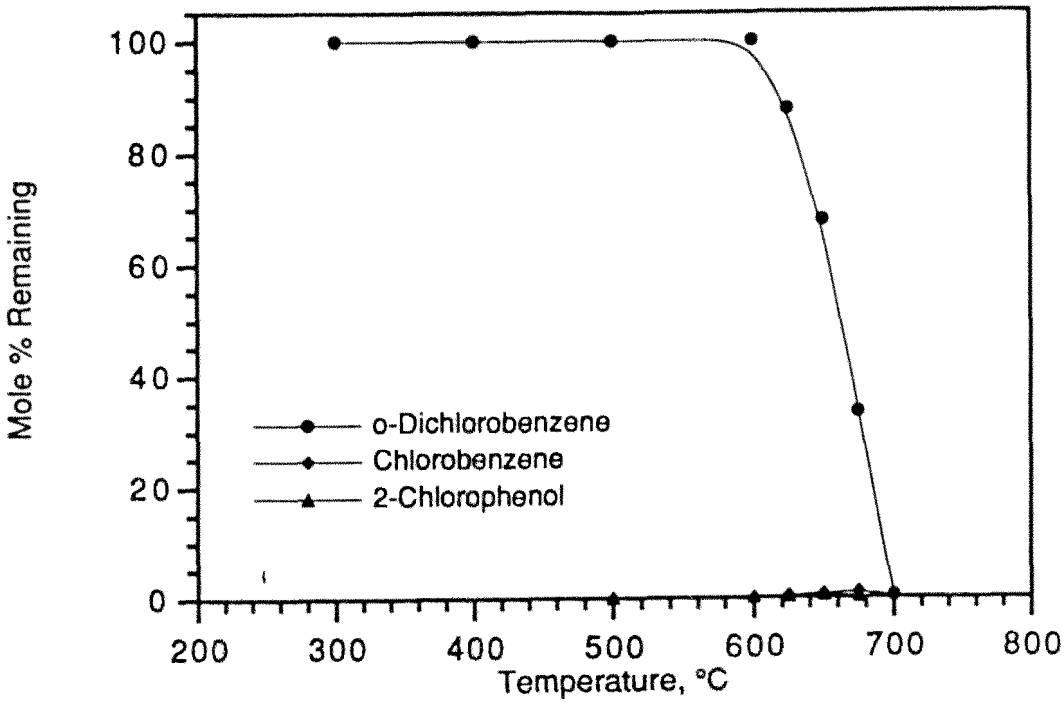

Figure 5.9. Summary of LS-PDU data for o-dichlorobenzene and its major PICs exposed for 10 sec in air showing the relatively small yield of the organic products.

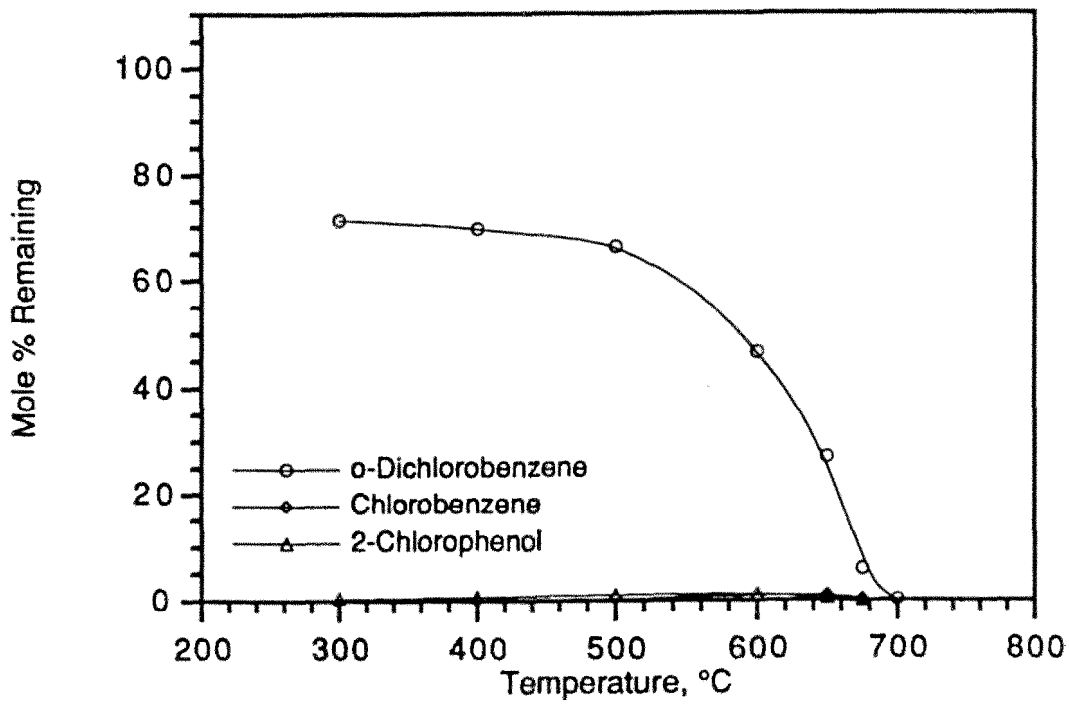

Figure 5.10. Summary of LS-PDU data for o-dichlorobenzene and its major PICs exposed to 18.1 W/cm^2 for 10 sec in air showing the relatively small yield of the organic products.

5.5 CHLORINATED DIBENZO-P-DIOXINS

The LS-PDU tests on TCDD wererelatively brief and consequently detailed PIC analysis was not conducted. However, examination af the GC/FID data daes show a general perspective on the production of PICs from this compound. The LS-PDU GC/FID traces from a thermal exposure at 300°C (100% remaining), 600°C (35.4% remaining), and a photothermal exposure at 600°C (0.0285% remaining) are summarized in Figure 5.11. The 600°C thermal data shows the production of numerous PICs which often accompany the thermal decomposition of organic compounds. This is an interesting example in that it is one of the few cases where the LS-PDU reactor can be operating in a dominantly photothermal mode (i.e., where there is very high photothermal conversion, but limited thermal conversion) and the photothermal trace clearly shows that not only is the parent TCDD destroyed under these conditions, but nearly all of the associated products as well. Recall that the LS-PDU's cold trap is operated at -160°C, so that all but the lightest organic products are collected and analyzed. This emphasizes that the photothermal process differs significantly from conventional direct photochemical processes (i.e., near-ambient temperature processes that act directly on the contaminants without the use of sensitizers or catalysts) in that photothermal decomposition reactions lead to the complete mineralization of the waste feed. [11, 12, 13, 14]

5.6 MIXTURES OF TCE, DCBz, AND WATER VAPOR

Mix #1

As shown in Table 4.2 the initial concentrations of TCE and DCBz in the LS-PDU reactor were 300 and 51.9 ppm (58:1), respectively. Given that the concentration of TCE is 58 times greater than DCBz it is not surprising that the decomposition chemistry is dominated by TCE. This is clearly illustrated in Tables 5.7 and 5.8, and Figures 5.12 and 5.13, which summarizes the thermal and photothermal data, respectively, taking the initial concentration of TCE as the basis for comparison. Indeed, on this scale the DCBz is shown as a minor component that quickly drops below the level of interest (99% conversion) following a photothermal exposure.

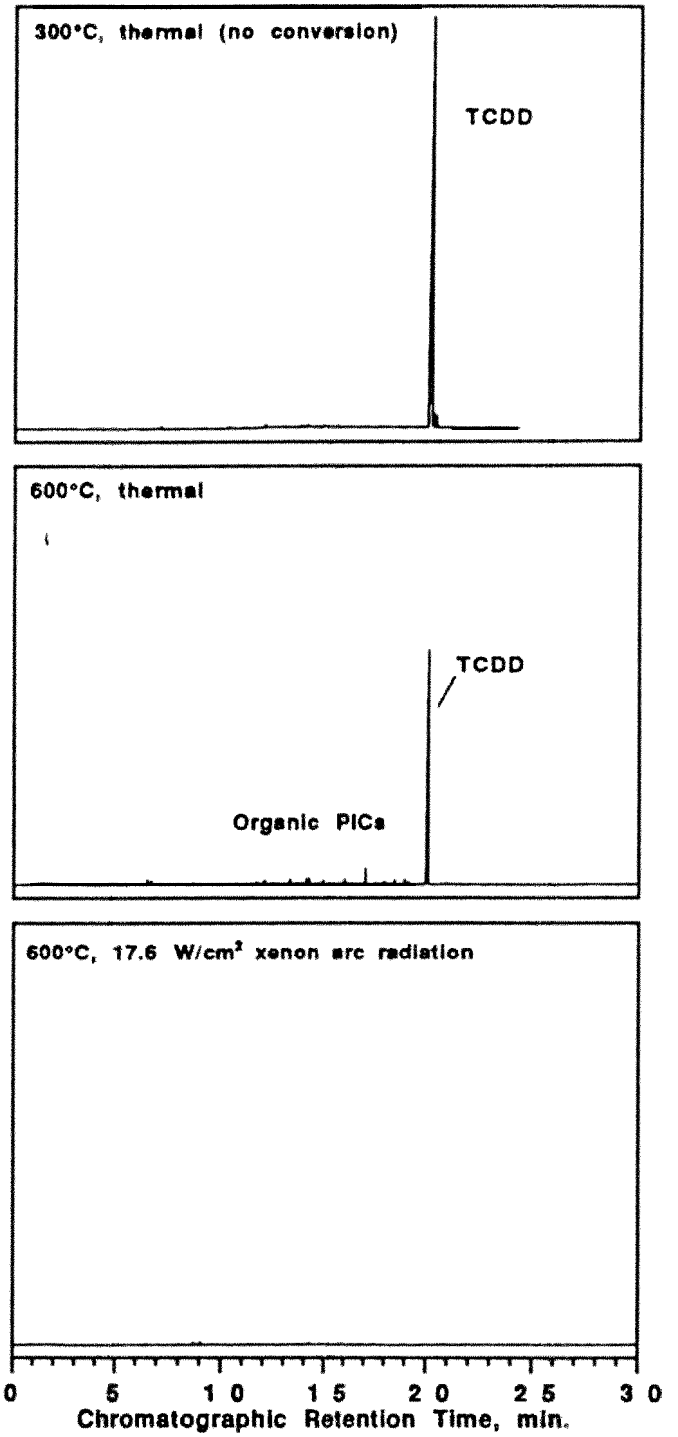

Figure 5.11. Example GC/FID chromatograms from TCDD exposed to 300 thermal, 600 thermal, and 600°C photothermal (17.6 W/cm^2) for 10 sec in air showing that the photothermal process destroys the complex mixture of PICs as well as the parent compound.

Table 5.7

Summary Of LS-PDU Data For TCE/DCBz/Water Mixture #1
Exposed For 10 sec In Air[1]

Temperature,°C	Trichloroethylene	o-Dichlrobenzene	Carbon Tetrachloride
300	100	1.83	---
400	100	1.83	---
500	70.6	1.23	0.447
550	35.1	0.520	2.58
600	5.58	0.291	4.24
650	0.339	0.149	2.40
700	0.0385	0.0309	0.212

[1]Data are mole % remaining; $_{i}$[Compound]/[Trichloroethylene]$_0$x100%

Table 5.8

Summary Of LS-PDU Data For TCE/DCBz/Water Mixture #1
Exposed To 17.6 W/cm^2 Xenon Arc Radiation For 10 sec In Air[1]

Temperature,°C	Trichloroethylene	o-Dichlrobenzene	Carbon Tetrachloride
300	82.0	1.15	0.156
400	60.9	0.899	0.714
500	19.5	0.136	2.85
550	7.68	0.117	4.09
600	1.61	0.0780	3.90
650	0.0962	0.0571	2.12
700	---	0.0169	0.0933

[1]Data are mole % remaining; [Compound]/[Trichloroethylene]$_0$x100%

As shown in Tables 5.7 and 5.8, and Figures 5.12 and 5.13, carbon tetrachloride was the only organic product produced in significant yield. Specifically, the thermal and photothermal yields both reached approximately 4% between 550 and 600°C. This contrasts sharply with the data reported earlier for TCE decomposed as a pure compound where the maximum yields of carbon tetrachloride were from approximately 15% (thermal) and 19% (photothermal). This reduction in yield may result from the additional hydrogen sources (i.e., o-dichlorobenzene and water) providing a stable "sink" for the chlorine providing a more favorable pathway for the formation of hydrogen chloride versus carbon tetrachloride. These data also show that the yield of carbon tetrachloride is only slightly affected by the photothermal exposure. Once again, this is consistent with observations discussed above on weakly absorbing compounds.

As in the earlier work with TCE as a pure compound, phosgene was observed in the GS/MS traces, but was not quantified.

Mix #2

Recall that a second formulation of the **TCE/DCBz/Water** mixture was tested in which the relative molar concentration of TCE and DCBz were approximately the same (1: 1). Interestingly, when the data from this mixture was analyzed with respect to PICs, no major organic PICs were found. This is consistent with the results comparing the PIC yields from TCE tested as a pure compound versus Mixture #l. Specifically, the yield of the major organic product carbon tetrachloride may be reduced by the presence of a hydrogen source, in this case DCBz. This illustrates that the composition of a mixture can influence the relative stability of the parent compounds and the yield of PICs. This suggests that treatability studies be conducted in conjunction with the first field trials to make a determination of the potential for PIC formation.

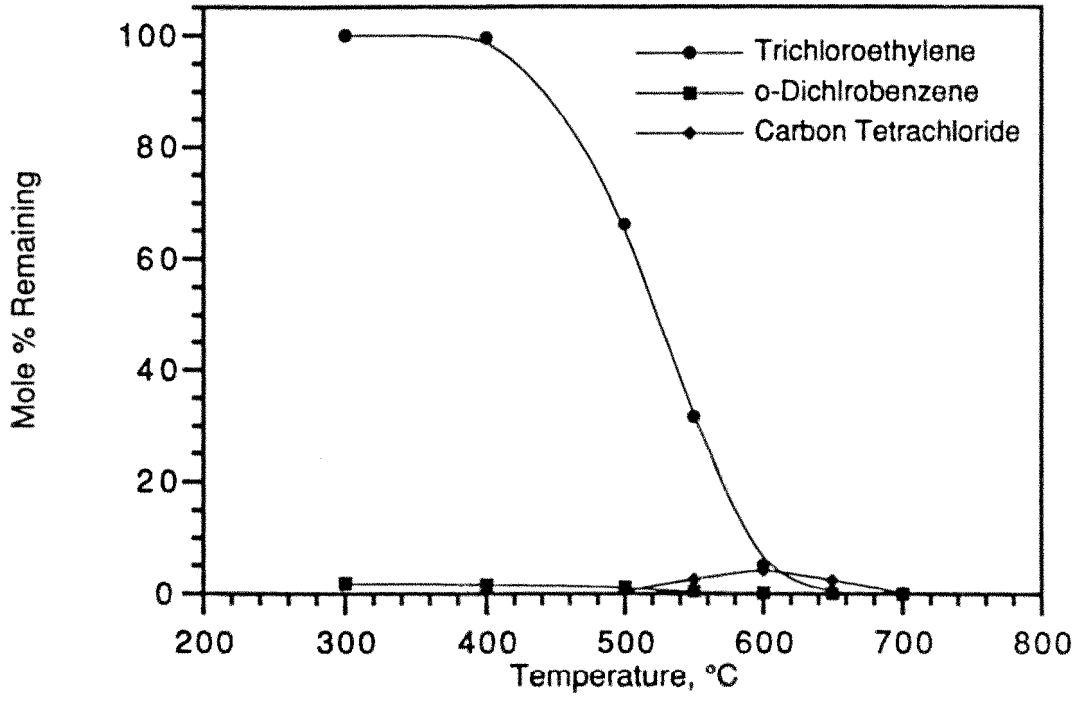

Figure 5.12. Summary of LS-PDU data for the trichloroethylene and o-dichlorobenzene components of a TCE/DCBz/water mixture exposed for 10 sec in air showing the relative yield of carbon tetrachloride, the only major organic product from this mixture.

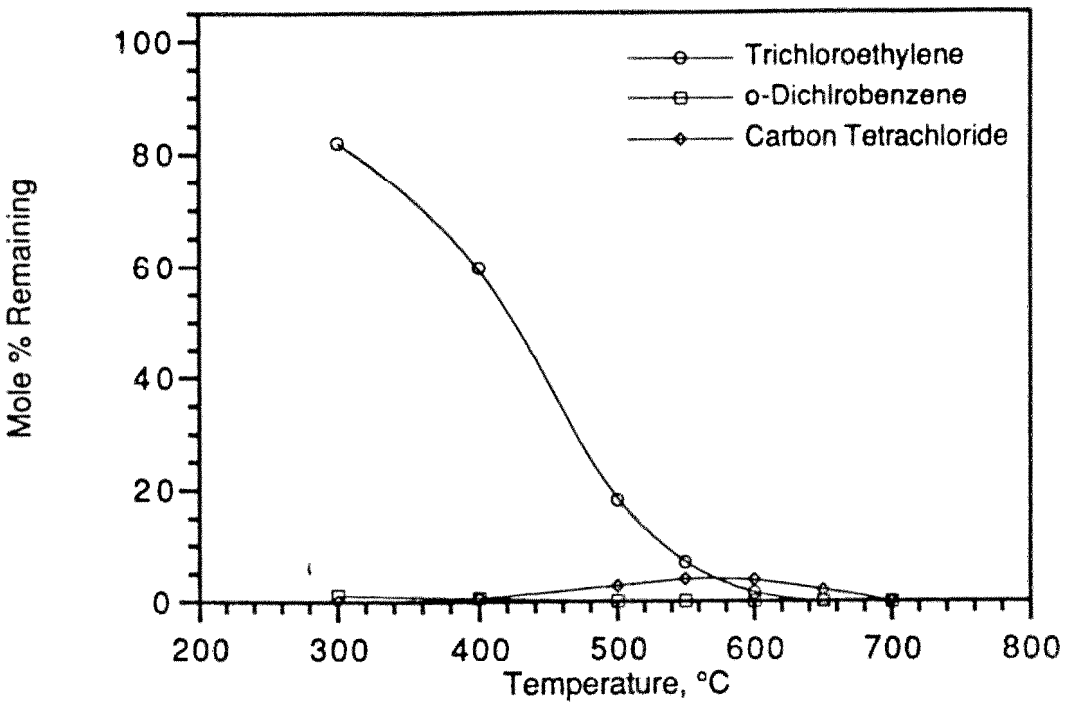

Figure 5.13. Summary of LS-PDU data for the trichloroethylene and o-dichlorobenzene components of a TCE/DCBz/water mixture exposed to 17.6 W/cm^2 of xenon arc radiation for 10 sec in air taking the initial concentration of TCE as the basis for comparison showing the relative yield of carbon tetrachloride, the only major organic product from this mixture.

5.7 SUMMARY

The discussion above shows that unlike conventional, low-temperature photochemical detoxification, the photothermal process is capable of destroying organic PICs which may be formed. Furthermore, the process is particularly effective in destroying PICs which absorb near-UV radiation. Also the data for TCDD, in which the LS-PDU destroyed the test compound very efficiently at a relatively low temperature, illustrates that the photothermal process is capable of destroying PICs when the reactor is operating in a predominately photothermal mode. Clearly, the photothermal process does not proceed through simple, stepwise dehalogenation as is often the case in conventional, low-temperature photochemical reactions.

One major product observed in these tests which is of particular interest is phosgene, $COCl_2$. Phosgene has been reported as a major product from low-temperature decomposition processes, and understanding its production and developing methods for its destruction are

important because of its relatively high toxicity. One possible reason for the high yields of phosgene in these, and similar tests, is that at the relative low temperatures used here, the major mineral carbon product is carbon monoxide rather than carbon dioxide. Furthermore, the decomposition of compounds with large amounts of chlorine relative to hydrogen is molecular chlorine rather than hydrogen chloride. Therefore, it is likely the phosgene is being produced by the reaction of carbon monoxide with molecular chorine as;

$$CO + Cl_2 \text{---} > COCl_2 \qquad (5.1)$$

This may explain why phosgene has not been observed from the decomposition of compounds like chloro- and dichlorobenzene where the major chlorine product is hydrogen chloride rather than chlorine. Therefore, it is likely that phosgene production may not be a problem in actual waste streams as long as there is an ample hydrogen source available. In circumstances where a waste contains a relatively large amount of compounds containing chlorine atoms and an insufficient source of compounds containing hydrogen atoms it may be possible to efficiently destroy the phosgene by reacting it with added water as;

$$COCl_2 + H_2O \text{--} > CO_2 + HCl \qquad (5.2)$$

In a full-scale system this could easily be achieved by the water which is naturally present in most process streams or injecting water into the feed stream. Since the mixture tests suggests that there is certainly no adverse effect of the presence of water vapor, the suppression of phosgene in a full-scale system should not present a significant problem.

In summary, as with the applicability to the types of waste feed, the only PICs which will present a significant challenge to the photothermal process are those which do not absorb UV radiation effectively. This suggests that radiation sources with the shortest possible UV radiation be used. Furthermore, the mixture test results illustrate that the mixture components can significantly alter PIC yields. This suggests that feasibility studies be conducted as a part of any scale-up activities to determine the probability of PIC formation.

SECTION 6

BASIC DESIGN FOR THE PROTOTYPE PDU

With the data presented in the preceding sections there is now a sufficient body of knowledge available to embark on the design of a prototype PDU. This discussion begins with a review of the potential radiation sources that may be used in a large-scale PDU and the selection of a specific illumination system for the prototype unit. The geometry of the reactor vessel which encloses the illumination system to form the basic reactor unit is discussed as well as how the configuration of this unit affects its performance. Finally, the overall configuration is examined to arrive at a specific proposed design. From this design the capital and operating costs are estimated.

6.1 LAMP SELECTION

Reviewing the commercial literature on industrial illumination systems shows that there are several types of lamps that are possible candidates for the prototype PDU. These include lamps such as mercury, xenon, mercury-xenon, low, medium, and high pressure, short arc and linear, continuous and flash lamps. Investigation of these lamps included reviewing the technical literature from American Ultraviolet Co., Hanovia, ILC Technology, Ushio Inc., and VBI Technologies and discussions with various technical representatives. The important characteristics considered included spectral distribution and relative UV output, total output, geometry, and service life. The primary candidates considered were high-energy short-arc lamps (recall this type of lamp is used in the LS-PDU), flash lamps, and linear medium-pressure mercury arc lamps. All three types of lamps offered relatively high output in the range of 10+ kW, but there were increasing concerns about service life of the short arc and flash lamps in the higher power ranges and there were concerns about these types of lamps being able to operate in a high temperature environment for long periods of time. Furthermore, most production short arc

lamps are relatively inefficient generators of UV radiation The flash lamps do much to overcome this problem, but suffer from relatively short service life. In contrast, mercury arc lamps offer relatively long service life (often greater than 2,000 hours), efficiently produce UV radiation, and should be able to operate at relatively high temperatures. Taking all these factors into consideration medium pressure mercury arc lamps were selected for the design of the prototype PDU.

The emission spectrum for a Havonia medium pressure mercury lamp delivering a nominal 1 W/cm^2 is shown in Figure 6.1. The emission spectrum for a comparable xenon arc lamp is also shown. This illustrates the principal differences between the xenon arc lamp used on the LS-PDU and the mercury arc lamps being considered for the prototype PDU. In the former anly about 2.5% of the total output is in the UV at wavelengths shorter than 300 nm and it is spread out as a continuous emission. In contrast, medium-pressure mercury lamps emit approximately 15% of their energy at these short wavelengths and is concentrated in several discrete emission bands. The significant improvement in the photon absorption rate constants of selected organic compounds using mercury versus xenon arc radiation is illustrated by the values given in Tables 6.1 and 6.2, respectively, for 1 W/cm^2 radiation from each source. The values in these tables may be used to calculate the photon absorption rate constant at other radiant intensities by using an appropriate scaling factor. Comparing these data shows an average 10 fold increase in photon absorption rate constant illustrating that as a radiation source mercury arc is clearly superior to high pressure xenon arc.

Hanovia produces mercury arc lamps for conventional photochemical and UV curing applications in a variety of sizes. Their largest lamps are rated at 200 and 300 W/in and can deliver total radiant energy on the order of 15 kW with nominal arc lengths of up to 75 and 50 in., respectively. Furthermore, the envelope temperature of these lamps is typically on the order of 800°C illustrating that they should be capable of operating in the high temperature environment of the PDU and their geometry should permit a relatively even illumination of the PDU interior.

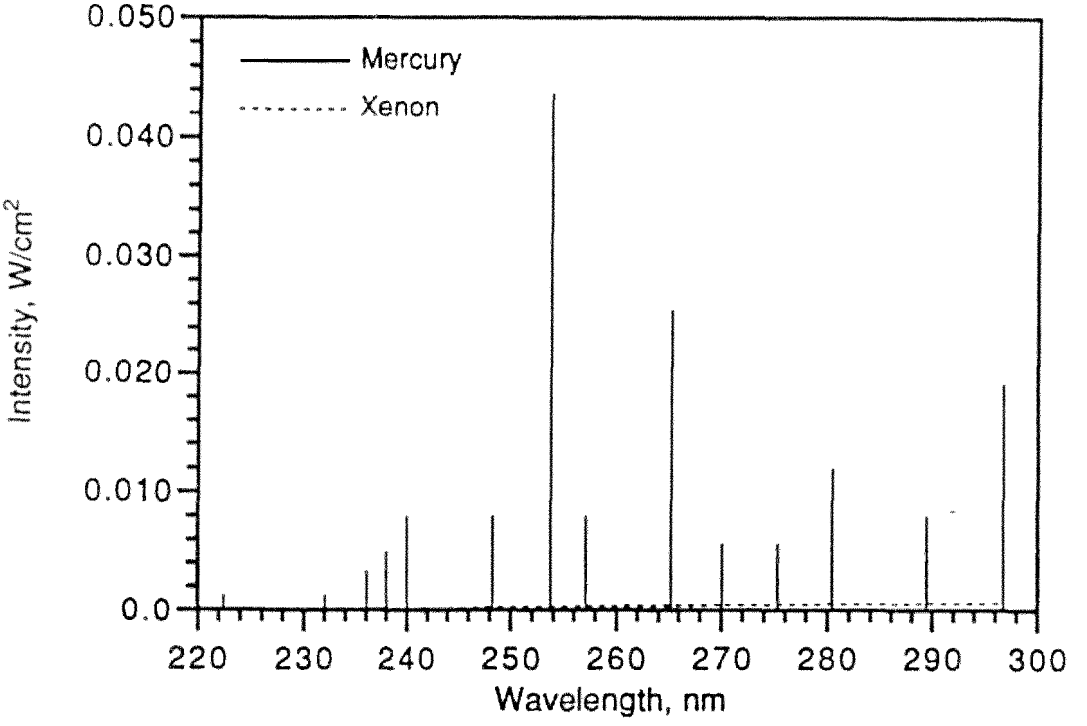

Figure 6.1. Comparison of the radiant intensity as a function of wavelength for 1.0 W/cm^2 of high pressure xenon and medium pressure mercury arc radiation illustrating that the radiation from the latter is concentrated in several high intensity bands in the UV.

Table 6.1

Photon Absorption Rate Constants Using 1 W/cm^2 Medium Pressure Mercury Arc Illumination

Temp	Clfrm	Ctet	TCE	PCE	Bz	MCBz	DCBz	Tol	EthBz	Xyl	TCDD
100°C		8.37e-4	3.21e-2		3.04e-2						
200	9.94e-5	1.58e-3	6.66e-2	2.84e-1	3.57e-2	6.12e-2	9.11e-2	6.67e-2	6.61e-2	8.33e-2	
300	3.63e-4	3.57e-3	9.44e-2	3.91e-1	4.24e-2	7.13e-2	1.14e-1	7.22e-2	7.38e-2	8.64e-2	7.85e0
400	9.63e-4	5.39e-3	1.38e-1	4.55e-1	4.95e-2	7.26e-2	1.23e-1	7.66e-2	7.94e-2	9.23e-2	7.80e0
500	2.91e-3	8.49e-3	1.76e-1	5.58e-1	5.49e-2	8.79e-2	1.80e-1	8.20e-2	8.55e-2	1.06e-1	1.10e1
600		1.51e-2	2.37e-1	6.12e-1	5.43e-2	1.05e-1	2.25e-1	7.89e-2	1.10e-1	1.14e-1	

Table 6.2

Photon Absorption Rate Constants Using 1 W/cm^2 Xenon Arc Illumination

Temp	Clfrm	Ctet	TCE	PCE	Bz	MCBz	DCBz	Tol	EthBz	Xyl	TCDD
100°C		4.93e-5	1.95e-3		2.05e-3						
200	6.67e-6	9.00e-5	4.13e-3	1.76e-2	2.78e-3	6.65e-3	1.41e-2	6.36e-3	6.13e-3	9.45e-3	
300	2.26e-5	1.99e-4	5.89e-3	2.75e-2	3.37e-3	8.02e-3	1.59e-2	7.20e-3	7.26e-3	1.10e-2	8.62e-1
400	5.30e-5	3.89e-4	8.81e-3	3.23e-2	4.49e-3	8.80e-3	1.64e-2	8.13e-3	8.35e-3	1.21e-2	9.78e-1
500	2.36e-4	6.59e-4	1.19e-2	4.36e-2	5.10e-3	1.15e-2	2.30e-2	9.50e-3	9.16e-3	1.44e-2	1.44e0
600		1.18e-3	1.62e-2	4.88e-2	6.23e-3	1.35e-2	2.69e-2	1.04e-2	1.36e-2	1.70e-2	

Key to abbreviations:

Clfrm	Chloroform
Ctet	Carbontetrachloride
TCE	Trichloroethylene
PCE	Tetrachloroethylene
Bz	Benzene
MCBz	Monochlorobenzene
DCBz	o-Dichlorobenzene
Tol	Toluene
EthBz	Ethyl Benzene
Xyl	m-Xylene
TCDD	1,2,3,4-Tetrachlorodibenzo-p-dioxin

6.2 BASIC REACTOR VESSEL DESIGN

With the illumination system selected, the design of the vessel which will house the radiation source can be designed. To begin it is informative to examine the radiation distribution around the lamp. To make this calculation a relatively simple model was developed to describe the radiation distribution surrounding a linear radiation source. The starting point for this model examines the radiation distribution about a point source. This point source model is then extended to a linear source by considering the latter as a line of point sources.

Examining the radiant intensity from a single point in a weakly absorbing media it can be shown that;

$$I = P/(4\pi d^2) \qquad (6.1)$$

where I is the radiant intensity (W/cm^2) at distance d (cm) from a point source radiating with a power of P (W). For a linear source consisting of n point sources, Equation 6.1 becomes;

$$I = \Sigma(P_i/(4\pi d_i^2)) \qquad (6.2)$$

where the summation is carried out over the length of the source. Therefore, the total radiation at any point in space near a linear source is taken as the sum of the intensity contributions from the individual points along the source. If each point source is considered to have the same power, Equation 6.2 simplifies to;

$$I = \Sigma(1/d_i^2)P_e/4\pi \qquad (6.3)$$

where P_e is the power (W) from a single element in the source. Equation 6.3 is the general model for calculating the radiant intensity as any point in space around a linear source (Equation 6.3 may actually be used for nearly any source as long as the appropriate function for d_i is used). Applying this simple model to a 15 kW, 200 W/in lamp gives the results summarized in Figure 6.2. This Figure illustrates that the radiant intensity drops off relatively quickly as the distance from the lamp increases. This would suggest a reactor vessel of narrow dimensions to keep the reactants as close to the lamp as possible. Furthermore, the radiant intensity diminishes quickly past the ends of the lamp, suggesting the length of the reactor be limited to approximately the length of the arc.

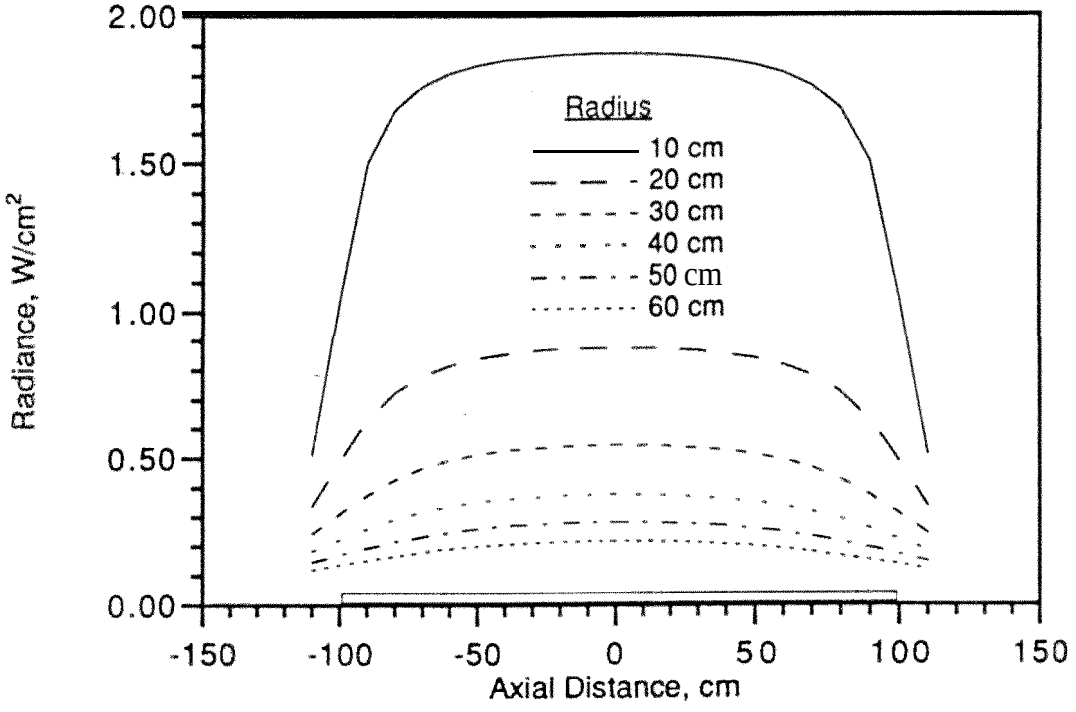

Figure 6.2. Radiant intensity as a function of radial and axial position from a 200 W/in. medium pressure mercury arc lamp with a nominal arc length of 200 cm (79 in.) illustrating that the radiant intensity is nearly constant over the length of the lamp and decreases rapidly off the ends of the arc. This suggests the PDU reactor vessel should not be significantly longer than the lamps.

The model for the intensity at a single point can be extended to an average intensity if the vessel is well mixed. Specifically;

$$I_{avg} = \Sigma I_i/n \qquad (6.4)$$

where I_{avg} is the average intensity (W/cm^2), I_i is the intensity at a single point (W/cm^2), n is the total number of points, and the summation is carried out throughout the volume of interest. This calculation was carried out for a cylindrical vessel with a fixed length of 250 cm enclosing a single 200 W/in lamp with a nominal arc length of 200 cm located on the vessel axis. The radiant intensity was calculated at points spaced 2.5 cm apart throughout the volume of the vessel. Points within 5 cm of the arc were excluded from the average to take into account the size of the tube which will enclose the lamp. The results, summarized in Figure 6.3, show that the mean radiant intensity decreases as the vessel radius increases. This is consistent with a simple cylindrical model where the wall (with surface area given by π(diameter)(length)) is evenly illuminated, losses out the ends are neglected, and the cylinder is of fixed length. For the perspective of designing a reactor with a high radiant intensity this again suggests a narrow reactor vessel.

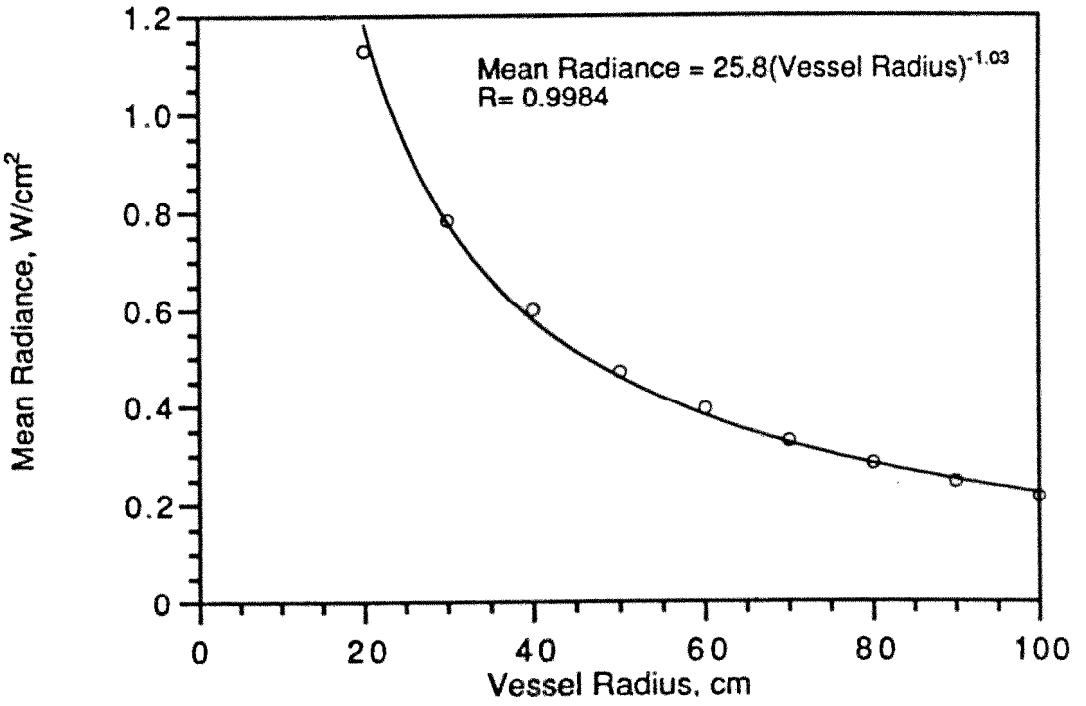

Figure 6.3. Mean radiant intensity as a function of vessel radius for a PDU chamber measuring 250 cm long enclosing a single 200 W/in. medium pressure mercury arc lamp with a nominal 200 cm arc showing that the mean radiant intensity decreases as the chamber radius increases.

Examining the plug flow reactor performance model given in Equation 1 .1shows that the radiant intensity (embodied in the photon absorption rate constant, k_{ab}) is one of two parameters directly affected by the vessel geometry, the second being the mean residence time, t. Specifically, the mean residence time may be expressed as;

$$t = V/F \tag{6.5}$$

where t is the mean residence time (sec), V is the volume of the reactor vessel (m^3), and F is the flow rate through the vessel (m^3/sec). In the case of a cylindrical reactor vessei;

$$t = \pi R^2 l/F \tag{6.6}$$

where R is the radius of the vessel (m) and l is the length (m). This shows that the mean residence time is proportional to the square of the vessel radius if the vessel length is constant. Taking into consideration that the mean radiance is proportional to the reciprocal of vessel radius, the product of rate of absorption and mean residence time (ca. Equation 1.1) should increase linearly with radius. Hence, the overall reactor performance should increase exponentially with vessel radius and even though the radiant intensitydecreases with the radius of the vessel, the overall performance model suggests a vessel of large diameter.

One consequence of a relatively large reactor is that it is possible to include more than ane lamp within the vessel, The impact of multiple lamps on the radiant intensity can be calculated by extending the simple model for a single lamp (Equation 6.3) as:

$$I = \Sigma\Sigma(1/d_i^2)P_e/4\pi \tag{6.3}$$

where the summations are carries out for each location i and each lamp j. This calculation was carried out for a cylindrical vessel with a diameter of 120 cm and a length of 250 cm enclosin g lamps rated at 200 W/in with a nominal arc length of 200 cm located on a 30 cm radius from the vessel axis, The results, summarized in Figure 5.4, show that the mean radiant intensity increases approximately linearly with the number of lamps. This suggests that a single chamber may include several lamps if necessary and the increase in radiant intensity will be approximately proportional to the number of lamps.

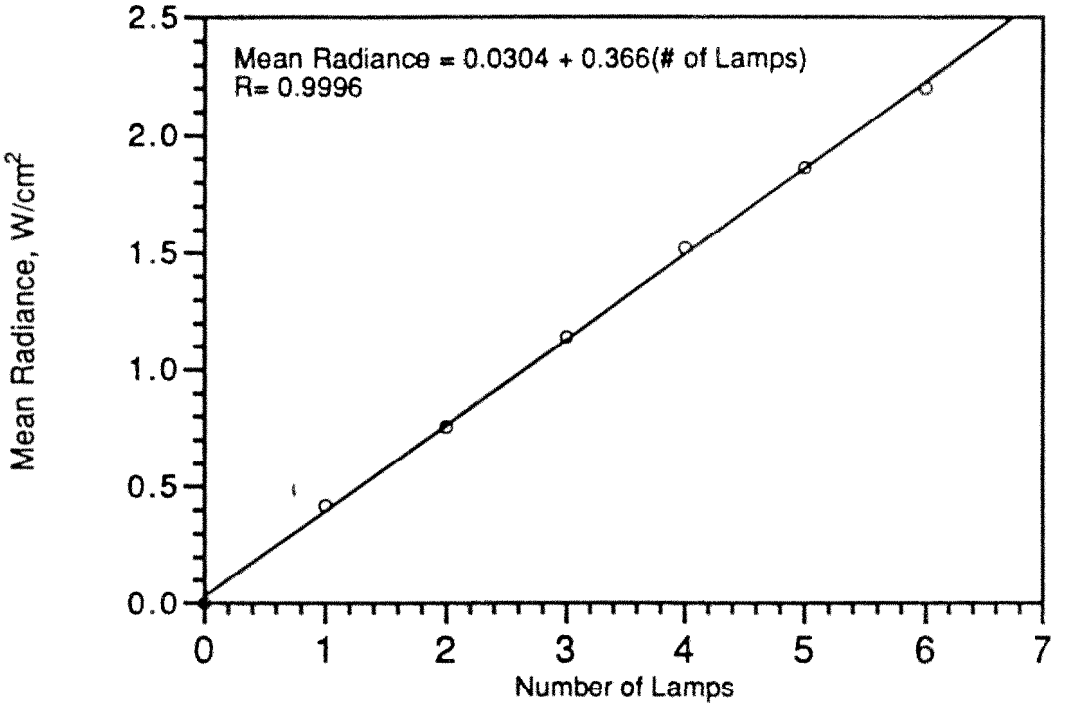

Figure 6.4. Mean radiant intensity as a function of the number of lamps for a PDU chamber measuring 250 cm long and 120 cm in diameter enclosing 200 W/in. medium pressure mercury arc lamps with a nominal 200 cm arc mounted on a 30 cm radius from the vessel axis showing that the mean radiant intensity increases approximately linearly with the number of lamps.

When considering a design with multiple lamps it is of interest to consider the placement of the lamps within the vessel. In this case the vessel described above for the multiple lamp calculations was modeled with 4 lamps mounted on a centerline radius that varied from 10 to 50 cm. The results are summarized in Figure 6.5, which illustrate the mean radiant intensity is a weak function of lamp location until the lamps are mounted close to the vessel wall where the intense radiation near the lamps is assumed to be absorbed by the non-reflecting surface of the vessel. This suggests that the system performance will not be overly sensitive to position of the lamps as long as they are somewhat centrally located and not mounted near the vessel wall.

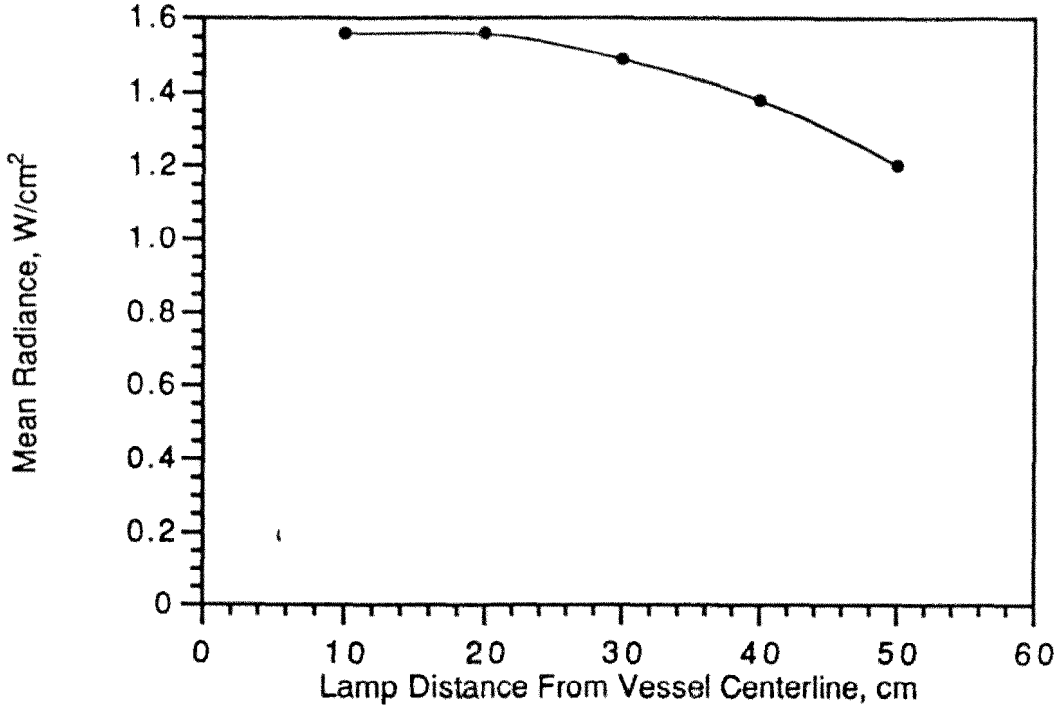

Figure 6.5. Mean radiant intensity as a function of the radius on which the lamps are mounted for a PDU chamber measuring 250 cm long and 120 cm in diameter enclosing four 200 W/in. medium pressure mercury arc lamps with a nominal 200 cm arc showing that the mean radiant intensity decreases as the lamps are mounted closer to the vessel walls which are assumed to be non-reflective.

In summary, there are several factors to be considered in designing the prototype PDU. Specifically, the type and size of lamps, the size and geometry of the reactor vessel, and the number and placement of the lamps within the vessel and each of these elements can be altered to meet a required specification. In general, however, the discussion above suggests using linear mercury arc lamps housed parallel to the axis of a cylindrical vessel which is only marginally longer than the arc length and of relative large diameter. A conceptual schematic for such a vessel is shown in Figure 6.6. Now that a basic reactor system has been established, the laboratory data can be used to predict the performance of this, and similar systems.

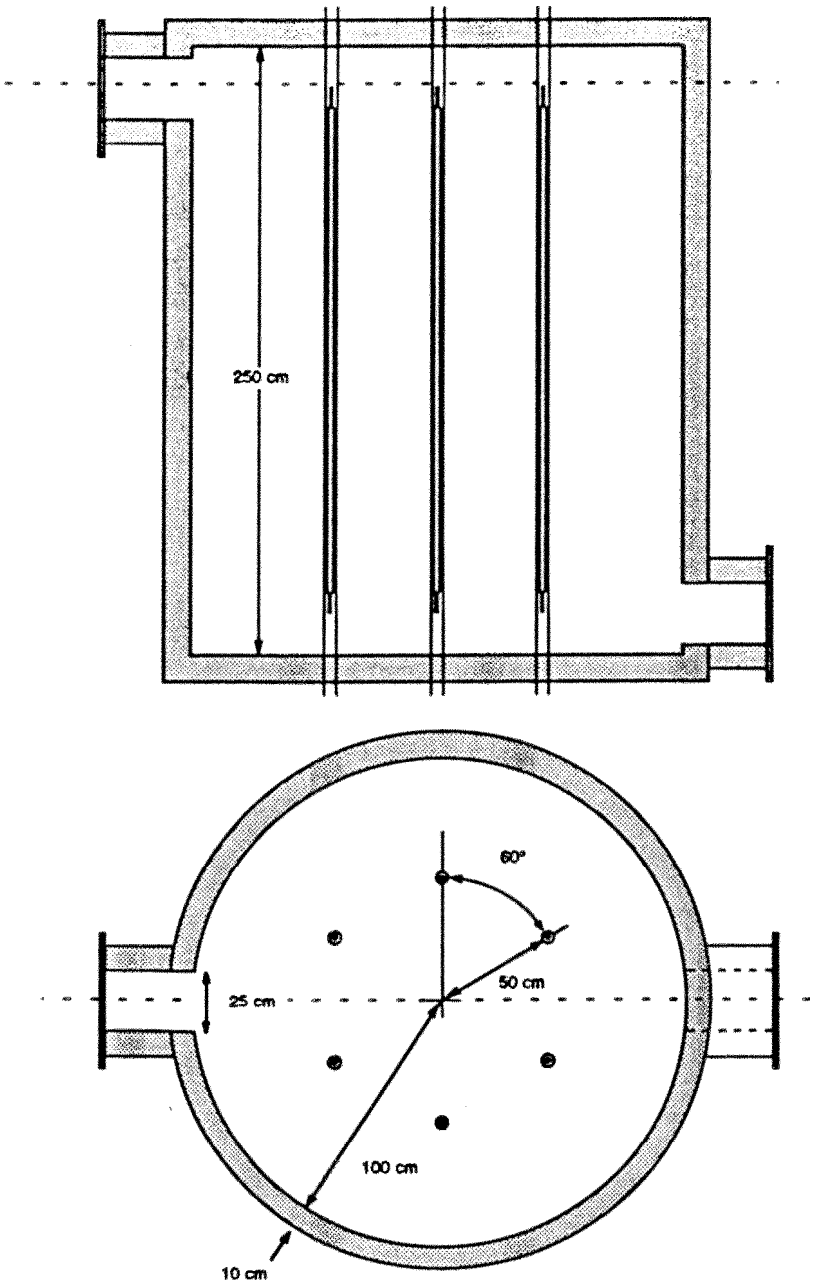

Figure 6.6. Basic design for a prototype PDU chamber based on the laboratory tests with the LS-PDU and ***assuming the use*** of six 200 W/in. medium pressure mercury arc lamps with a nominal arc length of 200 cm. Measuring 200 cm in diameter and 250 cm long, the vessel would have an internal volume of approximately 270 ft^3 and a mean radiant intensity of 1.23 W/cm^2.

6.3 PREDICTED PDU REACTOR PERFORMANCE

A diagram of a basic PDU reactor vessel is given in Figure 6.6. This Figure shows a PDU reactor vessel housing six medium pressure mercury arc lamps with a nominal arc length of 2 m. The vessel is 250 cm long and 200 cm in diameter giving an internal volume of approximately 8 m^3, or 270 ft^3. With the lamps mounted on a 50 cm radius and delivering 200 W/in, the mean radiant intensity would be 1.23 W/cm^2. In the paragraphs that follow the predicted performance of a PDU based on this design is discussed.

Recall that the performance model presented in Equation 1.l is applicable to a plug flow reactor (PFR). However, it is difficult to envision the flow through the reactor shown in Figure 6.6 behaving in a plug flow manner. Therefore, it is inappropriate to use a plug flow model. Indeed, since this model gives the highest theoretical conversion it would predict overly optimistic performance and lead to a design which would give disappointing results. In the extreme case the reactor performance may approach that of a completely stirred tank reactor (CSTR) where the performance is described by;

$$fr = \{1 + [(k_{gnd} + \phi k_{ab})t]\}^{-1} \qquad (6.6)$$

In practice it is likely that the actual flow through the reactor will be intermediate between the extremes of PFR and CSTR. Fortunately, the intermediate regime can be readily described using established models such as the tanks-in-series (TIS) model;

$$fr = \{1 + [(k_{gnd} + \phi k_{ab})t/N]\}^{-N} \qquad (6.7)$$

where N is the equivalent number of "tanks" (CSTR elements) needed to correctly describe the residence time distribution of the reactor system. The advantage of this model is that by appropriately selecting the value for N, any residence time distributions from plug flow (N of infinity) to completely mixed flow (N of unity) can be modeled.[l5] Using the pseudo first order rate parameters and photothermal quantum yields from the tests with the LS-PDU, the absorption spectra from the HTAS, and the emission spectrum from the lamp manufacture, Equations 1.7 (for the calculation of k_{ab}) and 6.7 can be used to predict the overall reactor performance.

Taking TCE as an example, the PDU performance was estimated using the reactor design shown in Figure 6.6. Based on our experience with reactors of similar geometry, the residence time distribution through the PDU vessel was taken as equivalent to two "tanks" (i.e., setting N equal to 2 in Equation 6.7). The model results are summarized in Figure 6.7 as the time required to achieve 99% conversion at 300, 400, 500, and 600°C as a function of the number of PDU chambers operating in series. This Figure clearly illustrates that the system performance increases rapidly with increasing temperature and by operating several chambers in series. With respect to the latter, these results show that as the number of chambers increases the overall system performance rapidly approaches that of a PFR. Indeed, from the perspective of time required to reach a specified level of conversion, there is only marginal improvement above 4 chambers, suggesting from a performance standpoint a PDU system should consist of at least 4 chambers. From a capacity standpoint the PDU can be easily scaled by adding additional chambers in series, or sets of chambers in parallel.

The model results presented in Figure 6.7 can also be expressed in terms of system capacity expressed as the volumetric flow rate of gas through the system. Specifically;

$$C = (VN'/t_{99})(T_{ref}/T_{PDU}) \qquad (6.8)$$

where C is the system capacity (cfm), V is the volume of each PDU chamber (270 ft^3), N' is the number of chambers, t_{99} is the time required to reach 99% destruction (min), T_{ref} is the temperature of the reference state (°K), and T_{PDU} is the mean temperature of the PDU (°K).

Equation 6.8 was used to predict the overall system capacity for a PDU based on the chamber illustrated in Figure 6.6 processing materials selected from the laboratory tests. The reference temperature was taken as 293°K (20°C). The results for TCE and PCE are shown in Figure 6.8 and 6.9, the components of BTEX in Figures 6.10, 6.11, 6.12, and 6.13, MCBz and DCBz in Figures 6.14 and 6.15, and for TCDD in Figure 6.16. These model results illustrate that the overall system capacity increases nearly linearly with the number of chambers. Therefore, from a capacity standpoint the size of the PDU may be scaled by simply adding the required number of chambers to the system.

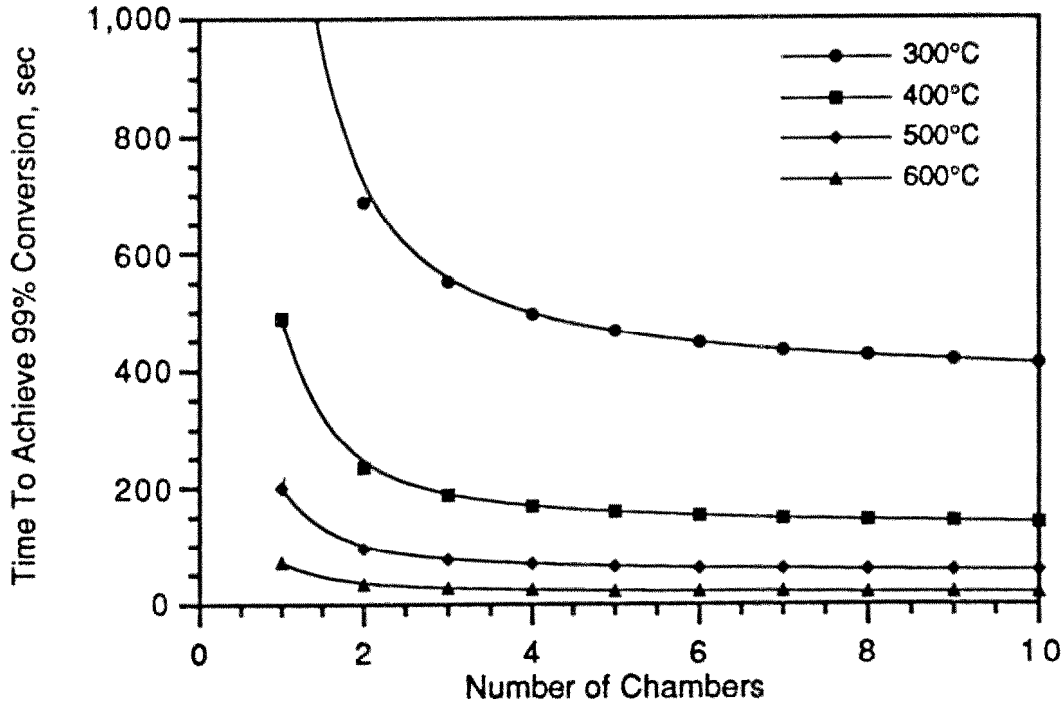

Figure 6.7. Predicted time to achieve 99% destruction (t_{99})of trichloroethylene using a series of PDU chambers as illustrated in Figure 6.6 operated in series assuming each chamber may be modeled as 2 CSTRs in series. This illustrates that the overall system efficiently approaches that of an ideal plug flow reactor as the number of chambers increases and that the rate of improvement rapidly slows with more than 4 chambers. This suggests that a PDU system should be comprised of at least 4 chambers, or a system of chambers with a mean residence time equivalent to 8 CSTRs in series.

The model results summarized in Figures 6.8 through 6.16 illustrate that operating temperature has a significant impact on the overall system capacity. In the case of the chloroalkenes (ca. Figures 6.8 and 6.9) a steady increase in throughput is predicted as temperature increases. In all of the aromatic materials a somewhat limited effect of temperature is seen at temperatures below approximately 500°C. with a significant increase at higher temperatures. This suggests that if the system capacity is inadequate at temperatures below 500°C the cost of achieving temperatures greater than 500°C may be offset by the significant increase in the system capacity.

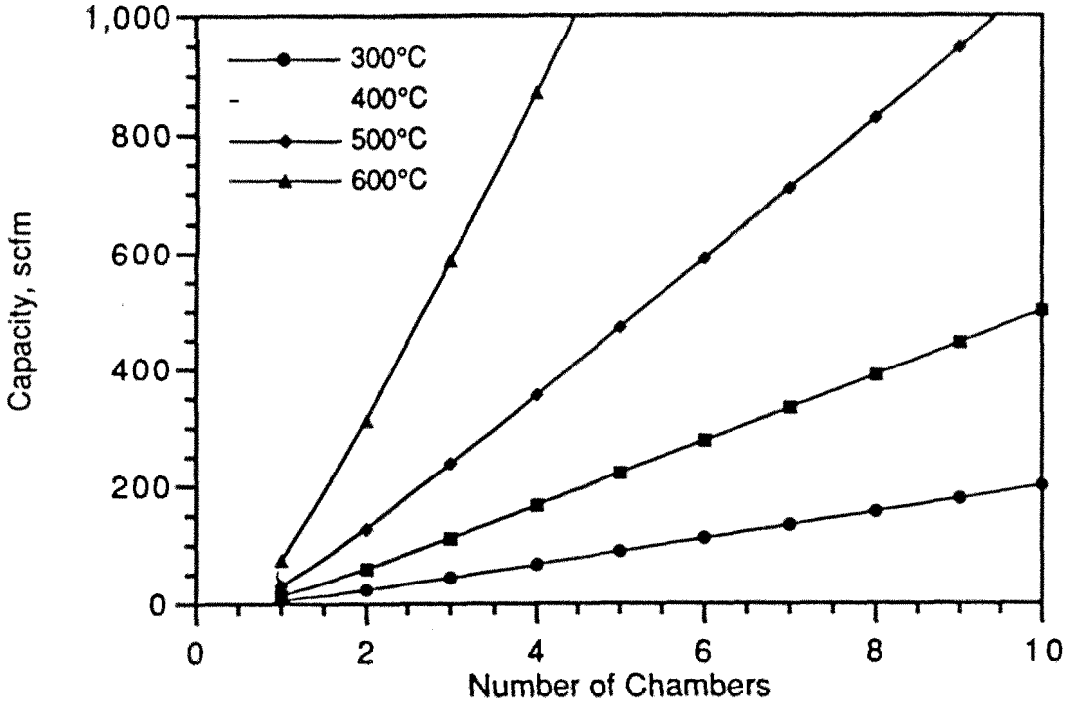

Figure 6.8. The predicted processing capacity of a PDU achieving 99% destruction of trichloroethylene as a function of mean operating temperature and number of chambers using the basic design illustrated in Figure 6.6 showing the capacity increases rapidly with temperature, and nearly linearly with the number of chambers.

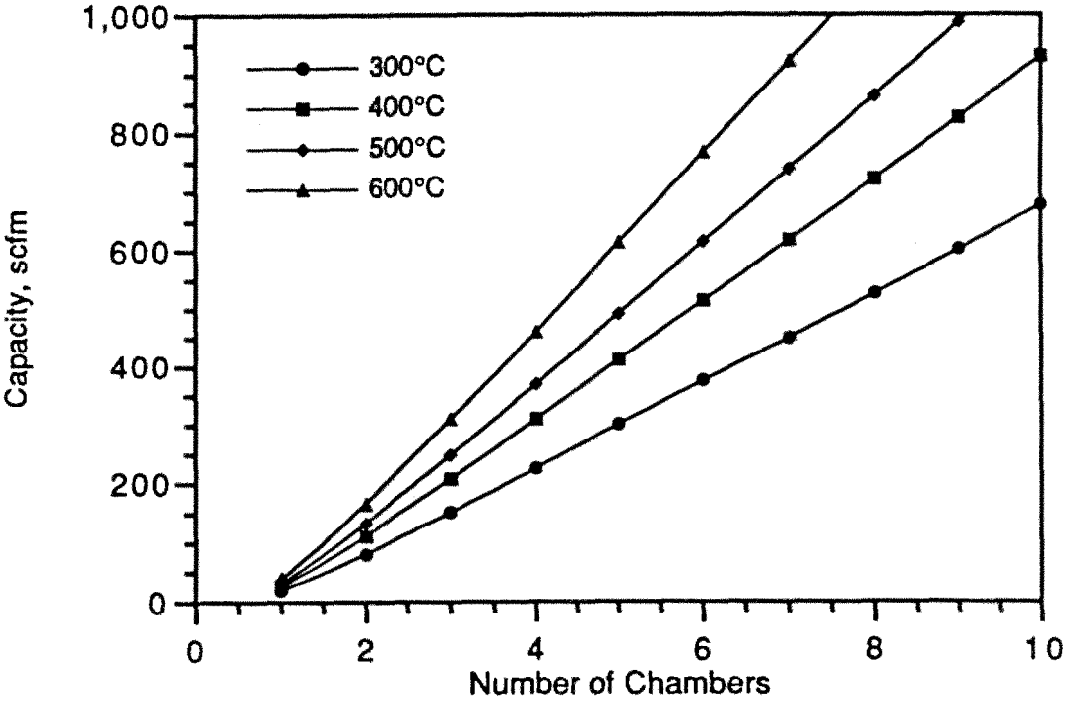

Figure 6.9. The predicted processing capacity of a PDU achieving 99% destruction of tetrachloroethylene as a function of mean operating temperature and number of chambers using the basic design illustrated in Figure 6.6 showing the capacity increases significantly with temperature, and nearly linearly with the number of chambers.

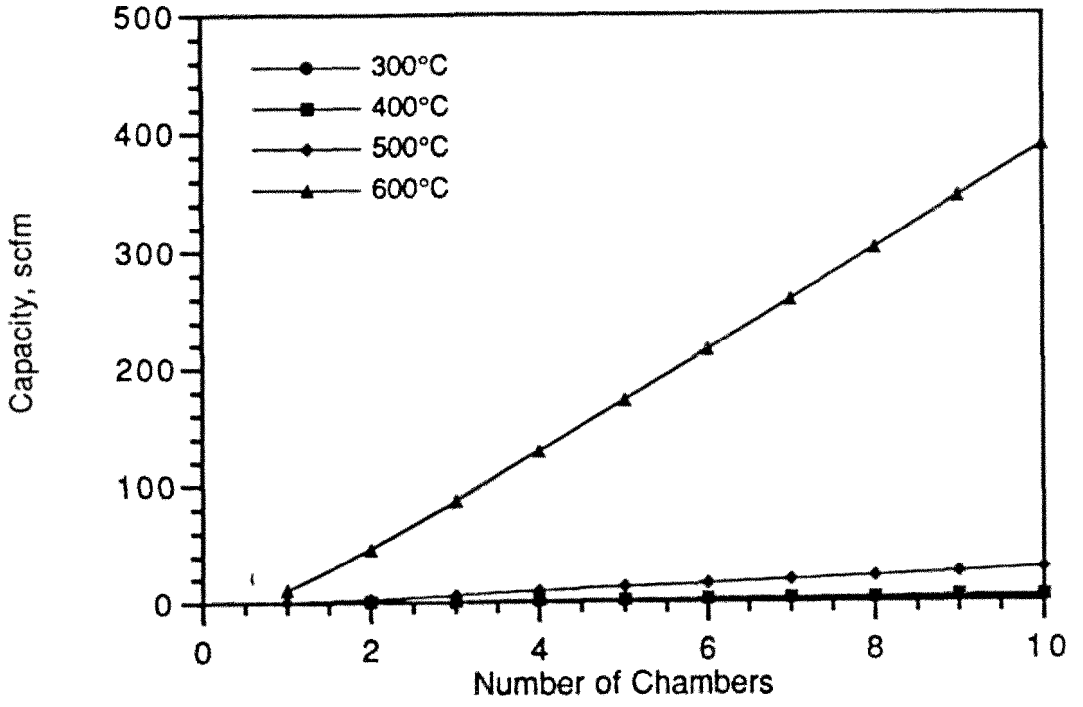

Figure 6.10. The predicted processing capacity of a PDU achieving 99% destruction of benzene in BTEX as a function of mean operating temperature and number of chambers using the basic design illustrated in Figure 6.6 showing the capacity increases significantly at temperatures above 500°C, and nearly linearly with the number of chambers.

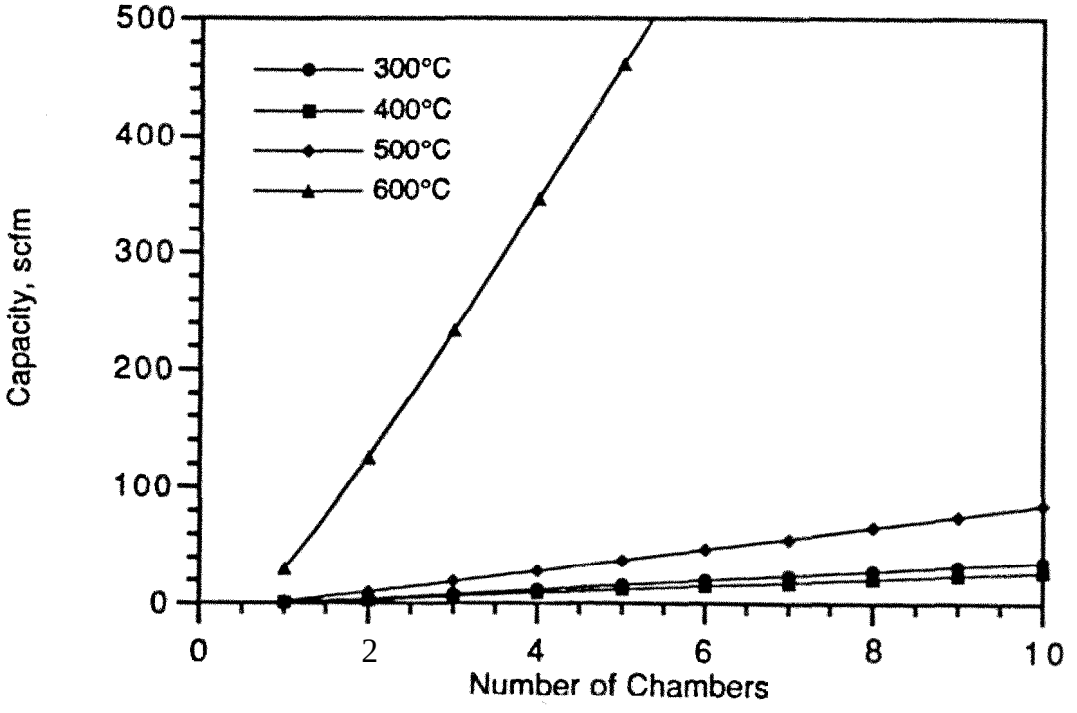

Figure 6.11. The predicted processing capacity of a PDU achieving 99% destruction of toluene in BTEX as a function of mean operating temperature and number of chambers using the basic design illustrated in Figure 6.6 showing the capacity increases significantly at temperatures above 500°C, and nearly linearly with the number of chambers.

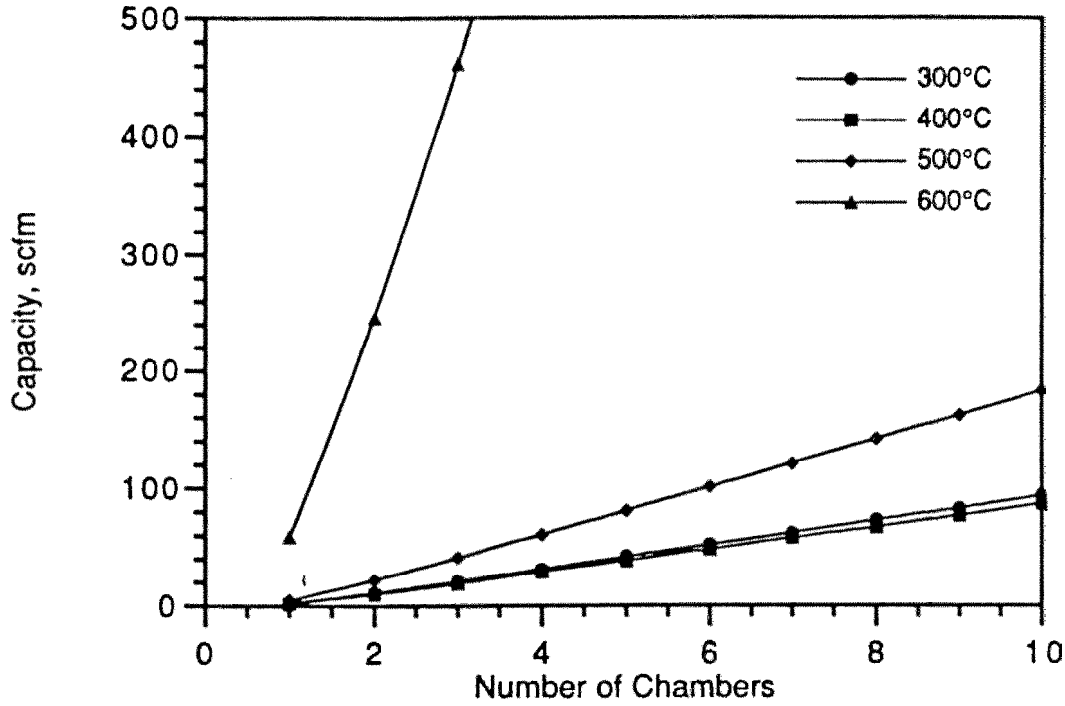

Figure 6.12. The predicted processing capacity of a PDU achieving 99% destruction of ethyl benzene in BTEX as a function of mean operating temperature and number of chambers using the basic design illustrated in Figure 6.6 showing the capacity increases significantly at temperatures above 500°C, and nearly linearly with the number of chambers.

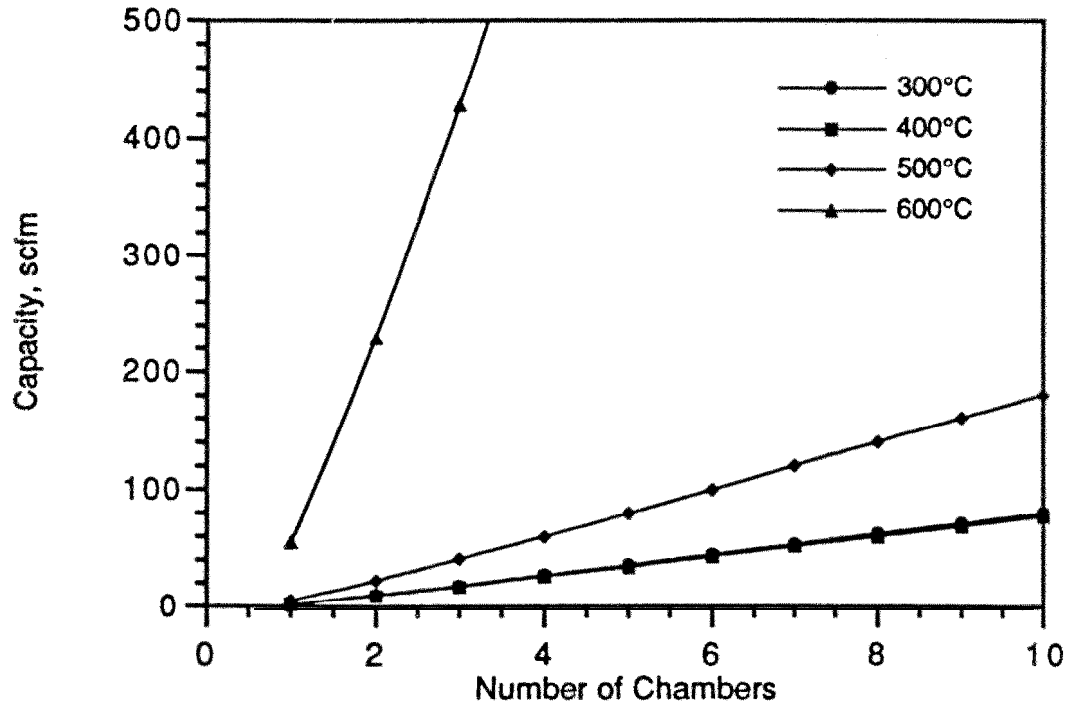

Figure 6.13. The predicted processing capacity of a PDU achieving 99% destruction of m-xylene in BTEX as a function of mean operating temperature and number of chambers using the basic design illustrated in Figure 6.6 showing the capacity increases significantly at temperatures above 500°C, and nearly linearly with the number of chambers.

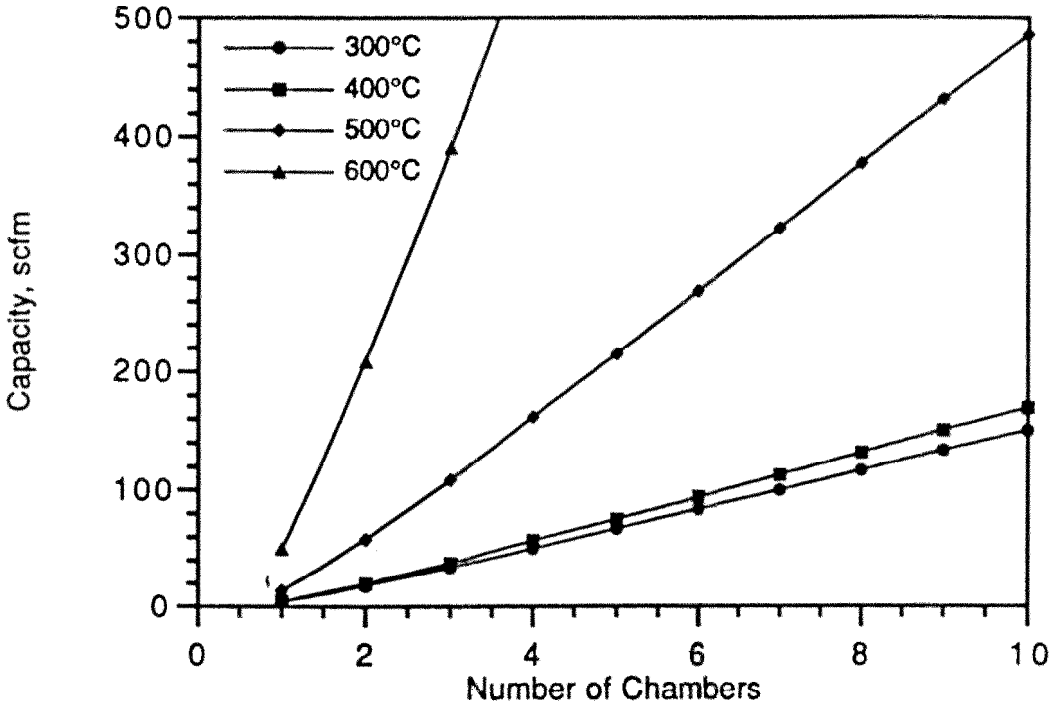

Figure 6.14. The predicted processing capacity of a PDU achieving 99% destruction of monochlorobenzene as a function of mean operating temperature and number of chambers using the basic design illustrated in Figure 6.6 showing the capacity increases significantly at temperatures above 400°C, and nearly linearly with the number of chambers.

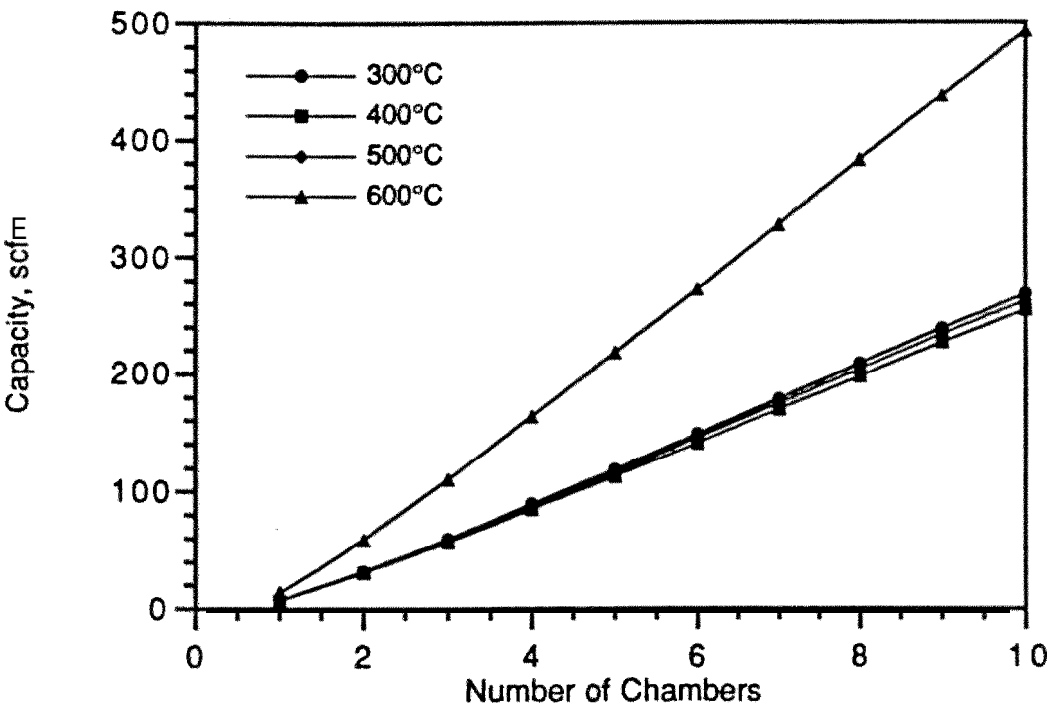

Figure 6.15. The predicted processing capacity of a PDU achieving 99% destruction of o-dichlorobenzene as a function of mean operating temperature and number of chambers using the basic design illustrated in Figure 6.6 showing the capacity increases significantly at temperatures above 500°C, and nearly linearly with the number of chambers.

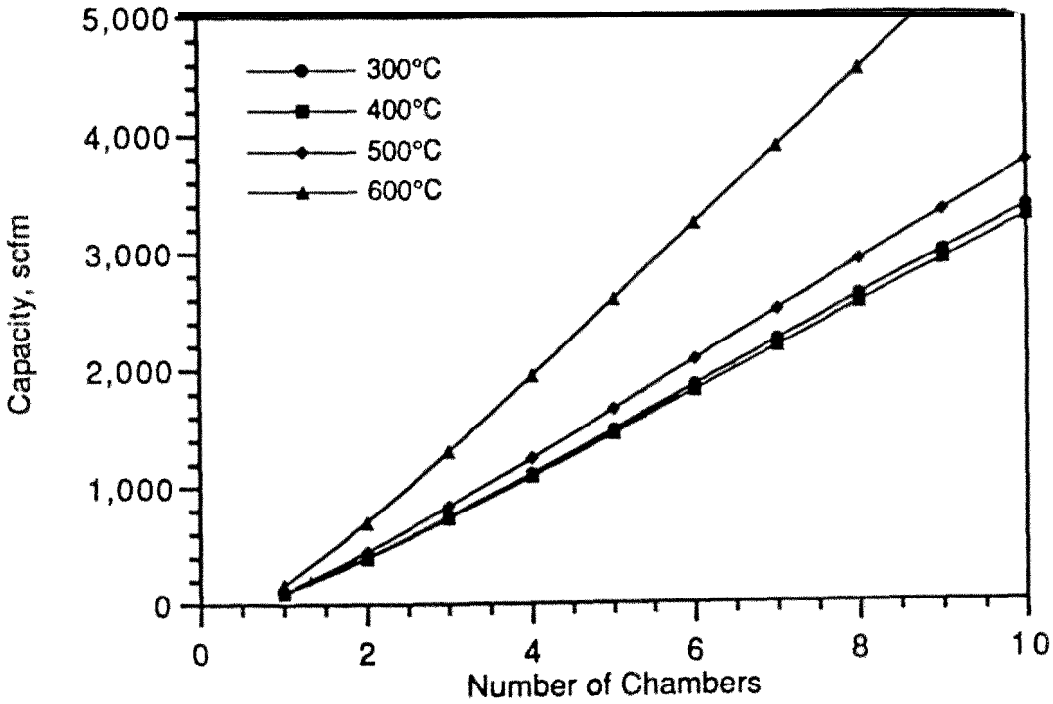

Figure 6.16. The predicted processing capacity of a PDU achieving 99% destruction of 1,2,3,4-tetrachlorodibenzo-p-dioxin as a function of mean operating temperature and number of chambers using the basic design illustrated in Figure 6.6 showing the relatively high system capacity for this compound and that the processing rate increases nearly linearly with the number of chambers.

6.4 ESTIMATED COST OF A PROTOTYPE PDU SYSTEM

The overall capital and operating costs for the PDU chamber illustrated in Figure 6.6 were calculated as summarized in Table 6.3. In this table the costs for the shell and insulating firebrick where taken as similar to that reported for a hazardous waste incinerator afterburner and corrected to 1995 costs.[16,17] The cost for the lamps, lamp wells, and lamp ballasts were from the manufacturer's literature (Hanovia, 1994). These estimates suggest the majority of the capital costs will be in fabricating the reactor shell, followed by the lamp wells, ballasts, and the estimated costs of the system support structure and equipment.

With respect to the amortized costs (using a simple linear depreciation model), Table 6.3 suggests the most expensive component will be the lamps and the lamp wells. The 2,500 hours used for the lamp life were based on the manufacture's estimate assuming 5 hours of operation for every lamp start. Discussions with the manufacturer indicated that since the lamps will likely see continuous service in the PDU significantly longer service life is possible which should reduce overall cost of the lamps, and hence the operating costs of the PDU. The second highest

amortized cost is the lamp wells which are expected to degrade from attack from dust and water vapor. The cost estimates assumes the lamp wells are replaced with new wells for every 10,000 hours of operation. If the wells can be replaced with refurbished units, this cost could be reduced.

Table 6.3
Estimated Costs For A PDU Chamber Fitted With
Six 200 W/in Medium Pressure Mercury Lamps

Item	Cost	Expected Life	Annual Cost
Carbon Steel Shell	$24,300 [1]	20 years	$1,215
Firebrick Insulation	$1,370 [2]	5 years	$274
Lamp Wells	$8,400	2 years[3]	$4,200
Lamp Ballasts	$8,500	5 years[4]	$2,125
Support Structure	$8,500 [5]	20 years	$425
Sub Total	$51,070		$8,239
Lamps	$3,000	6 months[6]	$6,000
Sub Total	$54,070		$14,239
Electrical Service[7]			$22,500
Grand Total			$36,739
Hourly Cost[8]			$7.34

[1]Assuming $86/ft^2.
[2]Assuming $1.44/ft^2-in.
[3]Assuming 10,000 hour life and 5,000 hours of operation per year.
[4]Assuming 20,000 hour life and 5,000 hours of operation per year.
[5]Assuming support structure and equipment is 20% of the chamber cost less support.
[6]Assuming 2,500 hour life and 5,000 hours of operation per year.
[7]Assuming $0.05/kW-hr and 5,000 hours of operation per year.
[8]Assuming 5,000 hours of operation per year.

With respect to consumable materials, only electricity for the lamps is considered here. As Table 6.3 shows electricity is the largest single contributor to the overall cost of the PDU. The relatively high electric energy requirement comes from the fact that only about 15% of the electrical energy is converted to useful UV radiation. If other lamps are made available, such as low pressure mercury or xenon excimer, this cost could be considerably reduced. This cost is in part offset by the thermal contribution to the system from the lamps. Specifically, in a well insulated vessel the 90 kW supplied to the chamber by the six 15 kW lamps is sufficient to heat approximately 600 cfm of air saturated with water vapor (as from a soil vapor extraction unit) from 15°C to 500°C. Therefore, depending on the specific site requirements, the heat from the lamps should reduce the size of a preheater, or eliminate it entirely.

In summary, the estimate summarized in Table 6.3 suggest the overall operating cost for a PDU based on the design presented in Figure 6.6 should be less than $ 10/hr-chamber including the depreciation of the equipment, replacement lamps, and required electrical service.

SECTION 7

CONCLUSIONS

Based on the results of the laboratory study of the photothermal detoxification process and the subsequent modeling of the performance of a large-scale PDU, the following conclusions may be made.

- Hazardous organic compounds whose molecular structure includes alkene or aromatic structures are likely to absorb near-UV radiation which is necessary for the photothermal detoxification process.
- The near-UV absorption spectrum of organic compounds shifts to longer wavelengths and increases in overall intensity with increasing temperature leading to an overall increase in efficiency of the photothermal process at high temperatures.
- Organic compounds which efficiently absorb near-UV radiation (i.e., chlorinated alkenes, chlorinated aromatics, chlorinated dibenzo-p-dioxins, etc.) are relatively easily destroyed by the photothermal process.
- Molecules which only weakly absorb near-UV radiation (i.e., alkanes and chloroalkanes) are not good candidates for a direct photothermal process using medium-pressure mercury lamps.
- The photothermal process is capable of destroying most organic PICs though caution should be taken to monitor for the emission of low molecular weight PICs as part of any scale-up activities.
- Of the high intensity lamps currently available, linear, medium pressure mercury lamps are the most suitable for a large-scale PDU for the treatment of chlorinated

alkenes, chlorinated aromatics. and dioxins due to the high UV output, long service life, and geometry of these types of lamps.

- A large-scale PDU should include at least four cylindrical reactor chambers operating in series, enclosing lamps mounted near the chamber centerline, and at a relatively high temperature (i.e., 500-600°C).
- The capacity of the PDU system can be adjusted through selection of appropriate operating conditions (i.e., number of lamps, operating temperature, etc.), operating chambers in series to increase efficiency and capacity, or sets of chambers in parallel.
- The overall capital cost for a large-scale PDU (270 ft^3 chamber enclosing six 200 W/in. lamps) should be on the order of $50,000 per chamber and an operating cost (including the amortized cost of the capital expenses) of less than $ 10/hr.

SECTION 8
REFERENCES

1. J. L. Graham and B. Dellinger, "Solar Thermal/Photolytic Destruction of Hazardous Organic Wastes," Energy, 12, No. 3/4, pp. 303-370, 1987.

2. J.L. Graham, B. Dellinger, D. Klosterman, G. Glatzmaier, and G. Nix, "Disposal of Toxic Wastes Using Concentrated Solar Radiation," In Emerging Technologies in Hazardous Waste Management II, American Chemical Society, Washington, DC, Chapter 6, pp. 83-109, April 1991.

3. R. Hulstrom, R. Bird, and C. Riordan, "Spectral Solar It-radiance Data Sets For Selected Terrestrial Conditions," Solar Cells, 15 (1985). pp. 365-391.

4. S. L. Murov, "Handbook of Photochemistry," Marcel Dekker, NY, 1973.

5. B. Dellinger, "Determination of the Thermal Stability of Selected Organic Compounds," Hazardous Waste, 1, No. 2, pp. 137-157, 1984.

6. S. P. McGlynn, T. Azumi, M. Kinoshita, "Molecular Spectroscopy of the Triplet State", Prentice-Hall, Inc., Englewood Cliffs, NJ, 1969.

7. A. Levy, "The Accuracy of the Bubble Meter Method For Gas Flow Measurements," J. Sci. Instrum., Vol 41, pp. 449-453, 1964.

8. W. G. Herkstroeter, "Special Methods in Absorption Spectroscopy," in Creation and Detection of the Excited State, Vol. 1, Part A, Edited by Angelo A. Lamola, Marcel Dekker, Inc., New York, NY, 1971.

9. J. L. Graham, D. L. Hall, and B. Dellinger, "Laboratory Investigation of the Thermal Degradation of a Mixture of Hazardous Organic Wastes-I," Environmental Science & Technology, 20, pp. 703-710, 1986.

10. B. Dellinger, "Emission of Toxic Organic Compounds, a Discussion of the Hazardous Waste Incineration Critical Review," APCA Journal, Vol. 37, No. 9, September, 1987.

11. E. Lipczynska-Kochany, J. R. Bolton, "Flash Photolysis/HPLCApplications. 2. Direct Photolysis vs Hydrogen Peroxide Mediated Photodegredation of 4-Chlorophenol As Studied by a Flash Photolysis/HPLC Technique," ES&T, Vo1.26, No. 2, pp. 259-262.

12. J. Hawarl, A. Demeter, R. Samson, "Sensitized Photolysis of Polychlorobiphenyls in Alkaline 2-Proponol Dechlorination of Arochlor 1254 in Soil Samples by Solar Radiation," ES&T, Vo1.26, No. 10, pp. 2022-2027.

13. H. Muto, M. Shinada, Y. Takizawa, "Heterogeneous Photolysis of Polychlorinated Dibenzo-p-dioxins on Fly Ash in Water-Acetonitrile Solution in Relation to the Reaction with Ozone," ES&T, Vol. 25, No. 2, pp. 316-322.

14. Chemical Engineering, p. 17, April 20, 1981.

15. O. Levenspiel, "The Chemical Reactor Omnibook", OSU Book Stores, Inc., Corvallis, OR, 1989.

16. G. A. Vogel, E. J. Martin, "Estimating Capital Costs of Equipment of Facility Components," Chemical Engineering, Vol. 90, No. 24, pp. 87-90, 1984.

17. M. S. Peters, K. D. Timmerhaus, "Plant Design and Economics for Chemical Engineers," 2nd Edition, McGraw-Hill Book Co., New York, NY, 1968.